



UNIVERSITY OF  
LIVERPOOL

# Ammonia Synthesis using a Dielectric Barrier Discharge Reactor

*A thesis submitted in accordance with the requirements of the University of  
Liverpool for the degree of Master of Philosophy.*

*By*

*Yuxing Tian*

*December 2019*

## ABSTRACT

Ammonia is an essential product used in such applications as pharmaceuticals, explosives and agriculture. Among these applications, about 85% of the  $\text{NH}_3$  is used for the production of fertiliser. The fertiliser production consumes more than 130 million tonnes of  $\text{NH}_3$  on an annual base and is believed to sustain nearly half of the global population. For now,  $\text{NH}_3$  has been manufactured by the Haber Bosch process. This process is carried out at high temperatures (400-600 °C) and pressures (200-400 atm). In addition, to separate the produced  $\text{NH}_3$  and to recycle the unreacted  $\text{H}_2$  and  $\text{N}_2$  in the flow, a periodic swing of temperature and pressure, and several separation stages, are necessary for industrial applications which consume even more energy. This makes the Haber Bosch process undesirable due to the substantial energy burden.

The motivation for the research carried out in this thesis begins in investigating an alternative method for artificial ammonia synthesis that provides promising solutions to reducing the adverse effects caused to the environment. This method requires an acceptable level of energy consumption, carbon emission and reliability for the industry. Plasma-driven  $\text{NH}_3$  synthesis might be potentially advantageous for scale-up applications. In the work of Chapter 3, the pure metal catalysed  $\text{NH}_3$  synthesis was performed under ambient conditions in a dielectric barrier discharge reactor (DBD). Metal materials were applied as internal electrodes to explore the influence of the combination of different metals on the experimental results. At the same time, I studied the results of the influence of gas proportion and gas flow rate under different experimental conditions. In addition, possible mechanisms are also discussed together with recent academic papers on the subject. The metal wool electrode was used to improve the  $\text{NH}_3$  concentration as well as to improve energy efficiency. Compared with the

rod electrode, the wool electrode substantially enhanced the synthesis performance regarding the conversion of  $\text{N}_2$  and  $\text{H}_2$ , the  $\text{NH}_3$  concentration and the energy efficiency of the synthesis process. From the catalytic results for pure metals, Cu wire showed the best energy efficiency reaching a  $1.04 \text{ g-NH}_3 \text{ kWh}^{-1}$ , as well as the highest conversion of 0.38%.

Chapter 4 focuses on the NTP ammonia synthesis in a rod electrode DBD reactor. It determines the optimum molar ratio and total feed flow rate of gases, as well as the optimum power input for  $\text{Fe}_2\text{O}_3$  and CuO based catalysts. Also, the work in this chapter shows the ability of  $\text{Fe}_2\text{O}_3$  and CuO based catalysts that significantly enhances the yield of ammonia, and this phenomenon obeys the Sabatier principle which is also known as the volcano plots. Various catalyst characterisation methods including XRD, TEM, TPD and XPS were used to investigate the correlation between catalyst characteristics and the experiment outcome, and reasons why copper-oxide based catalyst gave a better result.

## TABLE OF CONTENTS

List of corrections.....	2
Abstract.....	3
Table of Contents.....	5
List of figures.....	7
List of Tables .....	8
Acknowledgements.....	9
1. Introduction .....	10
1.1 Background and motivation.....	10
1.1.1 Introduction to nitrogen fixation .....	10
1.1.2 The importance and challenges of ammonia synthesis.....	11
1.1.3 The alternative methods for ammonia synthesis .....	14
1.1.4 Future perspective of the reaction of NTP into the ammonia synthesis.....	16
1.2 Plasma systems .....	17
1.2.1 Background of plasma physics and its classification.....	17
1.2.2 Non-thermal plasma and its generation methods.....	20
1.3 A review of the NTP assisted ammonia synthesis technologies .....	25
1.3.1 The development of the reactor for NTP assisted ammonia synthesis.....	27
1.3.2 The development of catalysts for DBD ammonia synthesis .....	38
1.4 Aims and objectives .....	42
2 Experimental .....	45
2.1 Experimental system.....	45
2.2 Analytic methods .....	49
2.2.1 Measurement and analysis of electric signals .....	49
2.2.2 Quantification of gas product using FT-IR.....	52
2.2.3 Plasma diagnostic using optical emission spectroscopy.....	53
2.2.4 Catalyst preparation and characterisation .....	53
3 NTP ammonia synthesis in a wire-electrode DBD reactor .....	57
3.1 Introduction .....	57
3.2 Results and discussions.....	57
3.2.1 Effect of electrode materials on the plasma-driven $\text{NH}_3$ synthesis .....	57
3.2.2 Effect of $\text{N}_2/\text{H}_2$ molar ratio on the plasma-driven $\text{NH}_3$ synthesis .....	59
3.2.3 Effect of total feed flow rate on the plasma-driven $\text{NH}_3$ synthesis .....	61
3.2.4 Effect of electrode materials on the electrical properties of the reactor.....	62

3.2.5	The enhancement mechanism of copper wire .....	65
3.3	conclusions.....	68
4	NTP ammonia synthesis in a rod electrode DBD reactor.....	69
4.1	Introduction .....	69
4.2	Rod electrode DBD reactor packed with metal oxide catalysts.....	69
4.2.1	Characterisation of fresh catalysts.....	69
4.2.2	Effect of gas ratio and feed flow rate.....	78
4.2.3	Effect of specific energy input (SEI) .....	80
4.2.4	Effect of temperature .....	83
4.2.5	Effect of metal oxide-based catalysts on plasma discharges.....	84
4.2.6	The enhancement mechanism of CuO/Al <sub>2</sub> O <sub>3</sub> .....	85
4.3	Conclusion.....	88
5	Conclusions and future work .....	89
5.1	Overview .....	89
5.2	Limitations.....	90
5.3	Future work.....	91
	References .....	92
	Appendices.....	97

# LIST OF FIGURES

Figure 1.1 The applications of ammonia, of which 88% artificial ammonia is used for fertiliser production, reproduced according to [7].	12
Figure 1.2 The stages involved in the Haber Bosch ammonia synthesis process, reproduced from [12].	13
Figure 1.3 Proposed circulation of NTP ammonia synthesis in a DBD reactor, reproduced from [37].	17
Figure 1.4 States of matter explanation, reproduced based on [38].	18
Figure 1.5 Voltage-current characteristic plot of electric discharge regimes [40].	19
Figure 1.6 Schematic diagram of the DBD plasma reactor used in the work of this thesis	22
Figure 1.7 An electric glow discharge tube featuring its most essential characteristics [40].	23
Figure 1.8 Schematic diagram of a microwave plasma reactor [47].	24
Figure 1.9 Glow discharge reactor for ammonia synthesis [30].	27
Figure 1.10 Rector Layout of high-frequency plasma reactors [33].	29
Figure 1.11 Schematic illustration of experimental apparatus [34].	30
Figure 1.12 Structure of the micro-gap dielectric barrier discharge reactor [28].	31
Figure 1.13 Dielectric barrier discharge reactor with a tubular membrane-like-catalyst [21].	32
Figure 1.14 Schematic diagram of the plasma jet used by Kubota, et al, [51].	33
Figure 1.15 Schematic of ferroelectric packed-bed DBD reactor [25].	34
Figure 1.16 NTP ammonia synthesis and adsorption system [29].	35
Figure 1.17 Synergistic catalytic absorption system designed by Peng, et al, [54].	36
Figure 2.1 Formulating the experimental setup for non-thermal plasma ammonia synthesis.	45
Figure 2.2 Schematic diagram and picture of the DBD reactor: (a) Wire-electrode DBD; (b) Rod-electrode electrode DBD.	47
Figure 2.3 (a) Typical circuit for measuring the discharge power of a DBD reactor [66], [67]; (b) Ideal Lissajous figure for a DBD reactor [68].	50
Figure 2.4 (a) Equivalent circuit of the DBD reactor [71]; (b) Transversal section of the Rod electrode DBD reactor [67], [71].	51
Figure 2.5 The flow chart for the preparation steps of the Fe/Al <sub>2</sub> O <sub>3</sub> catalyst.	54
Figure 3.1 NH <sub>3</sub> concentration and energy efficiency using electrode with different materials. (N <sub>2</sub> /H <sub>2</sub> = 1:1, total flow rate 100 ml min <sup>-1</sup> and discharge power 20 W).	59
Figure 3.2 Dependence of NH <sub>3</sub> concentration and energy efficiency on the N <sub>2</sub> /H <sub>2</sub> molar ratio. (Cu wire electrode, a total flow rate of 100 ml min <sup>-1</sup> and discharge power 20 W).	60
Figure 3.3 Effect of total flow rate on NH <sub>3</sub> production. (Cu wire electrode, N <sub>2</sub> /H <sub>2</sub> molar ratio 1:1 and discharge power 20 W).	61
Figure 3.4 Typical discharge waveform of the plasma-synthesis of NH <sub>3</sub> using different electrodes. (Total flow rate: 100 ml min <sup>-1</sup> , N <sub>2</sub> /H <sub>2</sub> = 1:1, frequency: 9 kHz; discharge power 20 W).	63
Figure 3.5 Lissajous figure obtained during the plasma synthesis of NH <sub>3</sub> . (Total flow rate: 100 ml min <sup>-1</sup> , N <sub>2</sub> /H <sub>2</sub> = 1:1, frequency: 9 kHz; discharge power 20 W).	64
Figure 3.6 The tri-nuclear structure of M <sub>3</sub> N (a) Cu (b) Ni (c) Ti, calculated by Iwamoto et al. [24].	67
Figure 4.1 XRD pattern of the fresh (before plasma chemical reaction) and spent (after plasma chemical reaction) catalysts.	70
Figure 4.2 TEM images of the fresh catalysts without reduction (a) Al <sub>2</sub> O <sub>3</sub> , (b) Fe <sub>2</sub> O <sub>3</sub> /Al <sub>2</sub> O <sub>3</sub> and (c) CuO/Al <sub>2</sub> O <sub>3</sub> .	72
Figure 4.3 NH <sub>3</sub> -TPD profile of the fresh (a) Al <sub>2</sub> O <sub>3</sub> (b) Fe <sub>2</sub> O <sub>3</sub> /Al <sub>2</sub> O <sub>3</sub> and (c) CuO/Al <sub>2</sub> O <sub>3</sub>	74
Figure 4.4 Comparison of total acid amounts for Al <sub>2</sub> O <sub>3</sub> , Fe <sub>2</sub> O <sub>3</sub> /Al <sub>2</sub> O <sub>3</sub> and CuO/Al <sub>2</sub> O <sub>3</sub>	74
Figure 4.5 N1s core level measurements for (a) packed with Al <sub>2</sub> O <sub>3</sub> (b) Fe <sub>2</sub> O <sub>3</sub> /Al <sub>2</sub> O <sub>3</sub> and (c) CuO/Al <sub>2</sub> O <sub>3</sub> after plasma reaction	77
Figure 4.6 Proportion of individual peaks assigned to N, NH, NH <sub>2</sub> and NH <sub>3</sub> for: (a) plasma only (b) packed with Al <sub>2</sub> O <sub>3</sub> (c) Fe <sub>2</sub> O <sub>3</sub> /Al <sub>2</sub> O <sub>3</sub> and (d) CuO/Al <sub>2</sub> O <sub>3</sub> ; The numbers above each bar chart indicate the percentage of an adsorbed species on the corresponding catalyst.	77
Figure 4.7 Ammonia concentration with different gas ratios (N <sub>2</sub> /H <sub>2</sub> = 1:3, 1:2, 1:1, 2:1, 3:1, total flow rate 50 ml min <sup>-1</sup> and discharge power 20 W).	78

Figure 4.8 Ammonia concentration with different gas flow rates ( $N_2/H_2 = 1:3$ , total flow rate 50, 100, 150, 200 $ml\ min^{-1}$ and SEI from 6-24 $kJ\ L^{-1}$ ).	80
Figure 4.9 Ammonia concentration with different discharge powers: (a) No catalyst; (b) Packed with $Al_2O_3$ ; (c) Packed with $Fe_2O_3/Al_2O_3$ ; (d) Packed with $CuO/Al_2O_3$ ( $N_2/H_2 = 1:3$ , total flow rate 50 $ml\ min^{-1}$ and discharge power 10, 20, 30, 40, 50, 60 W).	81
Figure 4.10 Energy efficiency with different discharge powers: (a) No catalyst; (b) Packed with $Al_2O_3$ ; (c) Packed with $Fe_2O_3/Al_2O_3$ ; (d) Packed with $CuO/Al_2O_3$ ( $N_2/H_2 = 1:3$ , total flow rate 50 $ml\ min^{-1}$ and discharge power 10, 20, 30, 40, 50, 60 W).	82
Figure 4.11 Plasma gas temperature of (a) No catalyst; (b) Packed with $Al_2O_3$ ; (c) Packed with $Fe_2O_3/Al_2O_3$ ; (d) Packed with $CuO/Al_2O_3$ ( $N_2/H_2 = 1:3$ , total flow rate 50 $ml\ min^{-1}$ and discharge power 10, 20, 30, 40, 50, 60 W).	83
Figure 4.12 Typical discharge waveform of the plasma-synthesis of $NH_3$ using metal oxide catalysts. ( $N_2/H_2 = 1:3$ , total flow rate 50 $ml\ min^{-1}$ and discharge power 60 W).	85
Figure 4.13 Emission spectrum for DBD: (a) plasma only (b) packed with $Al_2O_3$ (c) $Fe_2O_3/Al_2O_3$ and (d) $CuO/Al_2O_3$ (SPS = second positive system; FPS = first positive system; FNS = first negative system)	86

## LIST OF TABLES

Table 1-1 Classification of plasmas by temperature	20
Table 1-2 Summary of literature reported on plasma ammonia synthesis.	26
Table 1-3 The development of NTP catalysis.	37
Table 3-1 Electrical properties of the DBD reactor using different electrodes. ( $N_2/H_2 = 1:1$ , total flow rate 100 $ml\ min^{-1}$ and discharge power 20 W).	65
Table 4-1 Physical characteristics of the fresh catalysts.	71

## ACKNOWLEDGEMENTS

"There is nothing to writing. All you do is sit down at a typewriter and bleed."

**-Ernest Hemingway**

While modern people tend to use the keyboard rather than a typewriter, it does not change the bleeding nature of writing. Nevertheless, I am sure my words in this part has no intersection with this famous quote. Though my words lack the ability to express the full extent of experience and memory that the research conducted herein has given to me, please allow me to attempt as an engineer. My supervisor Professor Xin Tu and former postdoc Dr Li Wang time led me to the research level and have been continual sources of support for my project. Through those moments at a loss, I was provided with patience and encouragement to help me come by. Also, to everyone in my research group, I express my gratefulness for your readiness to assist and any contributions to the research in this thesis. Additionally, office 321 ought to be given credits to its healthy atmosphere of doing research.

To the Department of Electrical Engineering and Electronics, I have to say thank you for educating me in many aspects to become an engineer. Thank you for consistently maintaining the facilities in this building at right conditions that provide us with an active research environment. Besides, thanks to everyone who works at the workshop on the ground floor, without your help I am sure the work at the laboratory would be challenging to gain progress. Moreover, to whom I have bothered on the fifth-floor administrative office, I say thank you for making my postgraduate experience smooth and abundant.

Many thanks to my family and friends who have been staunchest supporters in my research by providing non-stop comfort, your love has undoubtedly made the years of research a rewarding experience. Particularly, thanks to my parents Biao Tian and Caihong Jiang who provided funding that enabled my studies to come to this point. Friends in LCGC fellowship, you have always been there reflecting God's amazing grace and lifting me up as always.

# 1. INTRODUCTION

The following chapter presents background information and the motivation for the research carried out in this thesis. The reasons why ammonia synthesis is of specific consideration and why it is imperative to human life are also explained.

To understand better the process of synthesising ammonia, the overall reaction and requirements are explained. After this, an overview of the general approaches regarding ammonia synthesis, including the Haber Bosch process, electrochemical, biological and plasma-induced are also discussed. Next, the classification of plasma is carried out to understand the rationale of various plasma generating methods. Moreover, the reception of plasma technology into the ammonia synthesis will be discussed in a brief literature review, highlighting the current level of research progress, and to supplement the understanding of the development stage of plasma ammonia synthesis. Finally, the aims and objectives section gives a clear idea of why this research should be conducted and what to achieve.

## 1.1 BACKGROUND AND MOTIVATION

### 1.1.1 INTRODUCTION TO NITROGEN FIXATION

Nitrogen is an essential element in proteins and related biological molecules, supporting animals and plants living on earth. Nitrogen fixation is a process by which nitrogen within the Earth's climate is changed over into ammonia or other atoms accessible to living beings. This process can be realised naturally, biologically and artificially. First, nitrogen can be fixed by lightning which converts nitrogen and oxygen into nitrogen oxide. It combines with water to create a nitrous acid, or nitric acid, that leaks into the soil and provides the essential plant food. Second, biological nitrogen fixation occurs when microorganisms (e.g. leguminous

rhizobia) converts nitrogen from the air into nitrogen compounds by an enzyme called nitrogenase. Recently, the biologically fixed nitrogen has reached around 297 million metric tonnes annually [1]. However, the increasing demand from the worldwide population has highlighted agricultural practices, implying that biological-fixed nitrogen is not adequate enough in raising emblems to bolster the developing population. This challenge leads to the third way of realising ammonia synthesis using artificial nitrogen fixation that utilises chemical reactions converting nitrogen to value-added nitrogen compounds which are used mostly for artificial fertiliser production. The Haber Bosch process dominates industrial ammonia synthesis process since it was commercialised in 1913. A market study carried out by "Ceresana Market Studies" [2] says "ammonia competition will soon be much more intense". The study concluded that the Haber Bosch process contributed to 198 million metric tonnes of ammonia annually worldwide in 2012 and will likely increase by 18% by 2019. Due to its significant contribution to the environment, the Haber Bosch process is considered one of the most significant inventions of the 20<sup>th</sup> century.

### 1.1.2 THE IMPORTANCE AND CHALLENGES OF AMMONIA SYNTHESIS

Ammonia is a chemical compound consisting of one atom of nitrogen and three atoms of hydrogen and is noted as  $\text{NH}_3$  in chemistry. It is a colourless gas under atmospheric pressure and ambient temperature. Ammonia dissolves effectively in water and alcohol. Also, it is easily liquefied at low temperature ( $-33.34\text{ }^{\circ}\text{C}$ ), and for such a reason, ammonia is used in refrigeration systems. The synthesis of ammonia is one of humanity's most massive volume manufactured chemical reactions by expending 2% of the world's entire energy per year [3]. As of 2014, about 88% of the human-made ammonia was broadly utilised in manufacturing nitrogen-based fertilisers either as its salts, solutions or anhydrous [4]. Also, nitrogen

fertilisers accounted for sustaining 40% of the world's population in 2014, and this number is gaining greater [5], [6]. Moreover, as shown in Figure 1.1 [7], ammonia is used to deliver various everyday products such as plastics, synthetic fibres, resins and other nitride-based chemical compounds. Besides, ammonia has the potential to play a noteworthy role in the future energy market, owing to its property of excellent energy storage media by storing a large amount of hydrogen in each molecule. A few speculations have proposed to utilise ammonia as a fuel for transport vehicles as well as for domestic heating purposes [8]–[10].

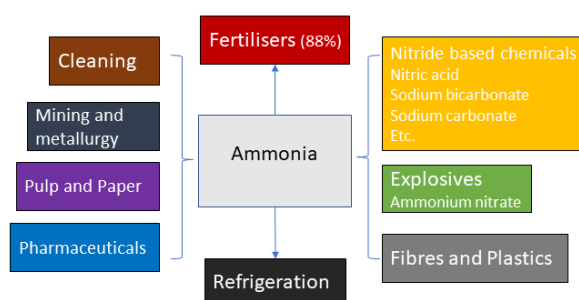


Figure 1.1 The applications of ammonia, of which 88% artificial ammonia is used for fertiliser production, reproduced according to [7].

The overall reaction of ammonia synthesis is shown in chemical equation 1. The main difficulties of this process are the dissociation of the strong triple-reinforced dinitrogen bonds ( $945 \text{ kJ mol}^{-1}$ ). Also, the dissociation of  $\text{N}_2$  is an unequivocally endothermic reaction. However, from the thermodynamic point of view, the change in enthalpy for this synthetic reaction is  $-46.35 \text{ kJ mol}^{-1}$ , which is below zero, indicating this is an exothermic process and is favoured by low temperature. Whereas, the ammonia compounds decompose at relatively high temperature since this is a reversible reaction. Therefore, to accommodate both temperature stipulations in one reaction, engineers brought in the ideas of utilising high pressure as well as catalyst techniques to avoid the reverse reaction and to diminish the activation energy.



The Haber Bosch process was named after two German chemists Fritz Haber and Carl Bosch and was first introduced in 1909. This process typically conducts at 400-600 °C with a compression ranging from 200-400 atmospheres over the iron-based catalysts to obtain an acceptable N<sub>2</sub> conversion of 15% and an NH<sub>3</sub> yield of 15-20% [11]. Figure 1.2 shows a diagram of the stages involved in the traditional Haber Bosch process, where fossil fuel and a large-scale reaction chamber are used. Although the Haber Bosch process produces more than 130 million metric tonnes of ammonia per year, it is also responsible for absorbing about 1-2% of global energy due to the conversion process. Wherein the needs of heating and compression ranging are the leading causes of energy consumption. In this thesis, the method of non-thermal plasma, as an intermedia, will be investigated as a potential method of overcoming the intense temperature and pressure conditions, as well as the depletion of fossil fuels used for the synthesis of ammonia.

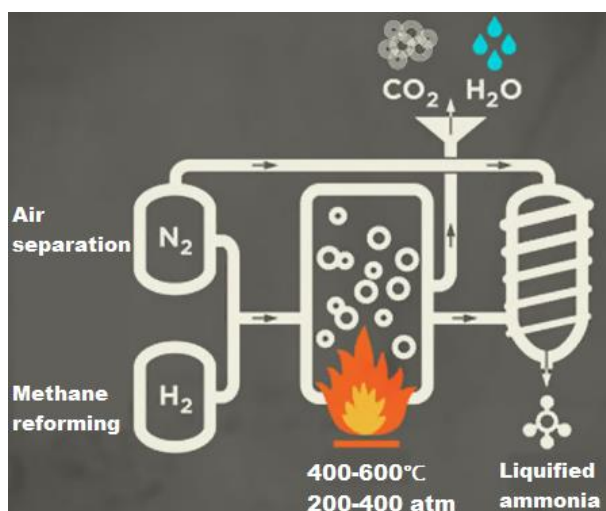


Figure 1.2 The stages involved in the Haber Bosch ammonia synthesis process, reproduced from [12].

### 1.1.3 THE ALTERNATIVE METHODS FOR AMMONIA SYNTHESIS

As described above, synthetic ammonia is crucial for producing valuable substances such as fertilisers and nitride-based chemicals. The object is to use different ammonia synthesis approaches to simplify the technological process (with low temperature and pressure) and thus improve its sustainability by allowing clean and carbon-free production. Although the Haber Bosch process so far is the foremost critical method of ammonia synthesis, this method results in major issues. The severe operating conditions are the main disadvantages of the Haber Bosch process, although there is the possibility of bringing down capital costs [13], [14]. Also, the high pressure required for the traditional Haber Bosch process further constrains the economies due to the high fossil fuel energy inputs for compression [14]. Moreover, the generation of hydrogen from either the electrolysis of water or the steam reforming of methane also needs attention. The former one is exceptionally energy-intensive, and the latter one requires fossil fuels. It is pointed out that the energy consumption of the Haber Bosch process will be almost three times higher (decreases to an energy efficiency floor of only  $68 \text{ g-NH}_3 \text{ kWh}^{-1}$ ) when applying renewable hydrogen source, for example, electrolysis of water (consumes  $360\text{-}480 \text{ kJ mol}^{-1}$ ) [15][16]. As a result, other ways of ammonia synthesis are therefore being considered taking into account renewable energy. Along with the Haber Bosch process, several alternative ammonia synthesis methods have been recently developed, including non-thermal plasma (NTP) [17], biological [18] and electrochemical ammonia synthesis [19],[20].

Plasma as an intermedia of synthesising ammonia has been widely studied recently. Peng and co-workers reviewed the non-thermal plasma-assisted ammonia synthesis technologies [17], and they pointed out that NTP is considered a promising technology for the future of

ammonia production. Moreover, it is known that NTP can enable thermodynamically unfavourable reactions to take place under ambient conditions. The NTP-driven chemical reaction has many advantages regarding mild reaction condition, rapid start and shutoff, and the potential to combine with other technologies. Furthermore, non-thermal plasma ammonia synthesis has the highest energy efficiency floor ( $303 \text{ g-NH}_3 \text{ kWh}^{-1}$ ) compared with the Haber Bosch process ( $126 \text{ g-NH}_3 \text{ kWh}^{-1}$ ) calculated by Cherkasov, et al, [15]. Most of the NTP ammonia synthesis uses  $\text{N}_2$  and  $\text{H}_2$  directly as the reactants. Then an electric or electromagnetic field will be applied to energise the reactant molecules to form  $\text{NH}_3$ . This approach has been widely investigated using DBD [21]–[29], glow [30], [31] and low-pressure microwave plasma [32]–[34] at low temperatures.

Biological ammonia synthesis is mainly about nitrogenase enzyme in microorganisms which catches and fixes the nitrogen from either nitrogen gas or nitrate/nitrite solutions to produce ammonia [18]. For biological ammonia synthesis, the energy is provided by the nutrient solution rather than provided by electricity. In this case, the energy supply system for this technology would be simpler compared with other artificial ammonia synthesis methods, such as electrochemical and plasma-induced. However, this technology comes with various well-known limitations. Firstly, this technology could only be carried out in the liquid phase, and the production rate is slow. Secondly, the engineering of complex enzymes is a significant obstacle to the improvement of this technology.

Electro-chemical ammonia synthesis uses electrolytes as a media to facilitates the transfer of hydrogen. Most of the studies reviewed by V.Kyriakou employed solid electrolytes using the material perovskite [20]. A major advantage is that electrochemical ammonia synthesis can also operate with liquid reactants, in which case the mesoporous electrolytes need to be

adopted. However, it is difficult to upgrade the structure of the reactor cell. Thus, the best way to enhance this technology is to design new electrolytes and catalysts that are coated on the electrodes to achieve high selectivity [35].

#### 1.1.4 FUTURE PERSPECTIVE OF THE REACTION OF NTP INTO THE AMMONIA SYNTHESIS

Ammonia synthesis with plasma as an alternative energy form has drawn people's attention. Non-thermal plasmas that operate at ambient temperature are widely investigated as a promising approach to produce ammonia from  $N_2$  and  $H_2$  mixture via NH radicals as a rate-limiting step. Utilising NTP to form  $NH_3$  rather than using the Haber-Bosch procedure could give valuable advantages:

- NTP ammonia synthesis can be operated under mild temperature and pressure conditions;
- they can be started and halted rapidly by actuating and deactivating the plasma system;
- they have the adaptability to be joined with sustainable energy sources, for example with wind power to reduce the overall carbon emission.

Accordingly, compared to the conventional high temperature and pressure process, a future plasma ammonia synthesis plant can eliminate the risk of using a compressor and the combustion of fossil fuel, achieving renewable energy involving small-scale plant for the designated use. Figure 1.3 shows the proposed circulation of ammonia synthesis using NTP in a DBD reactor, where only electricity was used to power the system and reactant gases are from air and water. Moreover, the idea of the development of a portable plasma device to synthesise ammonia on a small scale and produce fertilisers at the site of application has been investigated by the University of Minnesota. They have built a remarkable small-scale, on-site

ammonia plant using wind energy which adopts only air and water as the feedstock. The energy efficiency is reported at 60 g-NH<sub>3</sub> kWh<sup>-1</sup>, and a further update of the plant is expected to achieve an energy efficiency of 125 g-NH<sub>3</sub> kWh<sup>-1</sup>, which is better than the Haber Bosch process that averagely yielding 110 g-NH<sub>3</sub> kWh<sup>-1</sup> [36].

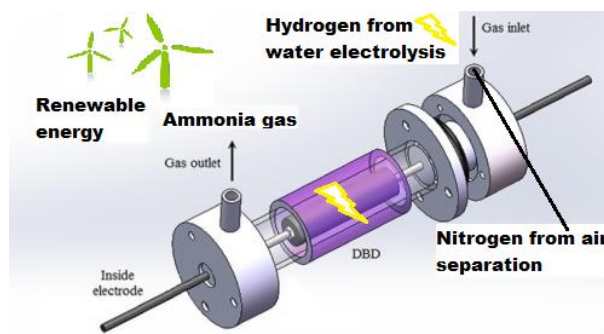


Figure 1.3 Proposed circulation of NTP ammonia synthesis in a DBD reactor, reproduced from [37].

## 1.2 PLASMA SYSTEMS

### 1.2.1 BACKGROUND OF PLASMA PHYSICS AND ITS CLASSIFICATION

The concept of plasma was firstly presented by Irving Langmuir in 1928 to depict the inward region of a glowing ionised gas delivered in an electrical discharge tube. Beyond that stage, plasma was also considered as the fourth state of matter that evolves from the gas phase. As shown in Figure 1.4, when enormous energy is applied, the substance molecules tend to be energised. Moreover, the matter is transformed into other states in the sequence of solid, liquid, gas and plasma.

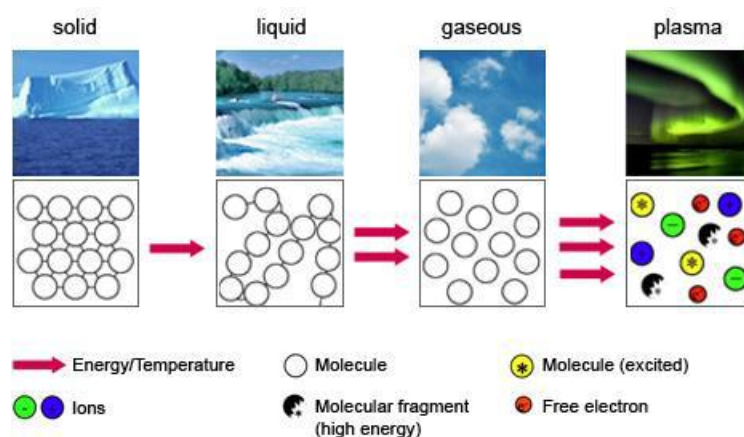


Figure 1.4 States of matter explanation, reproduced based on [38].

Plasma itself consists of many free electrons and positively-charged particles. Meanwhile, the numbers of positively and negatively charged particles are roughly equal. It has neither a specific shape nor a consistent volume unless it is enclosed in a container. Therefore, plasma can smoothly flow into, and take the shape of a container and will expand itself to fill that container evenly. However, the difference between plasma and gas occurs because of the loose charged particles. Due to the presence of charged particles, plasma can efficiently conduct electricity, and it can both produce and respond to electromagnetic fields so that plasma is sometimes called ionised gases.

To generate plasma, various energy types can be employed including thermal energy which is produced in plasma torches or in high-pressure discharges, and the energy brought by electromagnetic fields, e.g., microwave frequency discharge [39]. Electrically generated plasma is widely called “discharge plasma”, and Figure 1.5 shows the characteristics of the voltage and current of a discharge that is highly non-linear. It is confirmed that discharge characteristics, for example the breakdown voltage, is affected by the reactant gas, operation pressure and reactor configurations [40]. Generally, the plasma may be classified on the basis of the ion temperature, as high-temperature plasmas (HTP) and low-temperature plasmas

(LTP) which is summarised in Table 1-1 [41]. In high-temperature plasma, the temperature of ions and electrons are at the same level of about  $10^7$  K. Such plasmas happen at the centre of the sun or during the process of thermonuclear fusion. Low-temperature plasmas are subdivided into thermal and non-thermal plasmas. Meanwhile, non-thermal plasma is also named as cold plasma. In thermal plasma, electrons, ions, and background radicals are at the same temperature of  $10^4$  K. Plasma arc is a common form of thermal plasma, which is used for the applications of cutting, welding and other material techniques [42]. In non-thermal plasma or cold plasma, electrons are usually at a very high temperature of the order of  $10^5$  K, due to their light mass and selective acceleration, whereas the heavier ions remain relatively cold at room temperature through energy exchange by collisions with the background gas. Moreover, under atmospheric pressure non-thermal plasma is produced in the following discharges: pulsed corona, pulsed glow discharge, glow discharge, micro-hollow cathode discharge, dielectric barrier discharge, radio frequency discharge and microwave discharge. Compared to thermal plasmas, non-thermal plasmas exhibit higher selectivity, thus is most commonly used for technological applications and is of the research interest in this thesis.

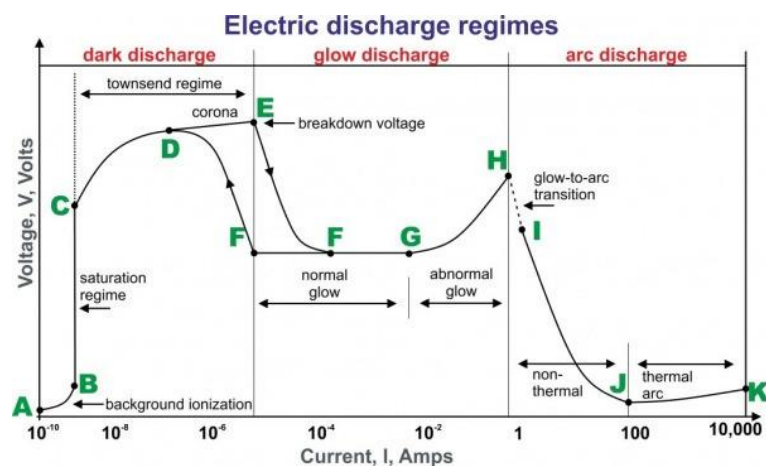


Figure 1.5 Voltage-current characteristic plot of electric discharge regimes [40].

Table 1-1 Classification of plasmas by temperature

Low-temperature plasma (LTP)		High-temperature plasma (HTP)
Thermal plasma $T_e \approx T_i \approx T \leq 2 \times 10^4 \text{ K}$	Non-thermal plasma $T_i \approx T \approx 300 \text{ K}$  $T_i \ll T_e \leq 10^5 \text{ K}$	$T_e \approx T_i \geq 10^7 \text{ K}$
e.g. Inductively coupled plasma torches	e.g. Low-pressure glow discharge, dielectric barrier discharge, corona, plasma jets	e.g. Fusion Plasmas

### 1.2.2 NON-THERMAL PLASMA AND ITS GENERATION METHODS

Non-thermal plasma exhibits higher selectivity and energy productivity compared with thermal plasma. This essential advantage is mainly due to the reality that most of the energy input is utilised to produce the energetic electrons, instead of radiating towards the bulk gas. The most common strategy of generating non-thermal plasma is by utilising an external electric field that leads to an electrical breakdown. Meanwhile, the electrical breakdown happens when the electric field surpasses the conduction band threshold, and thus the gas becomes conductive.

Previous studies have reported the use of a wide range of non-thermal plasma technology as a medium to synthesise ammonia. These non-thermal plasmas include corona discharge, glow discharge, high-frequency discharge such as radiofrequency and microwave discharge, gliding arc and dielectric barrier discharge. Recently, researches have shown an increased interest in applying the DBD reactor in ammonia synthesis. As an example, because of the discharge characteristics in the DBD plasma, the gap voltage, can be adjusted easily by changing the gas pressure or discharge gap width, making it simple to optimise the process [26], [43]. Moreover,

the mild operation condition of a DBD reactor, that requires no extra heating, is another reason that it is widely investigated. Furthermore, catalysts and packing materials can be easily packed into the DBD reactor. This makes DBD plasma favourable for plasma-catalytic reactions for the synthesis of ammonia.

#### *1.2.2.1 DIELECTRIC BARRIER DISCHARGE*

DBD describes a configuration where the electrodes are blocked by a dielectric barrier layer, as shown in Figure 1.6. Typical configurations of DBD reactors include planar and coaxial types, as described in [44]. For the coaxial cylindrical DBD reactors, plasma is generated in the gap between two electrodes through a dielectric layer. The material of the dielectric layer is, for instance, quartz, glass or alumina. The relative dielectric constant " $\epsilon$ " represents the ability of a dielectric material to store electric energy, like a capacitor. It directly affects the discharge characteristics and plays an essential role in DBD plasma. A DBD reactor can either be powered by AC or pulsed DC electricity. Electrical charges are deposited on the dielectric surfaces during the discharge operation. The deposited charges shield the external electric field, and thus, the discharge is self-extinguished [45]. When the electric field is strong enough, electron avalanche occurs and causes small discharge channels, called micro-discharge or filamentary discharge. The existence of a dielectric layer avoids the formation of sparks between electrodes, and therefore, the plasma discharge is restricted in the micro-discharge channel. Another critical factor of DBD plasma is the discharge gap. A small discharge gap restricts the electric field and current flow in the gap and therefore reduces the micro-discharge.

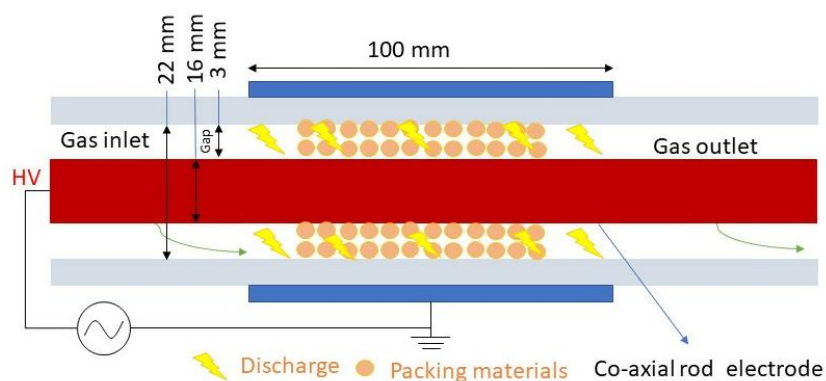


Figure 1.6 Schematic diagram of the DBD plasma reactor used in the work of this thesis

### 1.2.2.2 LOW-PRESSURE GLOW DISCHARGE (LPGD)

A glow discharge is a type of plasma formed by passing a direct current at 0.1 to several kV through gases. It is called the glow discharge owing to the fact of luminosity. A glow discharge operates typically under low pressure (lower than atmospheric pressure) because the breakdown voltage for the glow discharge depends non-linearly on the product gas pressure according to Paschen's Law, and a gas discharge requires a lower electric field to initiate the breakdown compared with the atmospheric pressure glow discharge (APGD). APGD remains at non-thermal state; however, due to the elevated pressure, the homogeneous glow is often unstable and easy to transit from glow to spark. Also, gas heating for APGD can achieve a few thousand Kelvin, while most LPGD is heating the gas at room temperature [42].

Glow discharge is the simplest configuration of the non-thermal plasma generating methods. Figure 1.7 shows an electric glow discharge tube; it consists of an anode and a cathode in a cell at low pressure (1-10 Torr). The tube is filled with reactant gases, and several hundred volts is applied between two electrodes. Initially, a small population of atoms is ionised by gamma rays. Next, the positively charged ions will travel towards the cathode while the electrons are driven towards the anode. This small population of initially charged particles

collides with atoms to ionise them and thus avalanche occurs. Eventually, under the same electric potential, a balance of ions and electrons will remain. Nevertheless, once atoms are excited, photons are released to carry the energy away and reduce the excess energy. The released photons can then be detected by optical atomic spectroscopy, and the properties of the atoms can be determined, according to the wavelength of the photons. Additionally, some collisions happen between the atoms of high enough energy which continuously causes ionisation. These ions can be detected by the atomic mass spectrometry and can reveal the type of atoms. Figure 1.7 also presents the main regions that may appear in a glow discharge. It shows the visible regions are anode glow, negative glow and positive column. In each normal glow discharge, the division of the regions is affected by the specific gas composition, pressure and cathode material [42]. For example, low pressure extends the discharge which means the entire discharge region is horizontally stretched, and the positive column may become an alternation of dark and bright regions [40]. In contrast, increased pressure will result in fewer regions. The positive column will be compressed, and the gap between negative glow and positive column will shrink to disappear. Eventually, with enough energy supply, spark or arc discharges will be generated if the gap between the anode and cathode reaches its lower limit provided there is no dielectric layer placed between them.

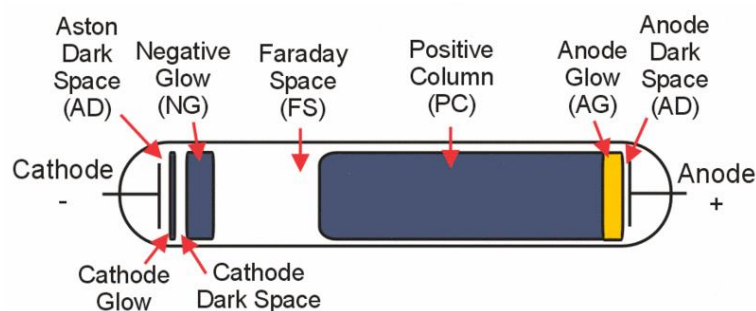


Figure 1.7 An electric glow discharge tube featuring its most essential characteristics [40].

### 1.2.2.3 RADIO FREQUENCY (RF) AND MICROWAVE DISCHARGES

An electromagnetic wave is also a general energy form that can ignite a breakdown and produce a plasma. This approach is called wave-heated plasma. RF and microwave discharges are two typical forms of wave-heated plasma that are sustained with an electromagnetic field without electrodes. In RF discharges, the flowing gas is either inductively or capacitively coupled with the power supply. Proper coupling is the key to preserve the energy efficiently transfer from the electromagnetic field to the flowing gas. The frequency to produce RF plasma is within the range 0.1-100 MHz, with the foremost accepted being 13.56 MHz [46].

Microwave plasma is usually generated by microwave coupled reactors as shown in Figure 1.8 [47]. In such a reactor, the microwaves are launched from a magnetron and fed into a tapered waveguide within a dielectric tube (quartz). This microwave power is guided to the middle of the process chamber that is transparent to the microwave radiation. An intense electric field then breaks the flowing gas down and causes ionisation by feeding massive energy to the electrons. Typically, the microwave plasma reactor operates at a frequency of 2.45 GHz and power of 2000 W, producing a temperature at the plasma region of 5500 °C, at atmospheric pressure [48]. The unique configuration of the electrode-less RF and microwave discharge means the extremely high temperature as the electrode cooling devices are not required. However, the high-frequency generator and power supplies are more complicated and expensive than that of DC plasma.

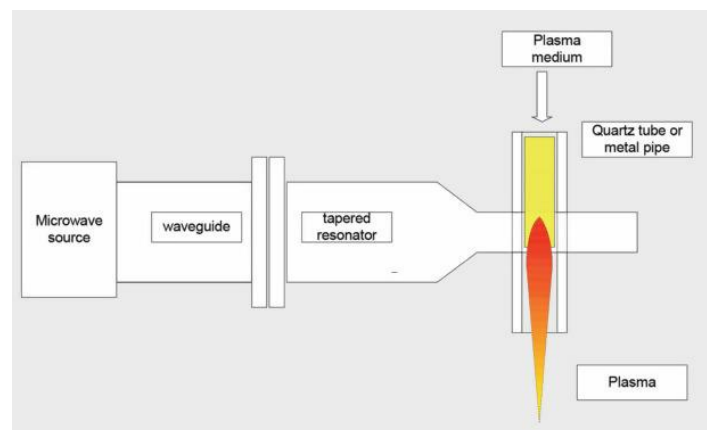


Figure 1.8 Schematic diagram of a microwave plasma reactor [47].

### 1.3 A REVIEW OF THE NTP ASSISTED AMMONIA SYNTHESIS TECHNOLOGIES

This section provides a review of the NTP assisted ammonia synthesis to give an insight into the progress of this technology. The first attempt at using NTP to synthesise ammonia was proved at the end of the 1980s when the concept of using NTP to effectively dissociate diatomic nitrogen and hydrogen under atmospheric pressure was demonstrated. Non-equilibrium plasmas which operate at low temperature and pressure are widely investigated as a promising alternative to produce ammonia from  $N_2$  and  $H_2$  mixture. Till now, NTP synthesis of ammonia has been reported based on the various plasma generation methods, including glow discharge plasma, high-frequency plasma and dielectric barrier discharge plasma, as summarised in Table 1-2. The proper development of the reactor would greatly improve the efficiency of the ammonia production system and increase the energy input ratio of the reactor. In addition, another critical factor to improve the process of NTP ammonia synthesis is the design of catalysts as summarised in Table 1-3. For this technology, numerous efforts have been made to promote the NTP ammonia synthesis reaction and improve its performance. In the following review, the design of an NTP reactor and corresponding catalysts will be discussed separately to demonstrate their capability of enhancing the synthetic process in terms of energy efficiency and ammonia conversion rate.

Table 1-2 Summary of literature reported on plasma ammonia synthesis.

Catalyst	Catalyst shape	Plasma type	Frequency	Plasma parameter	Total gas flow	Gas ratio (N <sub>2</sub> /H <sub>2</sub> )	Pressure	Temperature	Energy efficiency (g-NH <sub>3</sub> kWh <sup>-1</sup> )	NH <sub>3</sub> conversion	Ref.
MgO & CaO Al <sub>2</sub> O <sub>3</sub> ; WO <sub>3</sub> , and SiO <sub>2</sub> -Al <sub>2</sub> O <sub>3</sub>	Disks	Glow discharge	DC	DC, 6 mA	NA	1:3	5-10 Torr	No extra heating	NA	NA	[30]
MgO	Powder	DBD	5 kHz	Pulsed DC, 140 kV cm <sup>-1</sup> , 1 μs pulse width	200 ml min <sup>-1</sup>	0.9:1	1 atm	5 °C	NA	0.5%	[49]
MgO and glass spheres	Pellets	DBD	1 kHz	AC, 11-13 kV	70 ml min <sup>-1</sup>	1:1	1 atm	30 – 50 °C	NA	4.2%	[50]
Lead zirconate titanate, BaTiO <sub>3</sub>	Pellets	DBD	0.5-5 kHz	AC, 0-7.5 kV	11.5 ml min <sup>-1</sup>	1:3	1 atm	49 °C	0.9	2.7%	[25]
Lead zirconate titanate	Pellets	DBD	0.5-5 kHz	AC, 2.5-5.5 kV	5.7 – 76.7 ml min <sup>-1</sup>	1:3	1 atm	59 °C	0.7	7%	[26]
NA	NA	DBD	10 kHz	Pulsed DC, 80 μs pulse width, 1.8-2.15 kV	0.73 L min <sup>-1</sup>	1:4	1 atm	78 – 155 °C	1.83	1.25%	[28]
NA	NA	Microwave	2.45 GHz	1.3 kW	15 L min <sup>-1</sup>	1:4	1 atm	516-966 °C	0.78	2.5E-2%	[34]
NA	NA	DBD plasma jet	16 kHz	Pulsed DC, 300 W	30 L min <sup>-1</sup>		1 atm	No extra heating	1.16	1.7E-6% at 45 min	[51]
Cu	Wire-electrode	DBD	50 kHz	AC, 5 kV	100 ml min <sup>-1</sup>	1:3	1 atm	No extra heating	3.3	3.5%	[23]
Au, Pt, Pd, Ag, Cu	Wire-electrode	DBD	50 kHz	AC, 5 kV	100 ml min <sup>-1</sup>	1:3	1 atm	No extra heating	NA	NA	[24]
Ru/Al <sub>2</sub> O <sub>3</sub>	Powder	DBD	21.5 kHz	AC, 2.5-4.5 kV	30 ml min <sup>-1</sup>	1:3	1 atm	No extra heating	0.34	2.3%	[21]
Ru/MgO	Powder	DBD	8-16 kHz	AC, 5-10 kV	4 L min <sup>-1</sup>	3:1	1 atm	No extra heating	2.3	3.7%	[29]
Nanodiamonds and diamond-like carbon-coated Al <sub>2</sub> O <sub>3</sub>	Sphere powder	DBD	500 Hz and 1 kHz	AC, 12-17.5 kV	60 ml min <sup>-1</sup>	1:3	1 atm	113 °C	0.16	2.3%	[52]
Ru/Si-MCM-41	Powder	DBD	20-26 kHz	AC, 5-10 kV	4 L min <sup>-1</sup>	1:1	1 atm	No extra heating	1.7	NA	[53]
Cu	Wire-electrode		9kHz	20 W	250 ml min <sup>-1</sup>	1:1	1 atm	No extra heating	1.04	0.38%	Chapter 3
Cu/Al <sub>2</sub> O <sub>3</sub>	Sieved Pellet	DBD	9 kHz	AC, 12 kV	50 ml min <sup>-1</sup>	1:3	1 atm	No extra heating	0.52	0.67%	Chapter 4

### 1.3.1 THE DEVELOPMENT OF THE REACTOR FOR NTP ASSISTED AMMONIA SYNTHESIS

Previous studies have investigated a wide range of NTP reactors. Sugiyama, et al, [30] studied ammonia synthesis from  $H_2$ ,  $N_2$  mixed gas at room temperature using glow-discharge plasma. Figure 1.9 shows the structure of the utilised glow discharge reactor. A pair of tungsten electrodes were equipped at the up position of the vessel while glass wool is filled at the bottom with catalyst mounted on top. Also, the distance between the catalyst and the cathode was approximately 3 mm. The experimental procedure includes  $N_2/H_2$  of 3:1, at the pressure of 10 Torr, a high DC electric voltage, a constantly kept discharge current at 6 mA, all under room temperature.

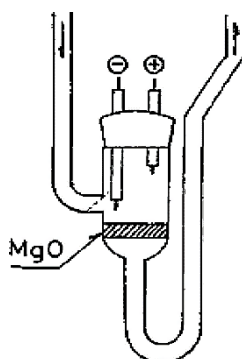


Figure 1.9 Glow discharge reactor for ammonia synthesis [30].

Yin and Venugopalan [31] investigated the effect of several electrode materials on the low-temperature plasma synthesis of ammonia in a glow discharge reactor which is similar with the one used by Sugiyama, et al, shown in Figure 1.9. Parameters included a discharge power of 200 W, current of 15 mA, 60 Hz frequency, and inter-electrode separations of 9.5 and 20.0 cm were applied as experimental conditions. Results showed that the yield of  $NH_3$  is significantly affected by the material of the electrode, for example, the yield of  $NH_3$  was more than doubled by using

platinum as the electrode as against using aluminium. However, the inter-electrode separation shows little impact on the  $\text{NH}_3$  formation. The  $\text{NH}_3$  yield, as well as  $\text{N}_2$  conversion, are in the order  $\text{Pt} > \text{SS} > \text{Ag} > \text{Fe} > \text{Cu} > \text{Al} > \text{Zn}$  for the different electrode materials.

Uyama, et al, [32] studied the effects of using various experimental conditions in the process of ammonia synthesis using microwave discharge plasma, with the pressure of 26-260 Pa, power input of 30-280 W, with a gas mixing ratio being varied from 0 (pure nitrogen) to 1 (pure hydrogen). They concluded that the ammonia product yield increases accompanied by the increasing of NH radicals, hydrogen atoms and hydrogen molecules. When the experiment was under lower pressures or higher input power, the authors discovered that a significant amount of NH radicals and hydrogen atoms were produced in the plasma so that the number of hydrogen molecules decreased. Therefore, they proposed that ammonia molecules were formed by the reaction of NH radicals, not only with hydrogen atoms but also with hydrogen molecules, and the decomposition of ammonia with hydrogen atoms would occur simultaneously.

Uyama, et al, [33] also compared the synthesis of ammonia using radio-frequency 13.56 MHz and microwave-frequency 2450 MHz at 1.2 kW discharges using the same reactor as shown in Figure 1.10. The results show that a double amount of ammonia was adsorbed on zeolite as an adsorbent by using microwave discharge rather than using RF discharge. The authors explained the reason why such an ammonia yield difference occurs as “the electron energy is considerably larger than the ionisation potential and the dissociation energy of the  $\text{N}_2$  molecule which are 15.6 and 9.8 eV respectively in the plasma prepared using microwave discharge. However, it is not able to be achieved by using RF discharge.”

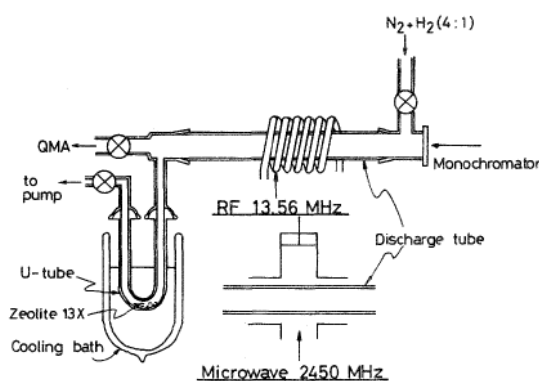


Figure 1.10 Reactor Layout of high-frequency plasma reactors [33].

In a major advance in 2008, Nakajima, et al, [34] investigated the synthesis of ammonia from  $N_2$  and  $H_2$  using microwave plasma at atmospheric pressure. The experimental apparatus is shown in Figure 1.11 with the experimental conditions of a maximum microwave generator power of 1.3 kW at a frequency of 2.45 GHz. They concluded that the proportion of the gas mixture at different steps of the reaction has a significant impact on the experimental results. Such as the amount of hydrogen plasma, hydrogen in the after-flow region and the dilution of argon gas at all time. More specifically, it was found that the increase of hydrogen flow rate reduces the ammonia production, while adding hydrogen gas injected into the after-flow region gives a higher concentration of ammonia by a factor of about 20. This fact strongly supports the notion that “input power is consumed for activating hydrogen rather than nitrogen as  $H_2$  flow rate increases.” It also shows the importance of quenching when the plasma reaction is conducted at atmospheric pressure. Furthermore, Nakajima, et al, tested the effect of dilution gas using argon. They reported that the argon flow rates up to  $10 \text{ L min}^{-1}$  results in a 25-30% higher ammonia production rate. However, the ammonia production rate starts to decrease when the flow of argon is beyond  $10 \text{ L min}^{-1}$ . They concluded that “by adding argon to plasma gas, the reaction may contribute to the formation of active nitrogen species, and consequently the production rate of ammonia is considered to increase with argon flow rate.” This is due to argon atoms

having almost same ionisation energy as nitrogen molecules ( $N_2$ : 15.58 eV; Ar: 15.76 eV), therefore, the charge transfer reaction is believed to occur in the plasma involving  $N_2$  and Ar [34]. Finally, Nakajima, et al, pointed out that from the experimental results the active nitrogen species are considered to play a vital role in the ammonia synthesis.

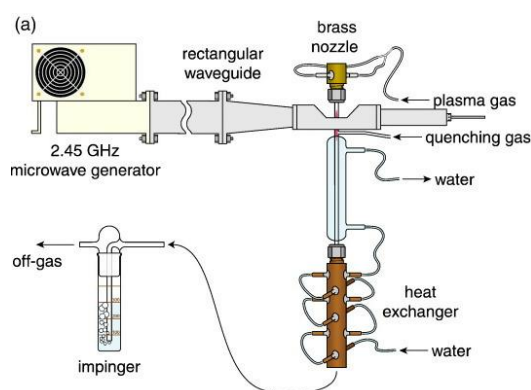


Figure 1.11 Schematic illustration of experimental apparatus [34].

NTP ammonia synthesis using DBD has been widely investigated since 2015. Because it provides an easy way of analysing plasma ammonia synthesis under atmospheric pressure and allows the testing of various catalyst materials as well as different experimental conditions and apparatus, such as the discharge power per area, applied discharge voltage, applied frequency, gas temperature, gas volume ratio and the total feed flow rate of the gas. Each condition listed above has a crucial impact on the produced ammonia concentration as well as energy efficiency. Bai and co-workers [28], used the non-equilibrium plasma produced by a micro-gap DBD under atmospheric pressure to synthesise ammonia. The structure of the dielectric barrier discharge apparatus can be found in Figure 1.12. Thin films of  $\alpha\text{-Al}_2\text{O}_3$  were sprayed both on the surface of discharge and earthing electrodes as dielectric layers; with the thickness of 0.25 mm and a discharge gap of 0.47 mm. Also, other properties were applied to the dielectric barrier discharge such as the frequency of 10 kHz, and a pulse period of 80  $\mu\text{s}$ . With this approach, they reached

an energy efficiency of  $1.83 \text{ g-NH}_3 \text{ kWh}^{-1}$  with a gas residence time of 0.62 s. According to the results, it is concluded that the concentration of ammonia improves with the increase of discharge power per area, applied voltage, gas temperature and the molar ratio of  $\text{H}_2/\text{N}_2$ .

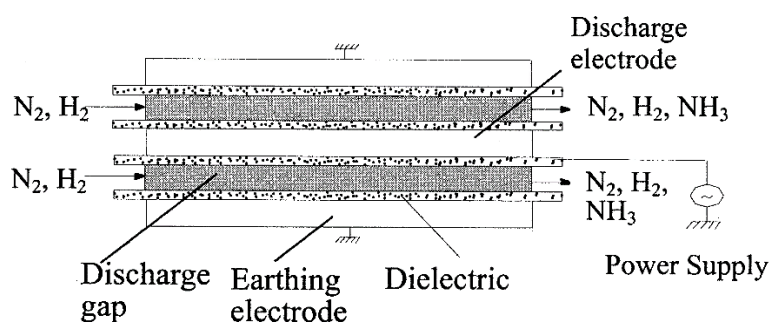


Figure 1.12 Structure of the micro-gap dielectric barrier discharge reactor [28].

Mizushima, et al, [21] reported results using a DBD reactor packed with a tubular membrane-like-catalyst, as shown in Figure 1.13. The apparatus consists of a stainless-steel tube of 4 mm diameter as the inner electrode, the membrane-like-catalyst alumina and ruthenium fixed on the electrode with ceramic adhesive, an 8 mm diameter and 1 mm thickness quartz tube vessel with tube-fittings and a piece of 90 mm length aluminium foil tightly surrounded as the outer electrode. A mixture of  $\text{N}_2$  and  $\text{H}_2$  was introduced into the plasma reactor which operated at ambient conditions and an applied voltage of 2.5–4.5 kV and a frequency of 21.5 kHz. It was found that the increasing flow rate leads to an increase in the energy efficiency, reaching up to  $0.9 \text{ g-NH}_3 \text{ kWh}^{-1}$ , possibly because of reduced decomposition of ammonia due to short residence time in the plasma region. Interestingly, even when ammonia yield and energy efficiency trends were similar, the optimal  $\text{N}_2/\text{H}_2$  values were found to be 1:3 and 1:5 with a catalyst and without a catalyst, respectively. The  $\text{NH}$  radical was found to be the precursor for the  $\text{NH}_3$  formation. It was concluded, based on unchanged current and energy consumption in the reactor with a

membrane, that ruthenium and alumina act not as plasma condition modifier but as a catalyst to promote ammonia formation.

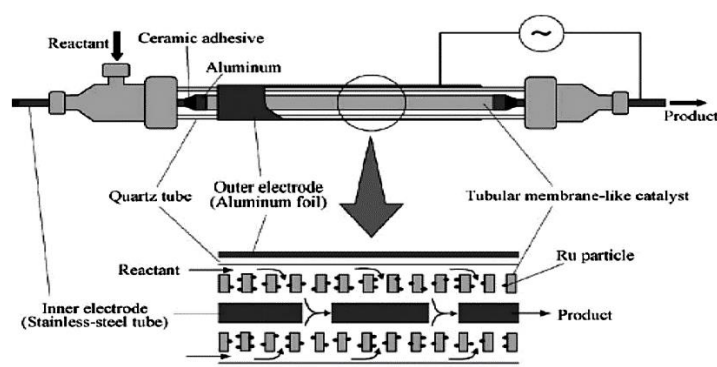


Figure 1.13 Dielectric barrier discharge reactor with a tubular membrane-like-catalyst [21].

Kubota, et al, [51] investigated the direct interactions between nitrogen plasma and corresponding liquid solutions which were either pure water or the mixture of water and ethanol, by applying an atmospheric plasma jet. The schematic diagram of the DBD plasma jet reactor is shown in Figure 1.14. They operated the reaction at the frequency of 16 kHz, nitrogen flow rate of 30 L min<sup>-1</sup> and input power of 300 W. The liquid solutions were not only used to provide the hydrogen source but also immediately absorb the produced ammonia. By using the nitrogen plasma jet injected to the mixture of pure water and ethanol, they achieved an energy efficiency of 1.16 g-NH<sub>3</sub> kWh<sup>-1</sup> which is relatively comparable to the results given by other types of DBD reactors.

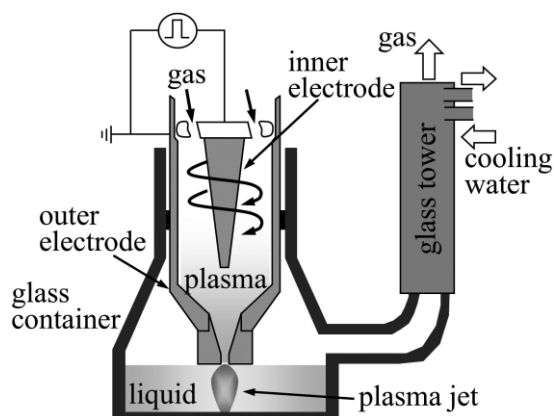


Figure 1.14 Schematic diagram of the plasma jet used by Kubota, et al, [51].

Gomez-Ramirez, et al, [25] designed a ferroelectric packed-bed DBD reactor, as shown in Figure 1.15, that uses the stainless-steel as an active electrode while the bottom wall of the reactor acts as an earthing electrode. Also, the inter-electrode gap is filled with ferroelectric material as a dielectric barrier so that the discharge gap can vary regarding different amounts of the ferroelectric material. As a result, the ferroelectric material, ceramic Lead zirconate titanate (PZT), gives both greater energy efficiency and higher ammonia yield than  $\text{BaTiO}_3$  with the consequence of  $0.9 \text{ g-NH}_3 \text{ kWh}^{-1}$  and 2.7% single-pass  $\text{N}_2$  conversion respectively. Therefore, PZT was claimed to be a substantially more effective moderator and catalyst than  $\text{BaTiO}_3$ . Also, other experimental parameters such as the  $\text{N}_2/\text{H}_2$  gas mixture ratio, applied voltage, discharge frequency, discharge gap and gas residence gap, also affect the case.  $\text{N}_2/\text{H}_2$  mixture ratio was found to provide the maximum energy efficiency in the range of 1:3 to 1:1, with higher  $\text{N}_2/\text{H}_2$  ratios resulting in a sharp decrease in ammonia production yield. Moreover, with both ferroelectric materials, the energy efficiency exhibited a maximum at 5.5 kV. At constant current, the energy efficiency decreased as frequency increased over the range of 0.5-4 kHz. The discharge gap as well also plays a vital role in the reaction, with the system attaining its maximum production value with the 10 mm discharge gap at 6 kV. Furthermore, residence time was shown

to be a significant operational parameter. Halving the residence time showed it can improve the efficiency impressively and it is likely due to its effect on restraining the decomposition of initially formed  $\text{NH}_3$ . Further enhancement of this ferroelectric packed bed reactor technique has been carried out by Gomez-Ramirez, et al, [26] through adjusting working parameters such as the inter-electrode spacing, the size of the ferroelectric pellets and the applied frequency as well as voltage. Under an optimised condition, the nitrogen conversions of more than 7% were achieved which is close to the performance of the Haber-Bosch method at 10-15%.

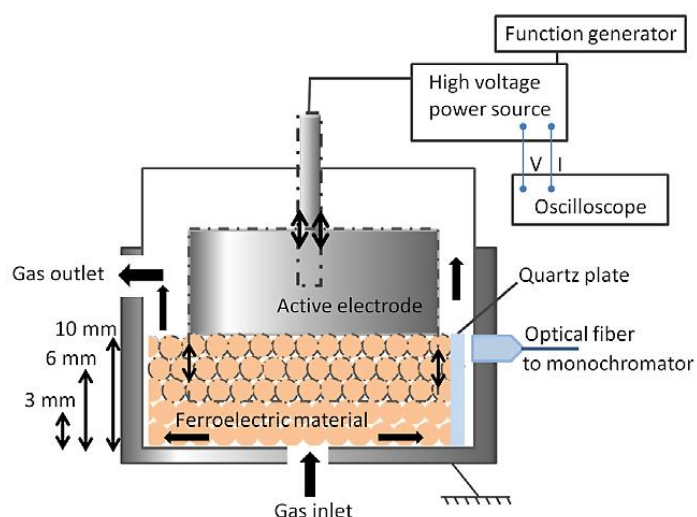


Figure 1.15 Schematic of ferroelectric packed-bed DBD reactor [25].

Peng, et al, [29] described an absorbing and recycling DBD system that could extract the produced ammonia and recycle the unreacted  $\text{N}_2$  and  $\text{H}_2$ , as shown in Figure 1.16. Through this research, ruthenium catalyst with carbon nanotube support and caesium promoter provided the highest ammonia yield under the NTP conditions with the efficiency of  $2.3 \text{ g-NH}_3 \text{ kWh}^{-1}$ . Frequency and applied voltage of 10 kHz and 6 kV were proven to offer the highest energy efficiency. Results also showed that  $\text{N}_2/\text{H}_2$  ratio of 3:1 produced the highest amount of ammonia, which further confirms that ammonia synthesis has higher efficiency under a nitrogen-rich

environment due to the relative difficulty in the disassociation of nitrogen. It should be noted that the gas ratio presented in this study does not agree with other reported works in this review, while most of the literature suggests a hydrogen-abundant environment is better for plasma ammonia synthesis.

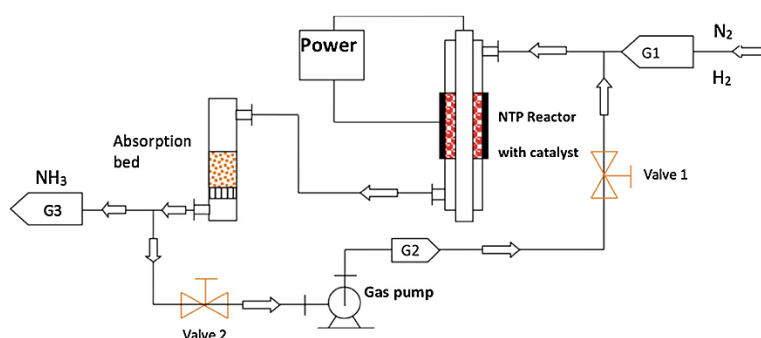


Figure 1.16 NTP ammonia synthesis and adsorption system [29].

The idea of separating the produced ammonia was later implemented in a more recent study by the same author [54]. Peng, et al, designed an in-situ catalytic absorption system using magnesium chloride as the absorber, as shown in Figure 1.17. Unlike the previous work, the absorber used in this study was also applied as a catalyst. Besides the synergistic effect between absorber and catalyst, the team also involved a pulse density modulation (PDM) to generate a homogeneous high frequency and high voltage electric field. They claimed that by using this entire system, the energy efficiency achieved in this study was 20.5 g-NH<sub>3</sub> kWh<sup>-1</sup> which is so far the highest reported in NTP assisted ammonia synthesis.

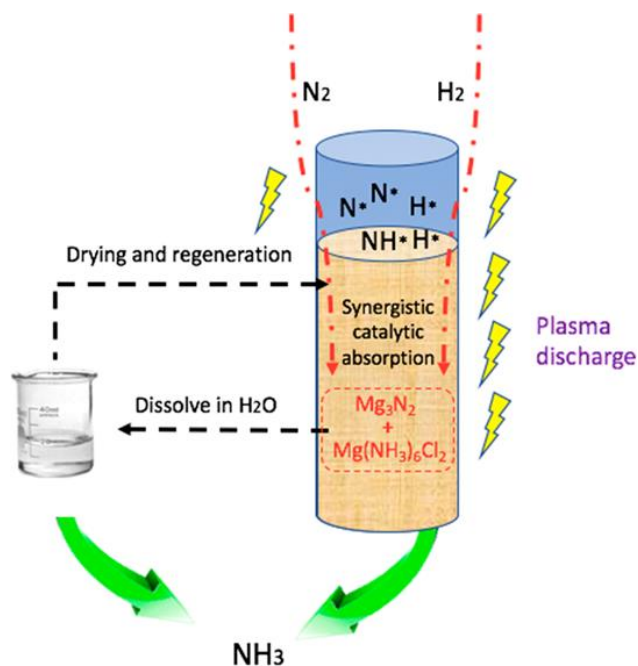


Figure 1.17 Synergistic catalytic absorption system designed by Peng, et al, [54].

In the most recent study, Wang, et al, [55] introduced a specially designed coaxial DBD plasma reactor using water as a ground electrode, which could take away the plasma generated heat and maintain the reaction at near-room temperature. Unlike common coaxial reactors with opaque ground electrodes, the transparency of the water electrode enabled Operando optical diagnostics using intensified charge-coupled device imaging and optical emission. Since the full plasma discharge area is exposed and can be visually accessed, the above operation can be conducted without altering the structure of the reactor.

Table 1-3 The development of NTP catalysis.

Catalyst type	Name of catalyst	Shape	References
No catalyst	-	-	[27]
No catalyst	-	-	[51]
Mono metallic	MgO and Al <sub>2</sub> O <sub>3</sub>	Powder smeared on the electrode surfaces	[28], [49]
Mono metallic	MgO	Glass spheres and MgO pellets	[50]
Mono metallic	BaTiO <sub>3</sub> and PZT	Pellets	[25], [26]
Mono metallic	Au, Pt, Pd, Ag, Fe, Cu	Metal wires	[23], [24]
Catalyst-support	Ru/Al <sub>2</sub> O <sub>3</sub>	membrane-like alumina tube	[21]
Catalyst-support	Functionalised-nano-diamond and diamond-like-carbon coatings on Al <sub>2</sub> O <sub>3</sub> spheres	Spheres	[52]
Catalyst-support	Ni on microporous silica adhere to glass and BaTiO <sub>3</sub>	Spheres	[56]
Catalyst-support	Ru/Al <sub>2</sub> O <sub>3</sub>	Seized pieces	[57]
Catalyst-support	Ni/Al <sub>2</sub> O <sub>3</sub>	Seized pieces	[55]
Catalyst-support-promoter	Ru/carbon nanotube support promoted by Cs	Seized pieces	[29]
Catalyst-support-promoter	Ru/Si-MCM-41 support promoted by Cs and Ba	Seized pieces	[53]
Catalyst-support-promoter	Ru/Al <sub>2</sub> O <sub>3</sub> promoted by Mg, K, Cs	Seized pieces	[22]

### 1.3.2 THE DEVELOPMENT OF CATALYSTS FOR DBD AMMONIA SYNTHESIS

A catalyst has been widely adopted in NTP ammonia synthesis to improve the synthetic process by yielding more ammonia and achieve better energy efficiency. As mentioned in 1.2.2.1, DBD allows the testing of various catalyst materials due to the simple reactor structure and regular discharge area. In this section, only catalysts being used in DBD ammonia synthesis will be discussed as they are compatible with the economic requirements for the future scalability. The following content will go through these three factors to describe the development of DBD catalytic for the synthesis of ammonia:

1. The presence of a catalyst in plasma chemical reaction;
2. Type of metallic catalyst system;
3. The shape and structure of the catalyst.

Firstly, although the presence of a catalyst in DBD ammonia synthesis is widely adopted, there are still a few studies that have not used catalysts, including the work by Bai, et al, [27]. They improved the yield of ammonia by adjusting the parameters such as the volume ration of  $\text{CH}_4/\text{N}_2$ , gas flow rate and gas temperature. The results showed that the highest ammonia yield was 8000 ppm, which is a promising result without involving a catalyst. Moreover, Kubota, et al, [51] conducted the synthesis of ammonia using a DBD plasma jet to enable direct chemical reactions between a nitrogen plasma jet and the liquid solution containing water and ethanol. Due to the special structure of the DBD plasma jet reactor and the fact that chemical reactions are happening on the liquid surface, the author did not introduce a catalyst at all. However, by injecting nitrogen plasma jet directly to the mixture of pure water and ethanol, Kubota, et al, achieved an impressive energy efficiency of  $1.16 \text{ g-NH}_3 \text{ kWh}^{-1}$ . At the same time, they made an

excellent point that collecting ammonia gas right after the reaction to prevent re-decomposition might improve the overall production of ammonia. This idea of separating and collecting the produced ammonia was further implemented by Peng, et al, [53], [54].

Secondly, regardless of the fact that all catalysts in use are metal catalysts, the following catalyst systems have been assessed: Mono-catalyst system where only one metal was used, has been investigated by Bai, et al, [28], [49], Hong, et al, [50], Gomez-Ramirez, et al, [25], [26] and Aihara, et al, [23], [24]. In 2000 and 2003 respectively, Bai, et al, reported their use of MgO and Al<sub>2</sub>O<sub>3</sub> powder smeared on the electrode surfaces of a micro-gap reactor. The first approach achieved an NH<sub>3</sub> yield of 5000 ppm and the second approach further improved this figure to 12500 ppm by flowing the mixture gas at a rate of 730 ml min<sup>-1</sup>. However, in these studies, the characterisations of the catalyst property were not discussed. Instead, they concluded that the MgO and  $\alpha$ -Al<sub>2</sub>O<sub>3</sub> effectively restrained the enlarging of discharge current and spark and this allows the increase of the electric field, and thus obtains high electron energy. Hong, et al, [50] synthesised ammonia in a DBD reactor packed with glass spheres and MgO pellet. Meanwhile, they focused on the effect of additional argon which claimed to increase the discharge power and uniformity. Moreover, Gomez-Ramirez, et al, [25], [26] used ferroelectric material BaTiO<sub>3</sub> and PZT in a planar DBD reactor to synthesise ammonia. As a result, compared to BaTiO<sub>3</sub>, PZT gave both greater energy efficiency and ammonia yield. This was explained as that the surface of PZT contributes more to prevent the ammonia decomposition than BaTiO<sub>3</sub>. They further proposed that the ammonia synthesis is linked to an increase in the electric field between the ferroelectric pellet and the materials are only partially catalytic. Aihara, et al, [23] used a metallic wire electrode to synthesise ammonia in a DBD reactor, achieving an NH<sub>3</sub> yield of 3.5% at an N<sub>2</sub>/H<sub>2</sub> molar ratio of 1:3 and the energy efficiency of 3.3 g-NH<sub>3</sub> kWh<sup>-1</sup>. They have proved that a

wire electrode can perform well as a catalyst. It is worth pointing out that the wool-like copper wires were also used as the high-voltage inner electrode. The team further reported the catalytic activity of Au, Pt, Pd, Ag, Cu etc. and found Au has the highest activity among others [24].

Numerous studies have indicated that the catalyst-and-support system is so far the most adopted plasma-catalytic system for NTP ammonia synthesis [21], [52], [55]–[57]. Mizushima, et al, [21] designed a membrane-like alumina tube. The ruthenium particles were deposited on the pore walls of the alumina by immersing the tube in a saturated solution of Triruthenium dodecacarbonyl  $\text{Ru}_3(\text{CO})_{12}$ . Hong, et al, [52] used  $\text{Al}_2\text{O}_3$  spheres as catalyst support for functionalised-nano-diamond and diamond-like-carbon coatings. Oxygenated nano-diamond has been shown to increase the production yield of ammonia, while hydrogenated nano-diamond has decreased its yield. However, neither type of nano-diamond significantly affected electrical discharge properties. Similarly, Akay, et al, [56] presented a novel catalyst in the form of 2 nm thick plates of nickel catalyst sandwiched between the silica support and adhere to high permittivity materials (glass and  $\text{BaTiO}_3$  spheres). They achieved an ammonia concentration of 9% at a power of 195 W. Furthermore, unlike Hong's and Akay's work, Xie, et al, [57] and Wang, et al, [55] have demonstrated the use of a transition metal catalyst loaded on  $\text{Al}_2\text{O}_3$  powders is superior to the impregnation method.

Another type of plasma-catalytic system is the catalyst-support-promoter system, in which alkaline metals such as Mg, Cs, Ba and K are added as a promoter. Research has shown that these promoters are able to increase the activity of catalysts by efficiently reducing the  $\text{N}_2$  dissociation energy barrier and promoting the destabilisation of the  $\text{NH}_x$  species [58], [59]. Peng, et al, in 2016 and 2017 [29], [53], respectively, tested two different catalysts for NTP ammonia synthesis. The first was a Ru-based catalyst with a carbon nanotube support, along with a Cs promoter and

microporous absorbents, including Molecular Sieve 13X and Amberlyst 15. With this catalyst, they achieved an optimised energy efficiency of  $2.3 \text{ g-NH}_3 \text{ kWh}^{-1}$  [29]. In 2017, and this team conducted the second catalyst, which was the Ru-based catalyst and promoters (Cs and Ba) deposited onto Si-MCM-41 support. They concluded that the Si-MCM-41 has a high surface area, low conductivity, organised and interconnected pores. These features improved the ammonia synthesis performance compared to metal oxide supports [53]. Kim, et al, [22] conducted the DBD ammonia synthesis over ruthenium catalysts promoted by Mg, K and Cs. They found that the effect of metal promoters was in the order of  $\text{Mg} > \text{K} > \text{Cs} > \text{no promoter}$ .

Finally, the third factor is the shape and structure of catalysts. It could affect the flow channels, gas residence time, surface area, and the number of active sites, etc., all of which were critical parameters for ammonia plasma synthesis. From Table 1-3, it is concluded that the shape of the catalyst used in DBD ammonia synthesis were powder that seized into pieces [21], [28], [29], [49], [53], [55], [57], spheres [52], [56], pellet-shaped [25], [26], [50] and metal wires [23], [24]. In view of all that has been mentioned so far, in the latter study performed by [23], the researchers reported that the wool-like copper catalyst can increase the electrode's surface area and allow for more productive ammonia synthesis over the electrode discharge. This conclusion also enlightened the breakthrough point of the work conducted in this thesis of using a wire electrode.

## 1.4 AIMS AND OBJECTIVES

As mentioned in former sections,  $\text{NH}_3$  not only has a decisive impact on agricultural development but also has the potential to be used for clean energy in the future. However, the ammonia synthesis method currently used in industry, named the Haber Bosch process has strict requirements on the reaction conditions and consumes a massive amount of fossil energy. Alternative methods including biological and electrochemical, are usually limited by energy efficiency and the environmental conditions and thus are not widely used. From the beginning of this century, non-thermal plasma technology has been widely investigated in the field of energy production due to its advantages, such as mild operation conditions, high activity of reactive species and the flexibility for small scale on-site usage.

The recent focus of NTP technology towards artificial ammonia synthesis has highlighted in optimising energy efficiency while applying clean energy during the synthetic process. The feasibility of the non-thermal plasma technology in an industrial scale application has been demonstrated by Minnesota university. As discussed in the literature review, both the plasma-only and the plasma-catalysis processes have been used in the field of ammonia synthesis. Despite only one group that abandoned a catalyst when using a DBD reactor, most of the other studies have involved catalysts. Among those researches of plasma-catalysis ammonia synthesis, two main approaches have drawn attention, which is a metallic wire electrode acting as a catalyst and a catalyst-support system. After a comprehensive study and appreciation of the related literature, the following problems are observed.

First, for the metallic wire electrode system, compared with plasma-catalytic ammonia synthesis, prevents plasma extinction without the addition of packing materials (or catalysts), and negates the risk of pressure-loss of the feed flow and has no problem of catalyst

deactivation. Also, compared with traditional catalysts, the metallic wire has significant advantages in manufacturing difficulty and pricing. Therefore, if it is determined that wire electrode can offer help with ammonia synthesis under plasma conditions in a reliable way, it will provide the basis for further research suggesting that it is still a potential option for scale-up applications. However, a more systematic understanding and more fundamental studies are still needed, not only for improving the conversion and energy efficiency under ambient conditions but also for providing information about the mechanism of plasma-synthesis of ammonia and supporting future progress. Moreover, the individual effects of the metallic electrode, the inner surface of the reactor and their catalytic characteristic are not apparent [30], [31], [60]–[63]. It is worth pointing out that the catalyst-support system has been investigated on the characteristics of the plasma. Mizushima, et al, [21] concluded based on the fact that the current and energy consumption in the reactor with catalysts remained unchanged, the catalyst was not acting as plasma condition modifier and hence not affecting the plasma characteristic. Similarly, Herrera, et al, [64] denied that the catalyst has modified the plasma characteristics. Therefore, if the metallic wires in the DBD reactor could modify the characteristics of the plasma becomes an outstanding question. Furthermore, it was Shah, et al, that spread the molten catalyst on the outside of glass tubes and placed the tubes in the RF plasma reaction chamber. An increase of 20% ammonia yield was achieved by using Ga-In alloy catalyst compared to using monometallic catalyst. Nevertheless, it has not been reported whether the same effect can be obtained by using alloys in DBD reactors as electrodes.

Second, rod electrode reactors are the most commonly used reactor. Combining NTP with heterogeneous catalysis (plasma-catalysis) demonstrably improves the performance of many plasma-activated reactions, for example with ruthenium-based catalysts. However, the

underlying mechanisms of the plasma-catalyst interactions are complex and not fully understood, especially limited on the understanding of metal-oxide catalysts. This work used the characterisation of metal-oxide catalysts to investigate the surface change and absorption of species during the reaction to give appreciation to the plasma-catalytic synergy.

Based on the above-mentioned problems, this thesis aims to improve the energy efficiency and production yield of ammonia synthesis under non-thermal plasma conditions. The experiment parts will focus on the influence of different reaction conditions on plasma ammonia synthesis, including gas ratio, gas flow rate and discharge characteristics etc. At the same time, this thesis will also discuss the contribution of catalyst characteristics, wherein the catalytic capacity of metal wires and metal oxides will be discussed, respectively. The study in this paper will provide a reference for the synthesis of ammonia using non-plasma technology on a small scale. With the development of this technology, it is believed that in the future, production of synthetic ammonia will no longer require the use of fossil energy and hence significantly reduce greenhouse gas emissions and contribute to the future hydrogen economy.

## 2 EXPERIMENTAL

### 2.1 EXPERIMENTAL SYSTEM

Figure 2.1 shows a schematic diagram of the experimental setup for plasma-synthesis of ammonia under ambient conditions. It comprises of four parts: a gas-supplying unit, a high voltage power supply, a DBD plasma reactor and a data collection unit for both the electrical signals and FT-IR spectra.

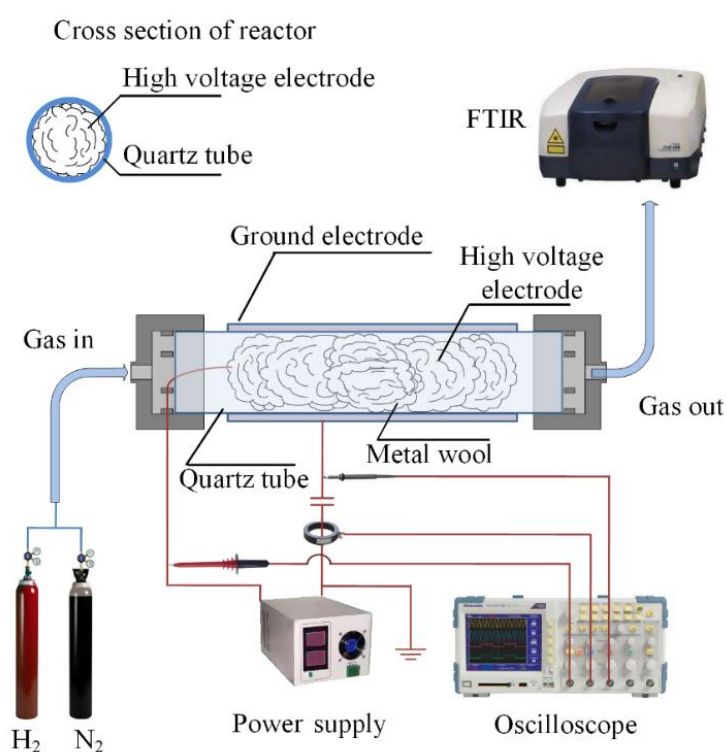


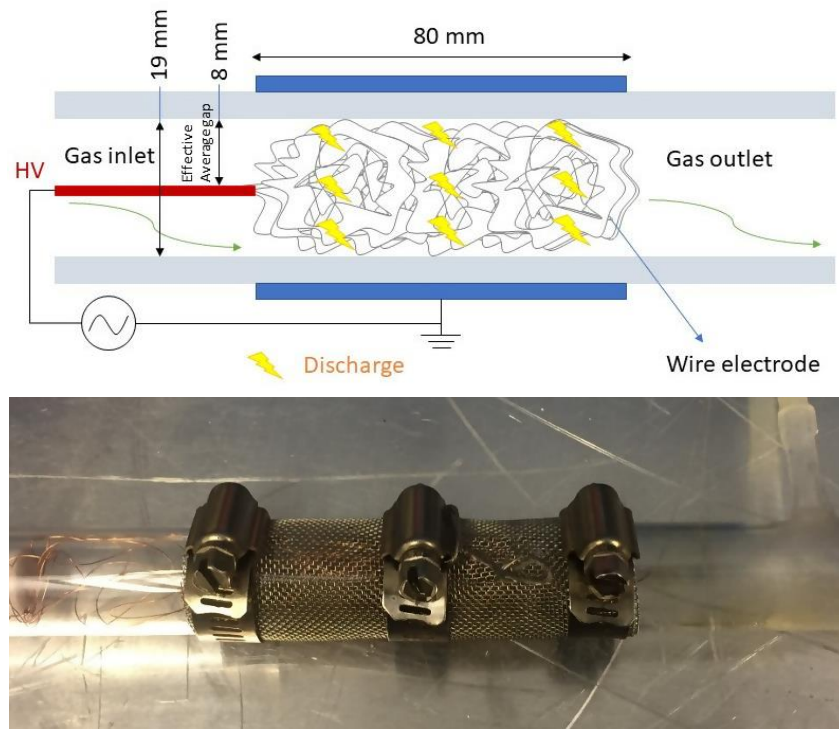
Figure 2.1 Formulating the experimental setup for non-thermal plasma ammonia synthesis.

The reactant gases  $N_2$  and  $H_2$  are provided by the gas cylinders and imported into the plasma reactor. Also, the pressure of the gas flow coming out of the cylinder is regulated at 1 bar, and the gas flow rate is controlled by the mass flow controllers (OMEGA). In the research of this thesis, two self-made plasma reactors of different specifications are used for the work in Chapters 3 and 4, as shown in Figure 2.2 accordingly. Both reactors are powered by a high

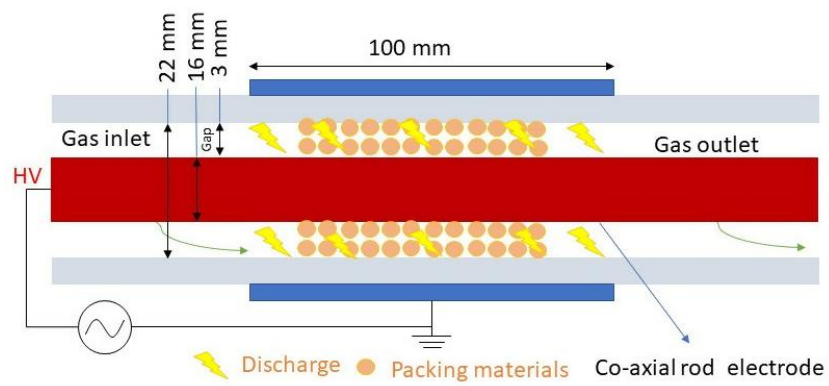
voltage AC power supply (CTP-2000K) with a maximum peak voltage of 30 kV and a frequency of 5-20 kHz.

The DBD reactor used in Chapter 3 is a wire electrode DBD reactor as shown in Figure 2.2 (a), with a quartz tube with an outer diameter of 22 mm and a wall thickness of 1.5 mm being used as a dielectric layer. A stainless-steel mesh wrapped around the quartz tube served as a ground electrode, while a metal rod or a loose metal-wool was placed in the middle of the quartz tube and acts as a high voltage electrode. All of the wire electrodes were prepared by unwinding the same size rod and then removed to ensure packing consistency. The metal wool was chosen from commonly-seen materials such as NiFe alloy, stainless steel, Ti, Ni and Cu. The metal wool consisted of fibre with the same diameter (0.2 mm) and total length (10 m), hence providing the same surface area ( $63 \text{ cm}^2$ ). A hollow stainless-steel electrode was also used for comparison. The discharge length was 80 mm with an average effective discharge gap of 8 mm.

For the reactor used in Chapter 4, a rod-electrode DBD reactor was used as shown in Figure 2.2 (b). A quartz tube with an outer diameter of 25 mm and a wall thickness of 1.5 mm was used as a dielectric layer. A stainless-steel mesh was wrapped around the tube working as the ground electrode, while a solid stainless-steel rod with a diameter of 17 mm was only used this time as the inner electrode. The discharge length was 100 mm with a discharge gap of 2.5 mm. Moreover, Chapter 4 contains experiments that require catalysts or dielectric materials to be packed. In this case, quartz-wool is applied to keep the packing materials within the plasma region whereas it is placed outside the plasma region. For the work conducted in Chapter 4, two kinds of transition-metal catalysts are compressed into pellets and sieved at 18-24 meshes. A total amount of 0.5 g catalyst (if needed) was partially packed into the reactor and sandwiched by quartz wool.



(a)



(b)

Figure 2.2 Schematic diagram and picture of the DBD reactor: (a) Wire-electrode DBD; (b) Rod-electrode electrode DBD.

In the research of this thesis, an FT-IR spectrometer (JASCO FTIR-4200, resolution of  $4\text{ cm}^{-1}$ ) was used to monitor the reaction product and collect the final ammonia concentration. It adopted a 10 cm effective pathlength gas cell (STORM 10 GAS CELL) with KBr windows (Specac). For the results obtained from FT-IR, each measurement was repeated three times, the standard deviation of the three values was calculated to obtain the average value and was reflected in the error bar. The optical emission spectroscopy (OES) diagnostics of the  $\text{N}_2\text{-H}_2$  plasma was performed using an optical fibre connected to a Princeton Instruments ICCD spectrometer (Model 320 PI) with a focal length of 320 mm.  $600\text{ g mm}^{-1}$  and  $2400\text{ g mm}^{-1}$  gratings were used to measure a wavelength range of 200-900 nm.

The gas temperature and the temperature of the catalyst bed in the discharge zone were measured using an infrared thermometer gun (Omega OS540). The temperatures at different locations in the plasma-catalytic zone were almost the same. The temperature was monitored on a regular basis to detect abnormal temperature changes.

## 2.2 ANALYTIC METHODS

### 2.2.1 MEASUREMENT AND ANALYSIS OF ELECTRIC SIGNALS

A self-designed power measurement system was used to monitor and control the discharge power in real-time. The voltage on an external capacitor ( $C_{ext} = 0.47 \mu\text{F}$ ) connecting the ground electrode and ground was measured to determine the total charge ( $Q$ ) transferred in the plasma reaction, while a high voltage probe measured the applied voltage (Testec, HVP-15HF) and a Rokowski coil measured the current (Bergoz, CT-E0.5). All signals were recorded by a digital oscilloscope (RIGOL, DS1104).

The discharge power was determined by calculating the area of the Q-U Lissajous figure which was firstly introduced by Manley in 1943 [65]. Figure 2.3 (a) illustrates a typical circuit for measuring the discharge power of a DBD reactor [66], [67] as well as an ideal shape of the Lissajous figure [68]. Also, the specific energy input (SEI), that describes the energy input into the plasma reactor, can be calculated by:

$$\text{SEI (kJ } L^{-1}) = \frac{60 \times P(W)}{q (mL \text{ min}^{-1})} \quad (\text{Eq. 2})$$

In this equation,  $P$  is the discharge power and  $q$  is the total feed flow rate.

Figure 2.3 (b) describes an ideal Lissajous figure, in which the peak-to-peak charge ( $Q_{pp}$ ), charge transferred per half cycle ( $Q_{trans}$ ) and the total capacitance ( $C_{total}$ ) can be obtained [69].

$$\frac{1}{C_{total}} = \frac{1}{C_d} + \frac{1}{C_{gap}} \quad (\text{Eq. 3})$$

$$C_{gap} = \frac{C_d \times C_{total}}{C_d - C_{total}} \quad (\text{Eq. 4})$$

The charge  $Q$  flowing through the DBD reactor can be calculated from the voltage dropped on the external capacitor  $C_{ext}$ , which in this study equals  $0.47 \mu\text{F}$ .

$$Q = C_{ext} \times U_c \quad (\text{Eq. 5})$$

The discharge voltage can then be determined by:

$$U_d = \frac{Q}{C_d} = \frac{C_{ext} \times U_c}{C_d} \quad (\text{Eq. 6})$$

Also, the gap voltage can be calculated as:

$$U_{gap} = U - U_d \quad (\text{Eq. 7})$$

Finally, the breakdown voltage can be determined by:

$$U_B = \frac{U_{min}}{1 + (C_{gap}/C_d)} \quad (\text{Eq. 8})$$

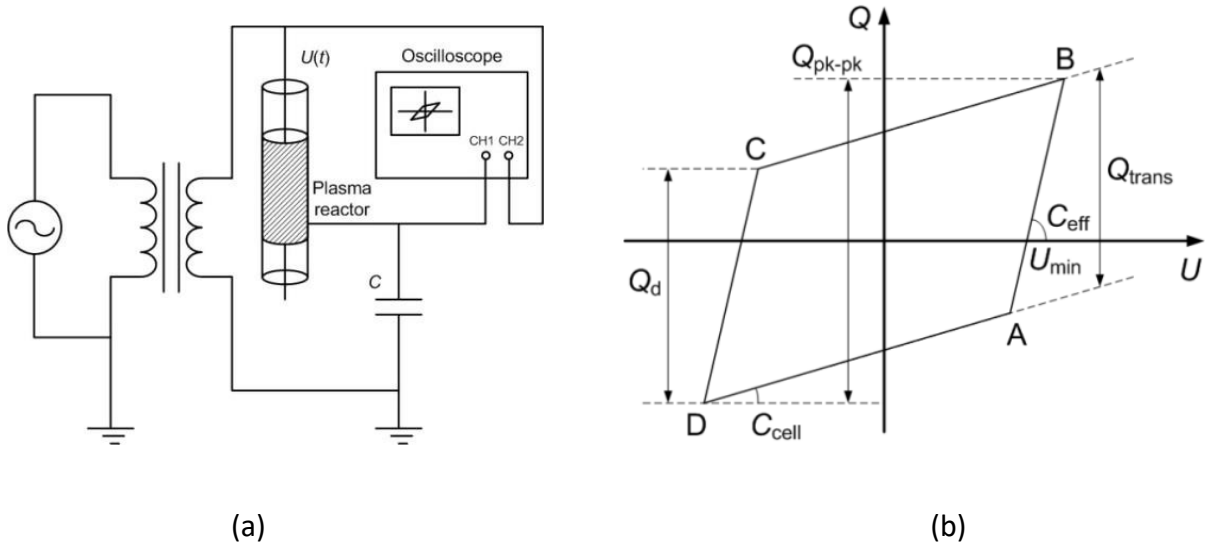


Figure 2.3 (a) Typical circuit for measuring the discharge power of a DBD reactor [66], [67]; (b) Ideal Lissajous figure for a DBD reactor [68].

Figure 2.4 (a) shows an equivalent circuit of the DBD reactor. It contains two capacitors that are in series [66].  $C_d$  is the capacitance of the dielectric material that stands for the

capacitance of the quartz tube in the rod electrode DBD reactor without packing.  $C_{gap}$  is the capacitance across the gap of the DBD reactor. Also, a resistive channel  $R_{gap}$  occurs when plasma is generated.  $C_d$  can be calculated using the equation below according to the topology of a rod electrode capacitor [70].

$$C_d = \frac{2\pi\epsilon_0\epsilon_d l}{\ln [(d + x)/d]} \quad (Eq. 9)$$

$\epsilon_0$  is the dielectric constant of a vacuum that equals to  $8.854 \times 10^{-12} \text{ F m}^{-1}$ ;  $\epsilon$  is the relative dielectric constant of dielectric material;  $l$  is the length of the plasma region;  $d$  and  $x$  are the inner radius of and the thickness of quartz tube, respectively, as shown in Figure 2.4 (b).

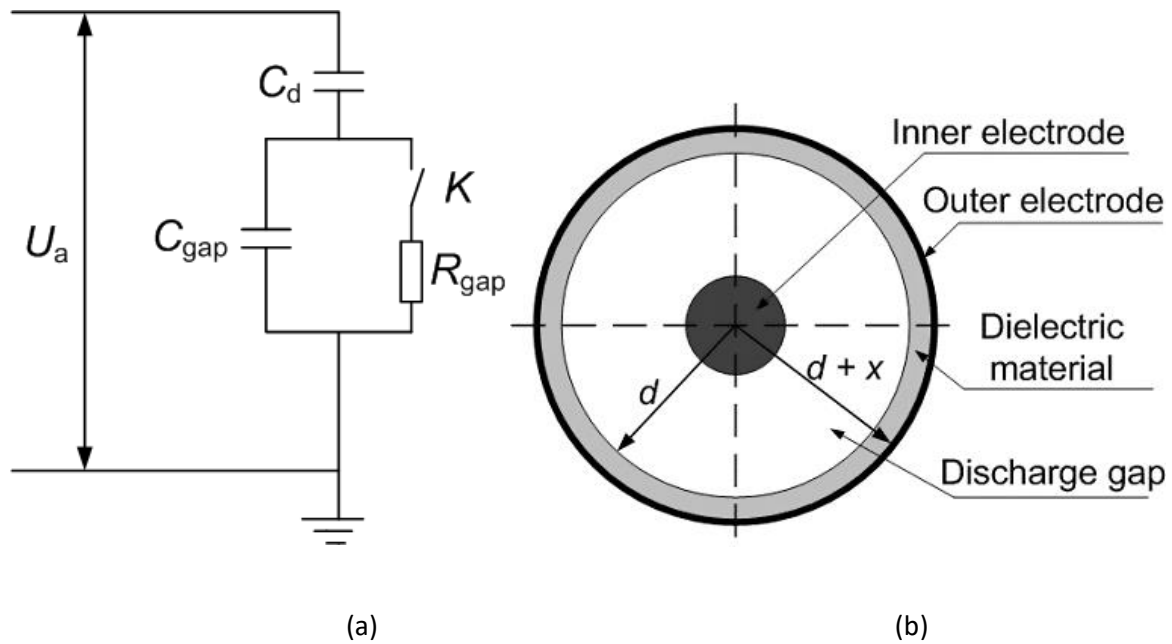


Figure 2.4 (a) Equivalent circuit of the DBD reactor [71]; (b) Transversal section of the Rod electrode DBD reactor [67], [71].

### 2.2.2 QUANTIFICATION OF GAS PRODUCT USING FT-IR

Fourier-transform infrared spectroscopy is applied to analyse the gas produced during the experiments in this thesis. FT-IR is a technique that measures the ability of a sample in absorbing or emitting light at each wavelength. This technique shines a multi-frequency beam onto the sample at once, and on the other side, giving the second data point containing a different combination of frequencies. Next, a computer with designated software collects the raw data and using a Fourier-transform, converts it into the actual spectrum. The concentration of the gas product is monitored until the steady-state is reached and ammonia is the only product gas of all experiments conducted in this thesis. Volume fraction part per million (ppm) was used to describe the gas concentration. Moreover, quantitative analysis was carried out by comparing the peak area under the spectrum to the standard ammonia FT-IR spectrum provided by OMNIC, since the peak area is proportional to the gas concentration [72].

The standard infrared spectrum of ammonia according to the OMNIC database indicates the numerical peak area is 0.482 when the wavenumber ranges from 954 to 970  $\text{cm}^{-1}$ , ammonia concentration is 100 ppm, and effective pathlength is 100 cm. Therefore, a relation between the obtained peak area value and the ammonia concentration can be concluded. Assuming  $\omega$  to be the values of peak area and  $\beta$  to be the value of ammonia concentration, a tenfold relation occurs due to the difference of optical distances. The concentration of ammonia in part per million (ppm) is defined as:

$$\frac{\omega}{0.482} = \frac{\beta/10}{100} \quad (\text{Eq. 10})$$

The energy efficiency of ammonia synthesis is defined as:

$$E (g-NHH_3 \text{ kWh}^{-1}) = \frac{\text{Moles of } NH_3 \text{ synthesised} \times 17 \times 1000 \times 1 (h)}{\text{Power (W)}} \quad (\text{Eq. 11})$$

### 2.2.3 PLASMA DIAGNOSTIC USING OPTICAL EMISSION SPECTROSCOPY

OES diagnostics of the N<sub>2</sub>-H<sub>2</sub> DBD was performed using an optical fibre connected to a Princeton Instruments ICCD spectrometer (Model 320 PI) with a focal length of 320 nm. The 600 g mm<sup>-1</sup> gratings were used to measure a wavelength range of 200-900 nm. OES was calibrated by the mercury pen-ray lamp. Measurements were aiming the plasma area at the middle of the reactor and each recording was taken after 15 minutes to ensure homogeneous discharge occurs.

### 2.2.4 CATALYST PREPARATION AND CHARACTERISATION

For the catalysts used in this study, both iron and copper-based catalysts were prepared by the impregnation of an aqueous solution of nitrate salts with  $\gamma$ -Al<sub>2</sub>O<sub>3</sub> powder at a weight percentage of 10 wt%. The amount of iron (Fe(NO<sub>3</sub>)<sub>2</sub> · 9H<sub>2</sub>O bought from Alfa Aesar) and copper (Cu(NO<sub>3</sub>)<sub>2</sub> · 2.5H<sub>2</sub>O bought from Alfa Aesar) nitrate precursors used was calculated according to the stoichiometric ratio. The flow chart in Figure 2.5 shows the detailed preparation process of the monometallic catalysts that use Fe/Al<sub>2</sub>O<sub>3</sub> catalyst as an example. First, the nitrate salts are weighted and mixed with de-ionised water. After mixing with de-ionised water, this nitrate solution is stirred for 2 hours. Once the nitrate solution is prepared, the support particle ( $\gamma$ -Al<sub>2</sub>O<sub>3</sub> powder) is added into the solution and impregnated overnight. Following this, the nitrate precursor/support particles solution is dried at 60-110 °C until the powder of nitrate precursor/support particles with the uniform size is obtained. The nitrate precursor/support powder is then calcined at 550 °C for 4 hours. The catalysts were then

sieved to 40-60 mesh. Finally, the catalysts are reduced under hydrogen plasma environment for 1 hour before each reaction. These catalysts, after plasma treatment, are henceforth called “fresh catalyst”.

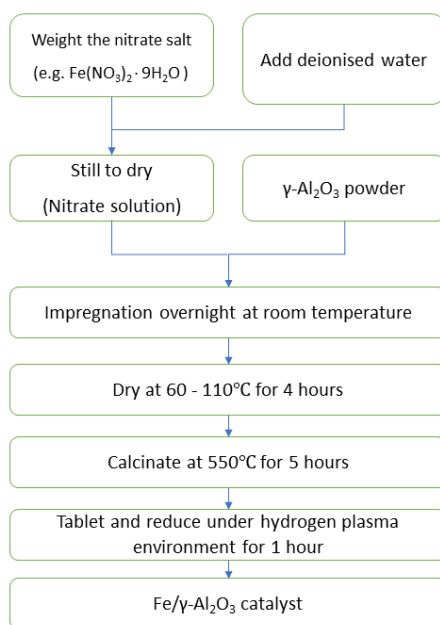


Figure 2.5 The flow chart for the preparation steps of the Fe/Al<sub>2</sub>O<sub>3</sub> catalyst.

Gas adsorption is used for studying a catalyst’s surface characteristics such as specific area, pore structure and pore distribution. Generally, nitrogen as one of the inert gases is used as adsorbents to resist chemical adsorption of catalysts. The isotherms of adsorption were assessed by measuring the amount of adsorbed gas at a constant temperature and a varied relative pressure. The divisions of adsorption and desorption ratio can be found in the isotherms of adsorption and the form of the isotherms depends mainly on the porous property. In this study, N<sub>2</sub> physisorption measurements were carried out using a Quantachrome Autosorb-1 instrument at 77 K to determine the specific surface area, pore size distribution, average pore diameter, and average particle diameter for each of the catalysts. All the catalysts, including the fresh catalysts and the spent catalysts, were pre-

treated at 300 °C under vacuum to remove any impurities from the surface. The specific surface area of the samples was calculated using the Brunauer–Emmett–Teller (BET) method.

X-ray diffraction (XRD) is a method that is used to classify the atomic crystal structure, relying on the positive interaction between the monochromatic X-ray and crystalline materials. The samples are designed for XRD analysis by grinding the solid materials into a fine powder that is then pressed and smoothed. The measurement records all possible diffraction directions of a lattice in the form of  $2\theta$  in a designated range. Then, peaks at different  $2\theta$  angles can be translated and recognise the crystal structure of the sample. In this study, XRD patterns of the fresh and spent catalysts were recorded by a Rigaku D/max-2200 diffractometer using a Cu- $K\alpha$  radiation source in the  $2\theta$  range from 10° to 80°.

Transmission electron microscopy (TEM) requires fine detail to be analysed and studied on an atomic level sample. Unlike standard optical microscopy, the precision of which is restricted by the diffraction of light energy, TEM utilises an electron beam to pass through an ultra-thin film sample. A reference picture can be replicated by calculating the electrons associated with the object. In this study, TEM analysis of the fresh catalysts was carried out using a Tecnai G2 F20 microscope operating at an acceleration voltage of 300 kV.

Temperature programmed desorption (TPD) is an effective tool for evaluating the strength of surface chemical bonds, surface acidity and adsorbed species on the catalyst surface. In TPD, pre-treatment allow the samples to immerse into the adsorbent to make sure the attachment of adsorbent onto the catalyst surface. The samples are then heated linearly to remove those

adsorbents from samples. The temperature at which the desorption occurs will indicate the species type, bond strength. In addition, the surface acidity can be suggested by the deconvolution of acid site curve and distinguished according to the temperature level. In this study, the acidity of the catalysts was evaluated by TPD of ammonia ( $\text{NH}_3$ -TPD) using a Micrometrics AutoChem 2910 instrument equipped with a mass analyser.

X-ray photoelectron spectroscopy (XPS) is a type of analysis based on the photoelectric effect of electron spectroscopy. In fact, any substance will produce electrons when irradiated by photoelectrons. By detecting these electrons, they could tell the knowledge on kinetics, strength and angular distribution related to electrons. Therefore, this information contributes to an understanding of the material as well as the electronic configurations of atoms and molecules. In this study, XPS analysis was performed on a Thermo ESCALAB 250Xi instrument using an Al K $\alpha$  X-ray source calibrated with C1s (284.8 eV). A low-resolution survey and high-resolution region scans were measured at the binding energy of interest for each of the spent catalysts.

### 3 NTP AMMONIA SYNTHESIS IN A WIRE-ELECTRODE DBD REACTOR

#### 3.1 INTRODUCTION

In this work, the synthesis of ammonia from nitrogen and hydrogen was carried out in a DBD reactor without extra heating and under atmospheric pressure. The effects of electrode materials on the  $\text{NH}_3$  production and energy efficiency was examined. The influence of process parameters, such as feed gas composition ( $\text{N}_2/\text{H}_2$  molar ratio) and total feed flow rate were also investigated. Moreover, the discharge characteristics of using different electrodes and possible surface reaction pathways for the plasma-driven  $\text{NH}_3$  synthesis were also discussed.

#### 3.2 RESULTS AND DISCUSSIONS

##### 3.2.1 EFFECT OF ELECTRODE MATERIALS ON THE PLASMA-DRIVEN $\text{NH}_3$ SYNTHESIS

Figure 3.1 shows the  $\text{NH}_3$  production using different electrodes, in terms of the  $\text{NH}_3$  concentration of product gas and the energy efficiency of the process. Compared with the rod electrode, the  $\text{NH}_3$  was more efficiently produced using the metal wool electrodes. It can be explained that the metal wool electrodes have a larger surface area ( $63 \text{ cm}^2$ ) than the rod electrode ( $45 \text{ cm}^2$ ) which has been calculated by the intersecting section area multiplied by the length of the wire. Copper wool achieved the highest  $\text{NH}_3$  production as the  $\text{NH}_3$  concentration in the product gas was 2983 ppm, and the energy efficiency of the process was  $0.68 \text{ g-NH}_3 \text{ kWh}^{-1}$ . The performance of metal wool electrodes for the  $\text{NH}_3$  production followed the order of  $\text{Cu} > \text{Ni} > \text{Ti} > \text{SS} > \text{NiFe}$ , suggesting that the plasma-driven ammonia production was affected by the material of the electrodes. The agreement between the present results

and the previous results is satisfactory, in particular with the results of the references [23], [55].

Although the applied voltage ( $U_{pp}$ ) and charge transfer ( $Q_{trans}$ ) were different for various electrode materials, as shown in Table 3-1, it is more likely due to the change of  $\text{NH}_3$  concentration in working gas, rather than that caused by the electrode materials as slight changes of  $U_{pp}$  and  $Q_{trans}$  have been observed. In other words, the effect of the material of the electrode could be assigned to the catalytic effect of the electrode surface. Interestingly, Wang, et al, investigated the  $\text{NH}_3$  decomposition using various supporting metal catalysts. They found that the reactivity of the catalysts followed the order of  $\text{Co} > \text{Ni} > \text{Fe} > \text{Cu}$ , which is the reverse order of the synthesis performance of electrodes in this work [73]. Their results support our idea that the electrode might serve as a catalyst in the plasma-synthesis of ammonia.

In the similar work conducted by Aihara and his co-workers using DBD plasma [23], they described the fact that after a long period of reaction, a bronze-coloured and non-uniform layer was observed on the inner wall of the reactor, which was later determined to be copper metal by X-ray photoelectron spectroscopy. However, in this work no significant metal deposition on the inner wall of the reactor was discovered at all. This could be due to different input power frequencies, as they adopted 50 kHz whereas only 10 kHz was used in this work. Moreover, Aihara and his colleagues tried to explain the advantage of the copper by utilising SEM to observe the change of the metal surface. It was found that the wool-like copper electrode surface became bumpy under the plasma treatment which allowed more exposure to the plasma environment and hence promoted the reaction.

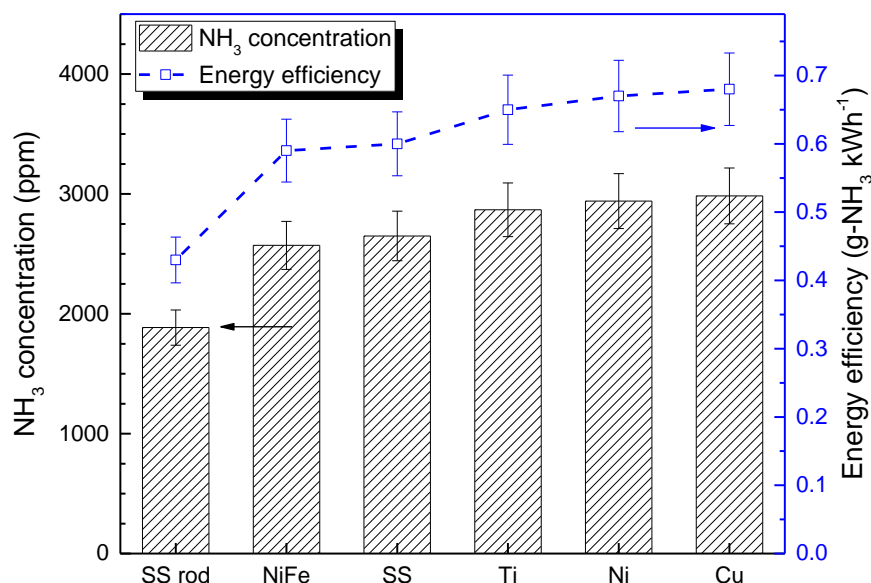


Figure 3.1 NH<sub>3</sub> concentration and energy efficiency using electrode with different materials. ( $N_2/H_2 = 1:1$ , total flow rate  $100 \text{ ml min}^{-1}$  and discharge power  $20 \text{ W}$ ).

### 3.2.2 EFFECT OF $N_2/H_2$ MOLAR RATIO ON THE PLASMA-DRIVEN NH<sub>3</sub> SYNTHESIS

Figure 3.2 shows the effect of  $N_2/H_2$  molar ratio on the NH<sub>3</sub> production. At ambient temperature, the atmospheric DBD plasma achieved the best NH<sub>3</sub> production when the  $N_2/H_2$  ratio was 1:1. This result can be explained as a trade-off between the reaction kinetics of NH<sub>3</sub> synthesis and the electrical properties of DBD plasma. On the one hand, compared with the stoichiometric  $N_2/H_2$  ratio (3:1), excessive  $N_2$  increased the N radicals produced by  $N_2$  dissociation, which is the rate-limiting step. On the other hand, higher  $N_2$  content might decrease the mean electron energy in  $N_2/H_2$  plasma, suppressing the plasma-dissociation of  $N_2$ . Previous studies showed that NH<sub>3</sub> production depends on the  $N_2/H_2$  molar ratio in the feed gas [22], [25], [29], [56], [74]. Gomez, et al, achieved a maximum energy efficiency for NH<sub>3</sub> production ( $0.44 \text{ g-NH}_3 \text{ kWh}^{-1}$ ) using PZT packing material and at an  $N_2/H_2$  ratio in the range of 1:3 to 1:1 [25]. One unanticipated finding was that Peng and co-workers reported

that slightly excessive  $N_2$  improved the energy efficiency for the plasma-synthesis of  $NH_3$ . They achieved the best energy efficiency of  $0.85 \text{ g-NH}_3 \text{ kWh}^{-1}$  at an  $N_2/H_2$  ratio of 3:1, while the further increase of  $N_2/H_2$  ratio decreased the energy efficiency [29]. They explained this inconsistency may be due to excessive  $N_2$  leads to a higher density of nitrogen molecular, and the possibility of active nitrogen molecule reacting with hydrogen would be increased. Hong, et al, calculated the electron density and temperature (electron energy) at various  $N_2/H_2$  ratios and found that the electron temperature was dependent on the  $H_2$  proportion, while a maximum value was reached when the  $N_2/H_2$  molar ratio was near 1:2 [74].

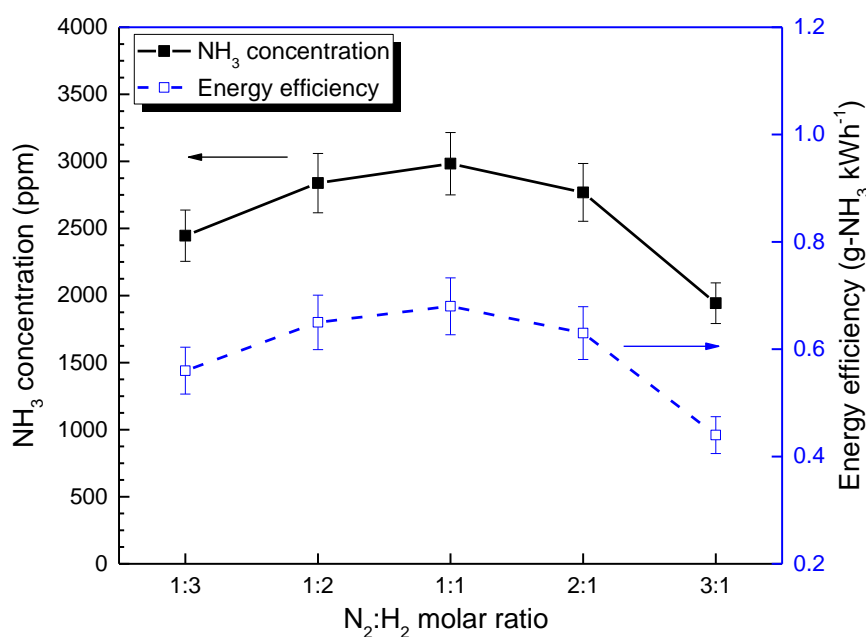


Figure 3.2 Dependence of  $NH_3$  concentration and energy efficiency on the  $N_2/H_2$  molar ratio. (Cu wire electrode, a total flow rate of  $100 \text{ ml min}^{-1}$  and discharge power  $20 \text{ W}$ ).

### 3.2.3 EFFECT OF TOTAL FEED FLOW RATE ON THE PLASMA-DRIVEN $\text{NH}_3$ SYNTHESIS

Figure 3.3 shows the effect of total feed flow rate on the  $\text{NH}_3$  production in DBD plasma. By increasing the total flow rate, the concentration of  $\text{NH}_3$  in the product gas was decreased, but the energy efficiency of the process was improved to  $1.04 \text{ g-NH}_3 \text{ kWh}^{-1}$  at a total flow of  $250 \text{ ml min}^{-1}$ . This finding can be explained as when the flow rate increased, the total amount of  $\text{NH}_3$  produced was increased, while the discharge power was fixed at  $20 \text{ W}$ . The energy efficiency was therefore increased. Indeed, it was indicated by [25] that a longer residence time brought by a smaller total flow rate would result in less ammonia production. This is due to the extended residence time assisted the back reactions especially the ammonia decomposition.

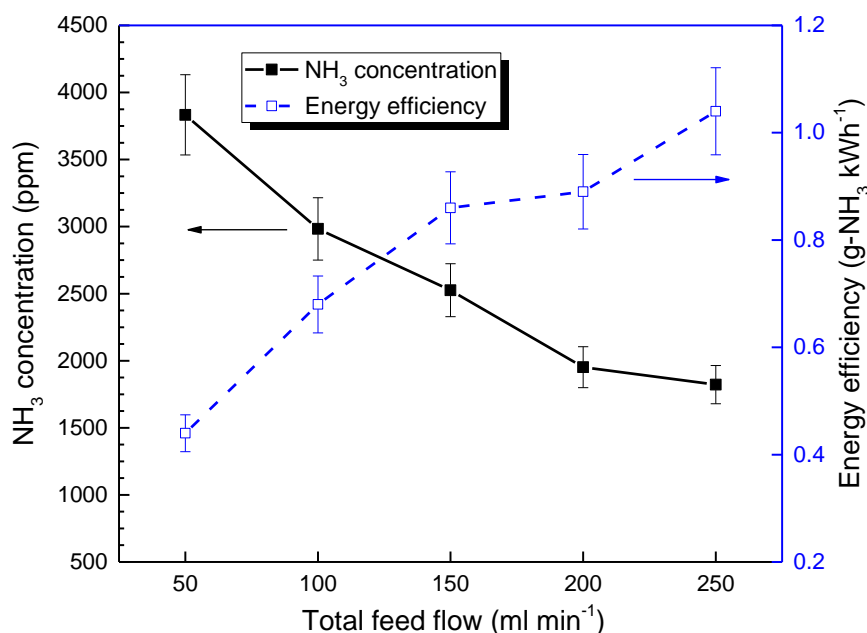


Figure 3.3 Effect of total flow rate on  $\text{NH}_3$  production. (Cu wire electrode,  $\text{N}_2/\text{H}_2$  molar ratio 1:1 and discharge power  $20 \text{ W}$ ).

### 3.2.4 EFFECT OF ELECTRODE MATERIALS ON THE ELECTRICAL PROPERTIES OF THE REACTOR

Figure 3.4 shows the typical voltage and current signals of the  $\text{NH}_3$  synthesis process. A few high spikes can be observed on the current profile, corresponding to the streamer discharges bridging the discharge gap. Numerous tiny current spikes can also be seen throughout the whole cycle, assigned to the surface discharges and micro-discharges between the dielectric layer and the metal wire. The current profile clearly suggests a mixed pattern of restrictive streamer discharge and surface discharge. It is reasonable since the fibre of wool-electrode is randomly distributed in and fills the quartz tube; the outer part of the wool electrode was in good contact with the inner surface of the quartz. The voltage applied across the reactor is also calculated when different electrodes were used for the plasma  $\text{NH}_3$  synthesis. The peak voltage roughly followed the order of SS rod > Ti > NiFe  $\approx$  SS > Ni  $\approx$  Cu. This is probably caused by the polarisation of the produced  $\text{NH}_3$  molecule. The dielectric strength of  $\text{NH}_3$  gas is lower than  $\text{N}_2$  and  $\text{H}_2$ , so that the produced  $\text{NH}_3$  changed the dielectric properties of the working gas, lowering the peak value of applied voltage.

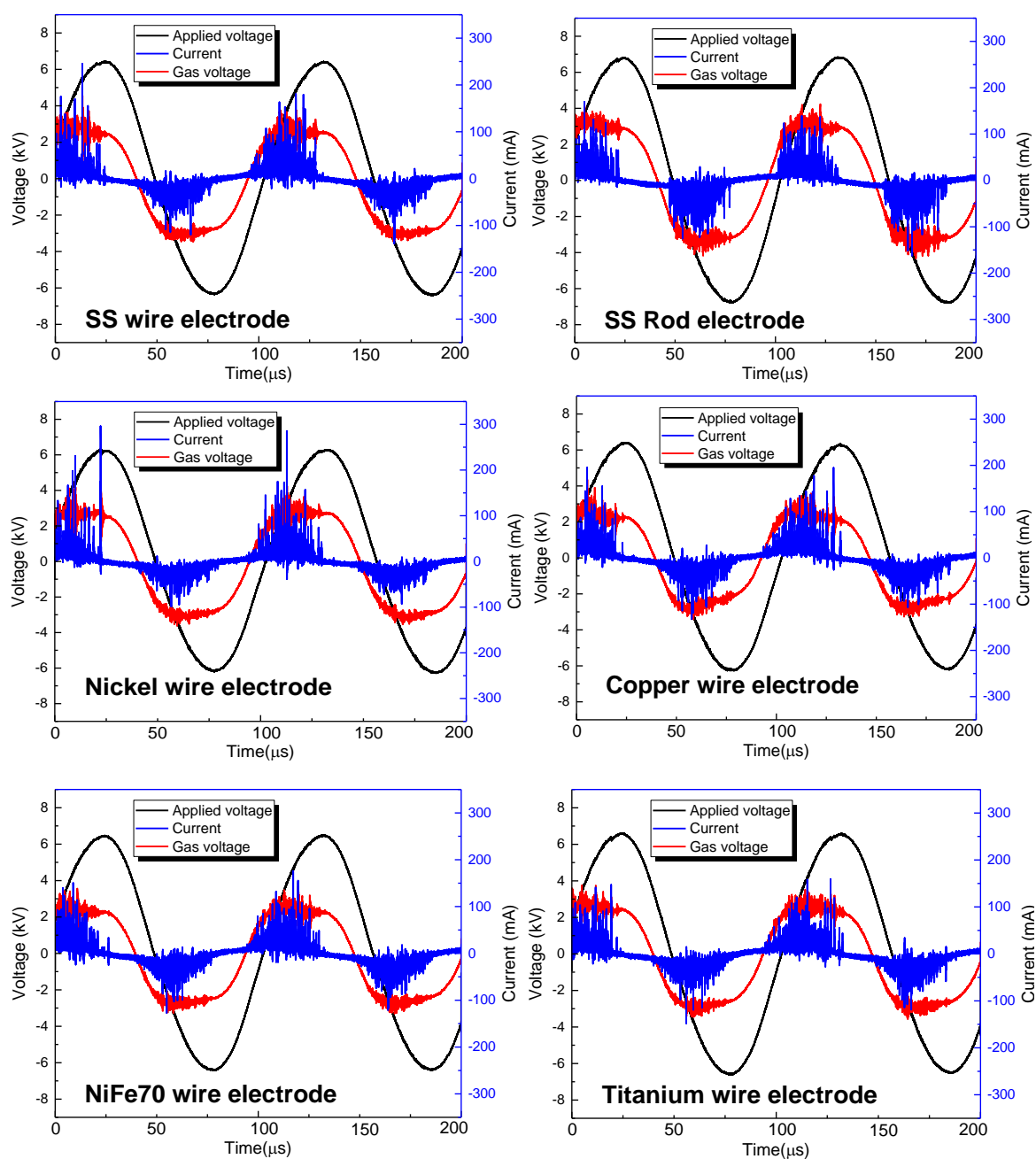


Figure 3.4 Typical discharge waveform of the plasma-synthesis of  $\text{NH}_3$  using different electrodes. (Total flow rate:  $100 \text{ ml min}^{-1}$ ,  $\text{N}_2/\text{H}_2 = 1:1$ , frequency: 9 kHz; discharge power 20 W).

Figure 3.5 shows the Lissajous figure obtained during the  $\text{NH}_3$  synthesis. The cases of using SS rod, Ti wool and Cu wool as the electrode was chosen as an example. When the SS rod was used, the Lissajous figure was flat, suggesting relatively high breakdown voltage and limited discharge current. The breakdown voltage  $U_b$  can be observed in the figure (1.33 kV).

However, when the Cu electrode was used, the Lissajous figure became thin, indicating the decrease of breakdown voltage and enhanced charge transfer. The figure morphed from parallelogram to oval shape and the breakdown voltage became difficult to determine, suggesting the discharge mode changed from partially discharging streamers to surface micro-discharges. In other words, the discharge spikes of using a Ti electrode were more intense than that using SS rod electrode. When the Cu electrode was installed, the discharge was even stronger than that using the Ti electrode. This result agrees with the peak voltage shown in Figure 3.4. Since the discharge power was fixed at 20 W, when the peak voltage decreases, the peak discharge current would increase accordingly, enhancing the charge transfer. The negligible difference in discharge characteristics was observed when changing the total flow rate or  $N_2/H_2$  molar ratio.

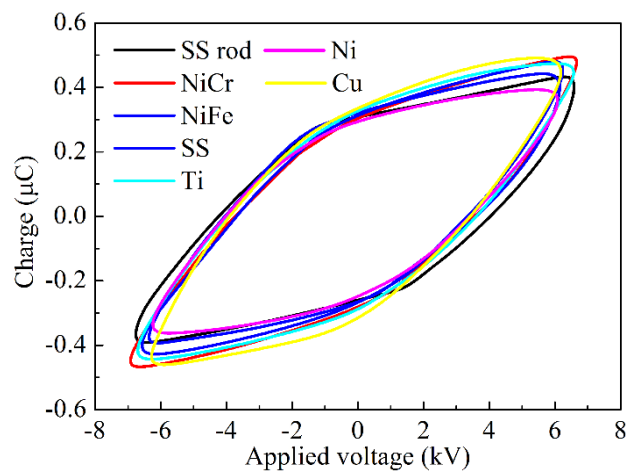


Figure 3.5 Lissajous figure obtained during the plasma synthesis of  $NH_3$ . (Total flow rate:  $100 \text{ ml min}^{-1}$ ,  $N_2/H_2 = 1:1$ , frequency: 9 kHz; discharge power 20 W).

Table 3-1 summarises the peak-to-peak voltage ( $U_{pp}$ ) and the charges transferred from one electrode to the other ( $Q_{trans}$ ) during discharge, as calculated. The values of  $U_{pp}$  are consistent according to Figure 3.5. Since the discharge power was fixed at 20 W, the discharge current

was improved due to the decreased applied voltage. The charge transfer was consequently enhanced. As discussed previously, the dissociation of  $N_2$  is a rate-limiting step for the  $NH_3$  synthesis from  $H_2$  and  $N_2$ . In the plasma-driven  $NH_3$  synthesis, the energetic electrons are essential for the excitation, ionisation and dissociation of  $N_2$  molecules, therefore being critical to the synthesis process. Decreased  $U_{pp}$  make the discharge more stable, enhanced the discharge current and increased the chance for the collision between electrons and reactant gas molecules. The average electron density in the plasma region was subsequently increased due to the enhanced current and can be confirmed by the improved charge transfer  $Q_{trans}$ . As a result, the increment of electrons would facilitate the conversion of  $N_2$  under plasma conditions.

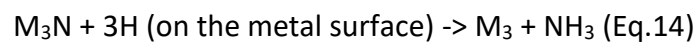
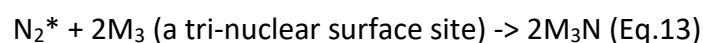
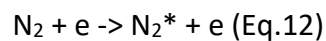
*Table 3-1 Electrical properties of the DBD reactor using different electrodes. ( $N_2/H_2 = 1:1$ , total flow rate  $100\text{ ml min}^{-1}$  and discharge power  $20\text{ W}$ ).*

Electrode material	$Q_{trans}$ ( $\mu\text{C}$ )	$U_{pp}$ (kV)
Rod	0.82	13.5
Ni-Cr	0.98	13.6
Ni-Fe	0.92	12.9
SS	0.84	12.7
Ti	0.92	13.3
Ni	0.76	12.4
Cu	0.95	12.5

### 3.2.5 THE ENHANCEMENT MECHANISM OF COPPER WIRE

It has been proposed that plasma synthesis of  $NH_3$  from  $N_2$  and  $H_2$  involves  $N_2^+$  ions and N, H atoms as initiators and NH radicals as intermediates [21], [27], [50]. Gomez, et al, confirmed the presence of  $N^*$ ,  $N_2^*$ ,  $N_2^+$  species according to correlated bands in DBD plasma by OES technique [25]. The asterisk refers to the excited status of the corresponding species. For instance, the excited nitrogen  $N_2(A^3\Sigma_u^+)$  (threshold 6.2 eV) is vital for the generation of  $N_2^+$  ions and excited N ( $^2D$ ) is a critical species for the formation of NH radicals, while N( $^4S$ ,  $^2P$ ) is

usually rapidly quenched at atmospheric pressure [56]. Since there are similarities of experiment methodologies between this work and that described by Aihara, et al [23], it is encouraging to adopt the OES result that was found by his group. What is surprising is that the intensity of  $N_2^+$  band ( $B^2\Sigma_u^+ \rightarrow X^2\Pi_g^+$ , first negative system) was far smaller than that of  $N_2^*$  band ( $N_2 C^3\Pi_u \rightarrow B^3\Pi_g$ , second positive system). This finding was further supported by a follow-up experiment by the same group [24]. Moreover, Aihara and his colleague found that the enhancement of  $N_2^*$  band ( $N_2 C^3\Pi_u \rightarrow B^3\Pi_g$ , second positive system) had a strong correlation with the increasing applied voltage and the little introduction of  $H_2$ . This result may explain why a nitrogen abundant environment in this work is not giving a better result for ammonia production yield. Furthermore, they have also reported that there was a concurrent increase in the  $NH_3$  production yield with a higher intensity of  $N_2^*$  band ( $N_2 C^3\Pi_u \rightarrow B^3\Pi_g$ , second positive system). Together, these results provide important insights into plasma ammonia synthesis over a metal wire electrode and that  $N_2^*$  species could be an active intermediate in the metal wire reaction system. Unlike those who considered  $NH$  radicals as intermediates that produced in the gas phase [21], [27], [50], Aihara, et al, argued that the adsorption of  $N_2^*$  species and H atom afterwards could happen on the surface of metal wires where the  $NH_3$  is generated. Each tri-nuclear surface site secures one N atom from the divided  $N_2^*$  and enables it to combine with the other three H atoms on the metal surface. This proposed  $NH_3$  formation mechanism on the metal surface is concluded in equations below:



Further calculation using density function theory (DFT) conducted by Iwamoto, et al [24], revealed the formation energies  $\Delta E_f$  of metal nitride  $M_3N$  as well as the adsorption energies of a nitrogen atom  $\Delta E_{ad}$  on the surface of metal wires. From their results, it can be found that the ability to adsorb nitrogen atoms is in the order of Cu ( $15.92 \text{ kcal mol}^{-1}$ ) > Ni ( $-10.45 \text{ kcal mol}^{-1}$ ) > Ti ( $-84.54 \text{ kcal mol}^{-1}$ ). In addition, the metal nitrides formation on the metal surfaces followed the same sequence. Hence, this indicated the correlation of  $\Delta E_{ad}$  with the catalytic activity in a proportional manner, and therefore explains why better results were given by copper than others. Besides, this study demonstrated that the adsorbed nitrogen is embedded in the dimple of triangular atoms which confirms the proposed structure of the tri-nuclear surface site, as shown in Figure 3.6.

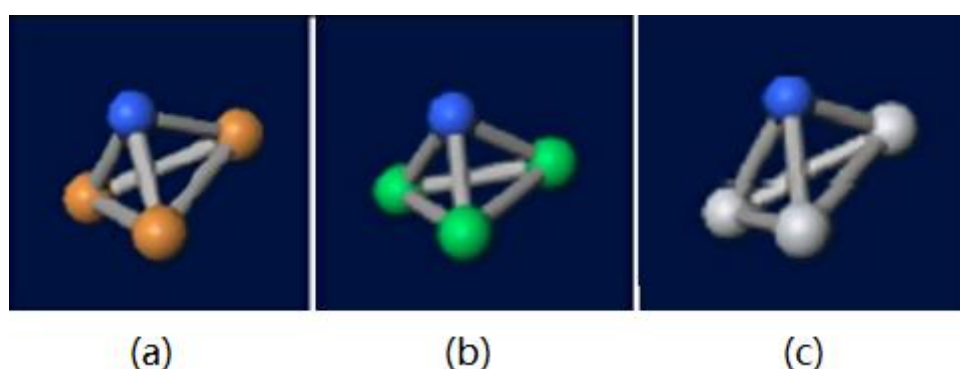


Figure 3.6 The tri-nuclear structure of  $M_3N$  (a) Cu (b) Ni (c) Ti, calculated by Iwamoto et al. [24].

In accordance with the discussion above, a recent study by Shah, et al [75], observed the formation of intermediate GaN on the surface of Ga-In alloy catalysts after the radio-frequency plasma treatment using SEM. The molten alloy catalysts were smeared on the outside of glass tubes and placed in the reaction chamber. This finding further could support the idea of the metal nitride formation on the metal surface in the plasma environment.

### 3.3 CONCLUSIONS

In this work, the  $\text{NH}_3$  synthesis in a dielectric barrier discharge reactor was performed without extra heating. The metal wool electrode was used as the inner electrode as well as a catalyst to improve the  $\text{NH}_3$  production and energy efficiency. Compared with the rod electrode, the wool electrode substantially enhanced the synthesis performance regarding the  $\text{NH}_3$  concentration in the product gas and the energy efficiency of the synthesis process. Results show that the  $\text{NH}_3$  production was dependent on the material of the electrode. After a comparative study of various materials, such as Cu, Ni, Ti and alloys, the copper-wool electrode exhibited the highest concentration of produced  $\text{NH}_3$  (2983 ppm) and the best energy efficiency ( $0.68 \text{ g-NH}_3 \text{ kWh}^{-1}$ ) at an  $\text{N}_2/\text{H}_2$  molar ratio of 1:1 and a flow rate of  $100 \text{ ml min}^{-1}$ . This result was ascribed to the catalytic effect of the surface of the wool electrode. By changing the total flow rate to  $250 \text{ ml min}^{-1}$ , the energy efficiency for the  $\text{NH}_3$  synthesis using a Cu wire electrode can be further increased to  $1.04 \text{ g-NH}_3 \text{ kWh}^{-1}$ . Also, the effect of electrode material on the electrical properties of the reactor was examined. Finally, the findings observed in this work mirror those of the studies by Aihara, et al, and Iwamoto, et al, that have examined the effect of metal nitride formation on the surface of metal wires, hence support the tri-nuclear intermediate structure that proposed by Aihara, et al.

## 4 NTP AMMONIA SYNTHESIS IN A ROD ELECTRODE DBD REACTOR

### 4.1 INTRODUCTION

In the previous chapter, plasma ammonia synthesis was carried out in a metal-wire electrode DBD reactor at atmospheric pressure without extra heating. In this chapter, NTP ammonia synthesis is conducted in a rod electrode DBD reactor. Due to the limit on the understanding of metal-oxide catalysts. This experiment determines the optimum molar ratio and total feed flow rate of gases, as well as the optimum power input for  $\text{Fe}_2\text{O}_3$  and  $\text{CuO}$  catalysts, wherein the metal oxide was recognised by XRD. Also, the work in this chapter shows the ability of metal-oxide, particularly the  $\text{CuO}$  based catalysts that significantly enhances the yield of ammonia, and this phenomenon obeys the Sabatier principle which is also known as the volcano plots. It is believed that the metal sites of metal oxides still play an important role. The characterisation of catalysts including XRD,  $\text{N}_2$  physisorption, TEM,  $\text{NH}_3$ -TPD and XPS have been conducted to determine the catalyst property. The discussion of the enhancement mechanism of  $\text{CuO}/\text{Al}_2\text{O}_3$  catalyst has been carried out. Before this experiment, the preparation of both  $\text{Fe}_2\text{O}_3$  and  $\text{CuO}$  based catalysts have been made and tested on their validity. It is worth adding that the present results would be the first experimental results showing that  $\text{CuO}$  has the highest catalytic activity.

### 4.2 ROD ELECTRODE DBD REACTOR PACKED WITH METAL OXIDE CATALYSTS

#### 4.2.1 CHARACTERISATION OF FRESH CATALYSTS

##### 4.2.1.1 *X-RAY POWDER DIFFRACTION (XRD)*

Figure 4.1 displays the XRD patterns of the fresh catalysts. It can be observed that there are three significant diffraction peaks at  $2\theta = 38.2^\circ$ ,  $45.9^\circ$  and  $67.3^\circ$ , which correlates to the  $\text{Al}_2\text{O}_3$

crystalline cubic structure. Such peaks can also be seen in the Fe/Al<sub>2</sub>O<sub>3</sub> and Cu/Al<sub>2</sub>O<sub>3</sub> spectrum. In addition, six intense peaks in the XRD pattern of Fe/Al<sub>2</sub>O<sub>3</sub> reveal strong Fe<sub>2</sub>O<sub>3</sub>-related reflections (24.0°, 33.2°, 35.6°, 40.8°, 49.5° and 54.0°). Meanwhile, CuO peaks are obvious at 2θ = 35.4°, 38.6° and 48.5°. The XRD pattern of each sample confirms the formation of metal oxides after catalyst calcination. However, according to the XRD pattern comparison before and after the plasma chemical reaction, it can be found that the catalyst has not been completely reduced and the oxide peaks still exist. It also shows that the oxide can directly participate in the reaction as a catalyst under the plasma condition.

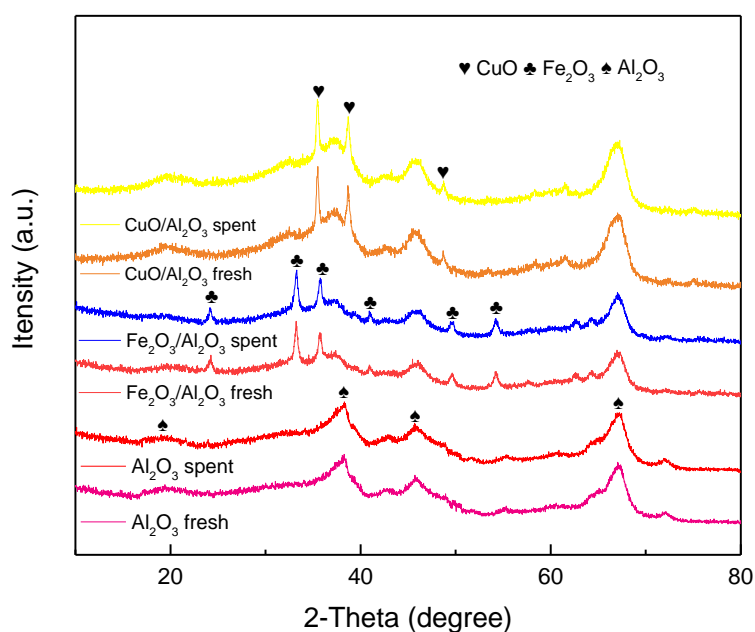


Figure 4.1 XRD pattern of the fresh (before plasma chemical reaction) and spent (after plasma chemical reaction) catalysts.

#### 4.2.1.2 N<sub>2</sub> PHYSISORPTION

The N<sub>2</sub> physisorption was carried out to characterise the textural properties of γ-Al<sub>2</sub>O<sub>3</sub>, Fe<sub>2</sub>O<sub>3</sub>/Al<sub>2</sub>O<sub>3</sub> and CuO/Al<sub>2</sub>O<sub>3</sub>. Table 4-1 shows the values of the surface area, mean pore diameter and pore volumes for each sample. It can be seen that the Brunaur-Emmett-Teller

(BET) specific surface area was decreased dramatically due to the coverage by the distribution of metals. It follows the order of  $\gamma\text{-Al}_2\text{O}_3 > \text{Fe}_2\text{O}_3/\text{Al}_2\text{O}_3 > \text{CuO}/\text{Al}_2\text{O}_3$ . Meanwhile, pore volume also showed the same trend, decreased from  $0.45 \text{ cm}^3 \text{ g}^{-1}$  for  $\gamma\text{-Al}_2\text{O}_3$  to  $0.35 \text{ cm}^3 \text{ g}^{-1}$  for  $\text{CuO}/\text{Al}_2\text{O}_3$ . However, the  $\text{CuO}/\text{Al}_2\text{O}_3$  had the most substantial mean pore diameter of 9.03 nm, compared to 7.69 nm for  $\gamma\text{-Al}_2\text{O}_3$ , indicating the combination of active metal and gas phase is more likely to happen and hence promote the chemical reaction.

Table 4-1 Physical characteristics of the fresh catalysts.

Catalyst	Specific surface area ( $\text{m}^2 \text{ g}^{-1}$ )	Pore volume ( $\text{cm}^3 \text{ g}^{-1}$ )	Mean pore diameter (nm)
$\gamma\text{-Al}_2\text{O}_3$	231	0.445	7.69
$\text{Fe}_2\text{O}_3/\text{Al}_2\text{O}_3$	158	0.349	8.69
$\text{CuO}/\text{Al}_2\text{O}_3$	153	0.345	9.03

#### 4.2.1.3 TRANSMISSION ELECTRON MICROSCOPY (TEM)

The surface morphology of the fresh catalysts was performed using transmission electron microscopy (TEM). Figure 4.2 (b-c) shows that the metal oxide particles were homogeneously dispersed over the  $\text{Al}_2\text{O}_3$  support. It can be observed that most of the particles were within a 20 nm diameter. For the  $\text{CuO}/\text{Al}_2\text{O}_3$  catalyst, similar morphologies have been reported in the recent study by Wang, et al [55].

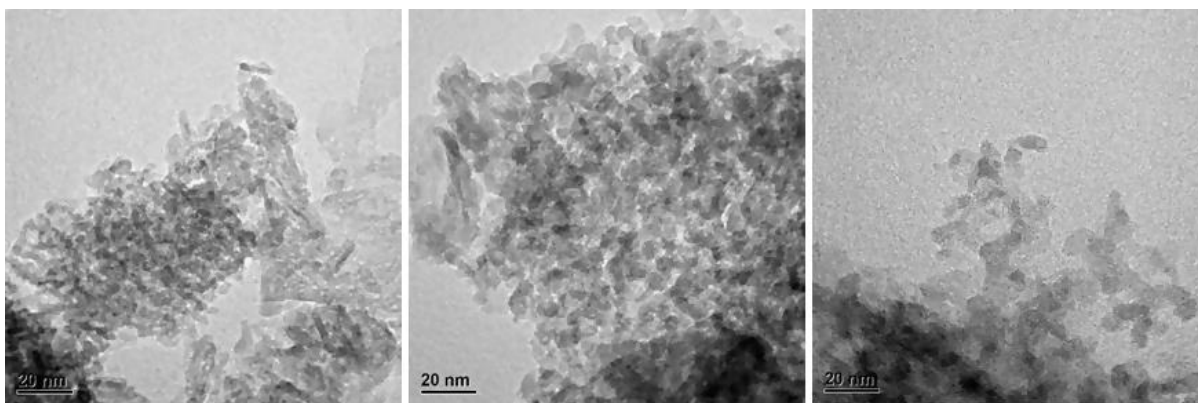
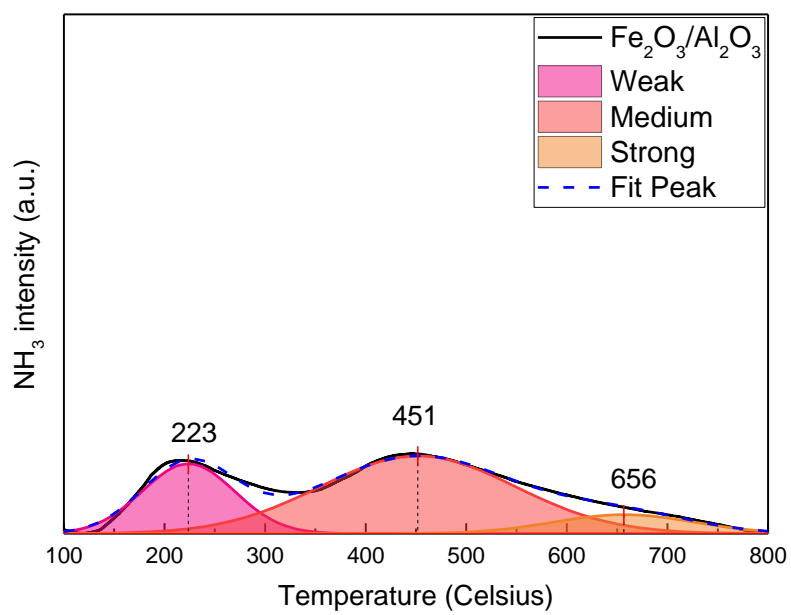
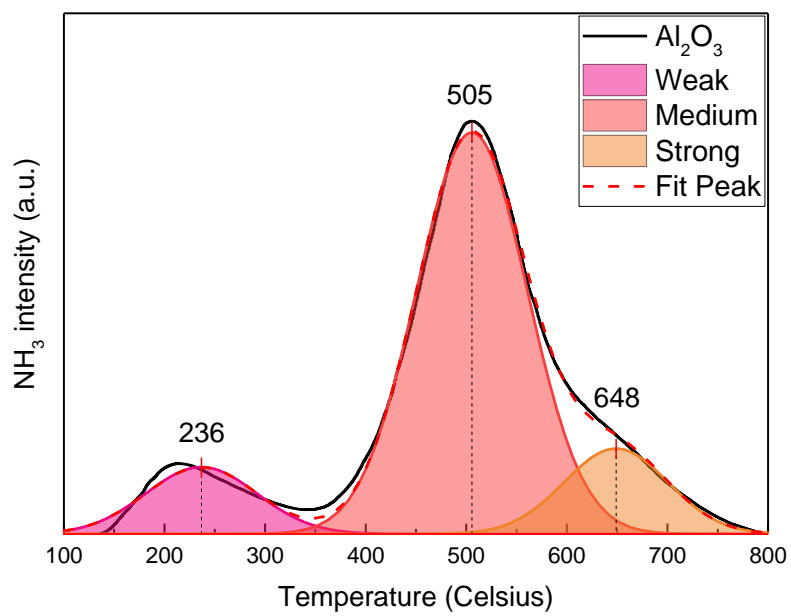


Figure 4.2 TEM images of the fresh catalysts without reduction (a)  $\text{Al}_2\text{O}_3$ , (b)  $\text{Fe}_2\text{O}_3/\text{Al}_2\text{O}_3$  and (c)  $\text{CuO}/\text{Al}_2\text{O}_3$ .

#### 4.2.1.4 TEMPERATURE PROGRAMMED DESORPTION OF AMMONIA ( $\text{NH}_3$ -TPD)

$\text{NH}_3$ -TPD was used to determine the surface acidity of the fresh catalysts. Figure 4.3 indicates the chemical desorption peaks of weak (150-300 °C), medium (300-600 °C) and strong acid sites (550-750 °C) [76] after the deconvolution of spectra. In addition, Figure 4.4 shows the amount of ammonia adsorbed on different acid sites as well as the total adsorbed ammonia for each catalyst. It is apparent from this chart that the concentration of medium and strong acid sites reduced with metal-oxide loading, while the weak acid sites remained unchanged. Also, there is a clear trend of decreasing the total number of acid sites when metal-oxide was deployed. Moreover, the desorption temperature of weak and medium acid sites decreased for  $\text{Fe}_2\text{O}_3/\text{Al}_2\text{O}_3$  and  $\text{CuO}/\text{Al}_2\text{O}_3$ . This suggests that the metal-oxide not only limited the total amount of acid sites but also loosened the strength of medium and strong acid sites of catalysts.



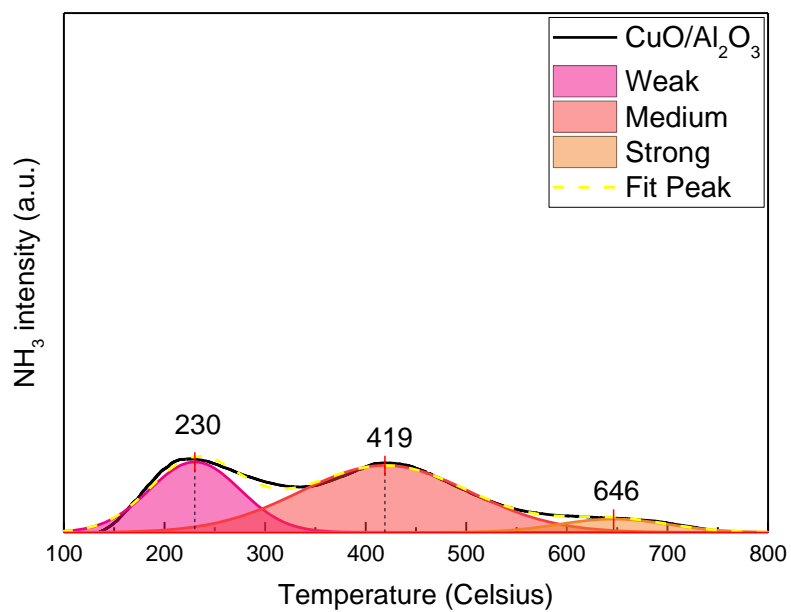


Figure 4.3  $\text{NH}_3$ -TPD profile of the fresh (a)  $\text{Al}_2\text{O}_3$  (b)  $\text{Fe}_2\text{O}_3/\text{Al}_2\text{O}_3$  and (c)  $\text{CuO}/\text{Al}_2\text{O}_3$

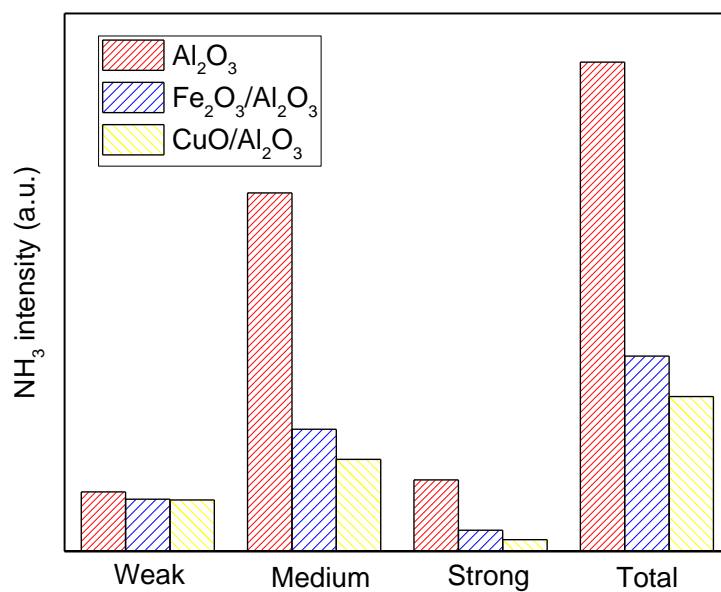
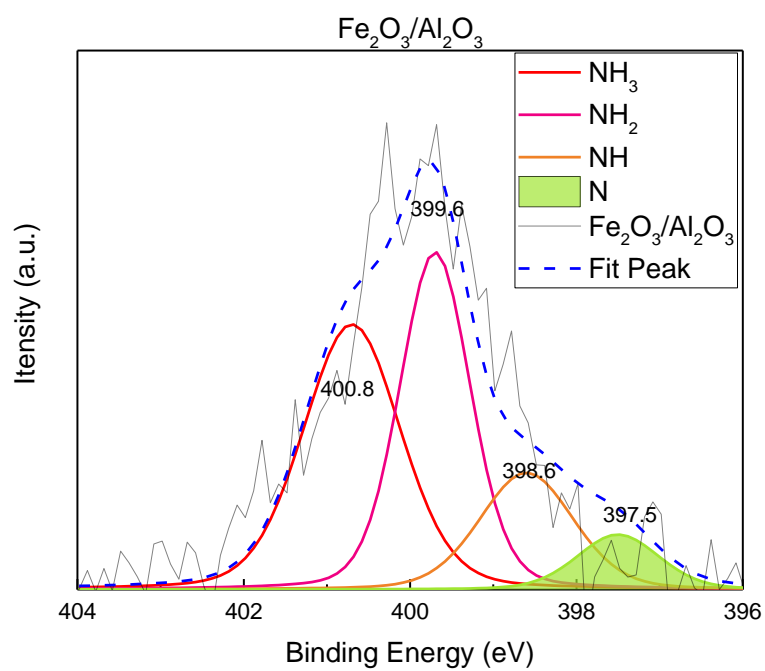
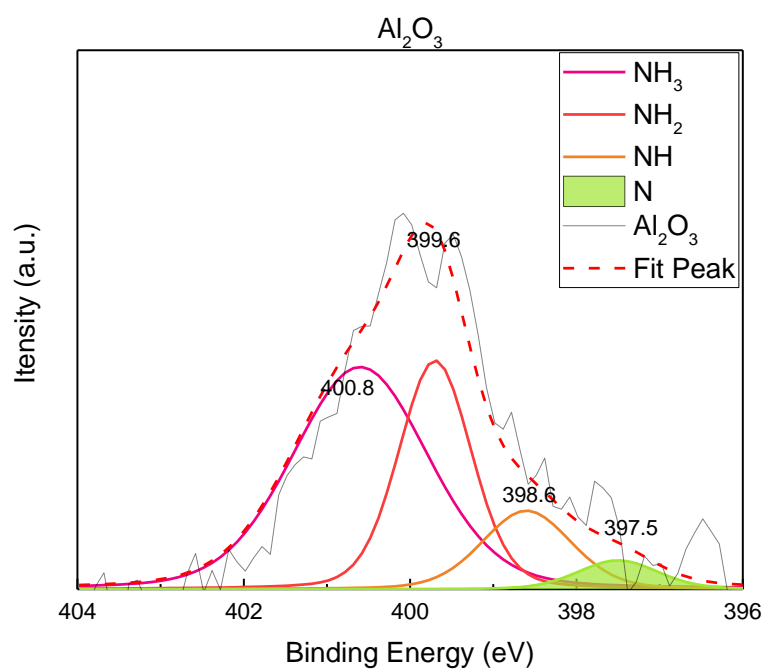


Figure 4.4 Comparison of total acid amounts for  $\text{Al}_2\text{O}_3$ ,  $\text{Fe}_2\text{O}_3/\text{Al}_2\text{O}_3$  and  $\text{CuO}/\text{Al}_2\text{O}_3$

#### 4.2.1.5 X-RAY PHOTOELECTRON SPECTROSCOPY (XPS)

The adsorption of N, NH, NH<sub>2</sub> and NH<sub>3</sub> species on the surface of spent catalysts were measured by X-ray photoelectron spectroscopy (XPS). Figure 4.5 shows the deconvolution of the spectra results of the N1s core level measurements for Al<sub>2</sub>O<sub>3</sub>, Fe<sub>2</sub>O<sub>3</sub>/Al<sub>2</sub>O<sub>3</sub> and CuO/Al<sub>2</sub>O<sub>3</sub>. Also, the quantified area of each individual peaks is shown in the figure. The assignments for N, NH, NH<sub>2</sub> and NH<sub>3</sub> peaks were determined from the NIST XPS database [77]. Two higher binding energy levels (400.8 eV, 399.6 eV) are assigned to the NH<sub>2</sub> and NH<sub>3</sub> bonds; while the other two peaks located at 398.6 eV and 397.5 eV stand for NH and N species, respectively. Figure 4.6 shows the proportion of individual peaks assigned to N, NH, NH<sub>2</sub> and NH<sub>3</sub>. It can be seen that the adsorption amount of NH<sub>3</sub> was inversely proportional to the ammonia yield of using different catalysts, in the order of Al<sub>2</sub>O<sub>3</sub> > Fe<sub>2</sub>O<sub>3</sub>/Al<sub>2</sub>O<sub>3</sub> > CuO/Al<sub>2</sub>O<sub>3</sub>. In addition, the concentration of NH<sub>2</sub> on the surface of CuO/Al<sub>2</sub>O<sub>3</sub> is far beyond other catalysts, indicating that the NH<sub>2</sub> species plays a significant role in the surface reaction. It can be seen that the concentration of N on the CuO/Al<sub>2</sub>O<sub>3</sub> surfaces was hardly detected than that of Al<sub>2</sub>O<sub>3</sub> and Fe<sub>2</sub>O<sub>3</sub>/Al<sub>2</sub>O<sub>3</sub>. This fact suggests that less direct N<sub>2</sub> dissociation occurs on CuO loaded catalysts and instead happens in the plasma gas phase.



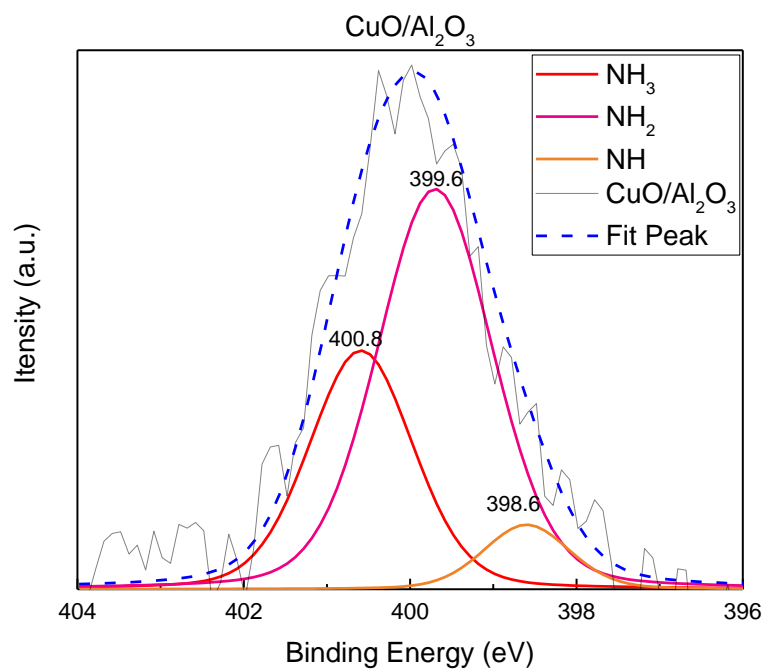


Figure 4.5  $\text{N1s}$  core level measurements for (a) packed with  $\text{Al}_2\text{O}_3$  (b)  $\text{Fe}_2\text{O}_3/\text{Al}_2\text{O}_3$  and (c)  $\text{CuO/Al}_2\text{O}_3$  after plasma reaction

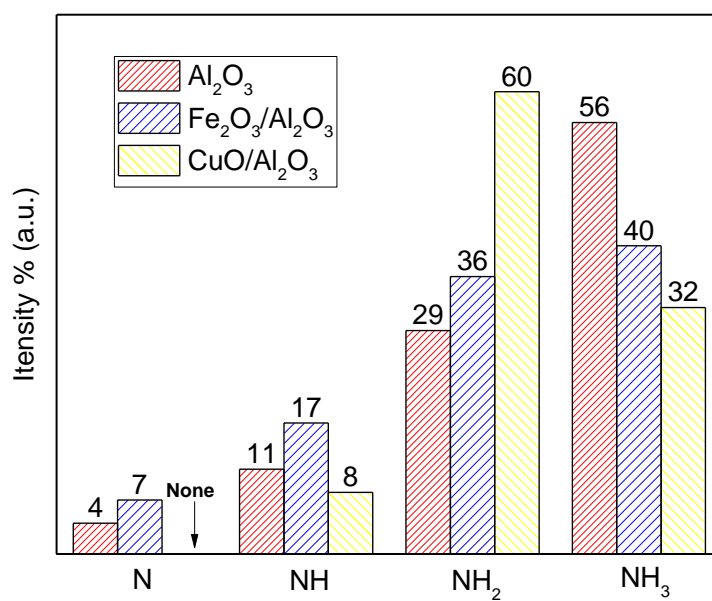


Figure 4.6 Proportion of individual peaks assigned to N, NH,  $\text{NH}_2$  and  $\text{NH}_3$  for: (a) plasma only (b) packed with  $\text{Al}_2\text{O}_3$  (c)  $\text{Fe}_2\text{O}_3/\text{Al}_2\text{O}_3$  and (d)  $\text{CuO/Al}_2\text{O}_3$ ; The numbers above each bar chart indicate the percentage of an adsorbed species on the corresponding catalyst.

#### 4.2.2 EFFECT OF GAS RATIO AD FEED FLOW RATE

Figure 4.7 shows the effect of the gas ratio on the  $\text{NH}_3$  synthesis concentration and energy efficiency of the plasma process without packing. It is apparent from this figure that a maximum  $\text{NH}_3$  synthesis concentration of 2641 ppm has been obtained at the  $\text{N}_2/\text{H}_2$  ratio of 1:3. This result conforms to the conventional ammonia synthesis process as per the stoichiometric ratio. However, the results shown in Figure 3.2 indicated an optimum molar ratio of 1:1 for a wire electrode reactor. This finding further supports the idea that the surface of the wire electrode worked as catalysts. This figure also shows that the energy efficiency of plasma processes dropped significantly when nitrogen content increases. This result may be due to the high energy demand of dissociating the  $\text{N}_2$  molecules and the lack of hydrogen species that leads to a lower concentration of ammonia.

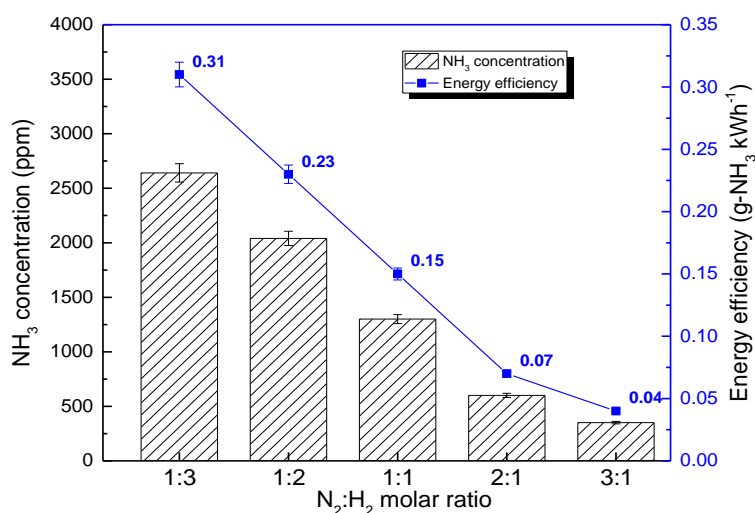


Figure 4.7 Ammonia concentration with different gas ratios ( $\text{N}_2/\text{H}_2 = 1:3, 1:2, 1:1, 2:1, 3:1$ , total flow rate  $50 \text{ ml min}^{-1}$  and discharge power  $20 \text{ W}$ ).

The effect of different feed flow rate on  $\text{NH}_3$  synthesis and energy efficiency of the plasma process without packing is presented in Figure 4.8. The maximum  $\text{NH}_3$  concentration was

achieved at the total flow rate of  $50 \text{ ml min}^{-1}$ . With the  $\text{N}_2/\text{H}_2$  molar ratio of 1:3 and the discharge power of 20 W, it is found that the increase of total feed flow rate significantly reduces the  $\text{NH}_3$  concentration. This result may be explained by the fact that the residence time of reactant gases in the discharge region decreases when the total feed flow increases, therefore lowering the possibility for activation of  $\text{N}_2$  and  $\text{H}_2$  through collisions with energised electrons. The residence time of the mixture of  $\text{N}_2$  and  $\text{H}_2$  in the discharge region decreases from 21.5 s to 5.4 s when total feed flow increases from  $50 \text{ ml min}^{-1}$  to  $200 \text{ ml min}^{-1}$ . Correspondingly, the  $\text{NH}_3$  concentration decreases from the maximum value to 910 ppm. Gomez [26], and his colleagues, investigated the dependence of  $\text{N}_2$  conversion on the flow rate of nitrogen in a packed-bed DBD reactor. A similar result was found that the  $\text{N}_2$  conversion percentage dropped from 6% of using nitrogen flow rate at  $20 \text{ ml min}^{-1}$  to a 3% of using nitrogen flow rate at  $80 \text{ ml min}^{-1}$ . Bai and his team, [28] also investigated the effect of total flow rate on the concentration of  $\text{NH}_3$ , and they applied a micro-gap DBD reactor and found a dramatic decrease of ammonia concentration when the total flow rate increases from  $1.5\text{-}4 \text{ L min}^{-1}$ , no matter what kind of  $\text{N}_2/\text{H}_2$  ratio was used.

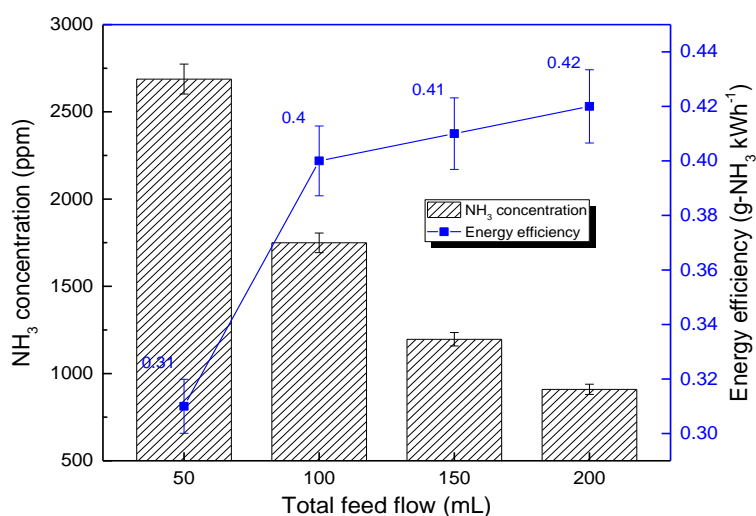


Figure 4.8 Ammonia concentration with different gas flow rates ( $N_2/H_2 = 1:3$ , total flow rate 50, 100, 150, 200  $ml\ min^{-1}$  and SEI from 6-24  $kJ\ L^{-1}$ ).

### 4.2.3 EFFECT OF SPECIFIC ENERGY INPUT (SEI)

Figure 4.9 illustrates the effect of discharge power on the  $NH_3$  concentration. It can be seen that with the increase of discharge,  $NH_3$  concentration increases with a notable amount. However, the increase rate of  $NH_3$  concentration is limited after reaching the discharge power of 30 W. For the no catalyst experiment, the  $NH_3$  concentration reaches its maximum value at the power of 50 W, and it tends to keep this value even if the discharge power increased. In contrast, when packed with  $Al_2O_3$  catalyst support,  $Fe_2O_3/Al_2O_3$  (10 wt%) and  $CuO/Al_2O_3$  (10 wt%), the  $NH_3$  concentration is almost linear with the increase of discharge power.  $CuO/Al_2O_3$  gives the highest  $NH_3$  concentration of about 6700 ppm, which is the highest  $NH_3$  concentration achieved in the research of this thesis. This study stopped at the discharge power of 60 W to mainly protect the experimental devices.

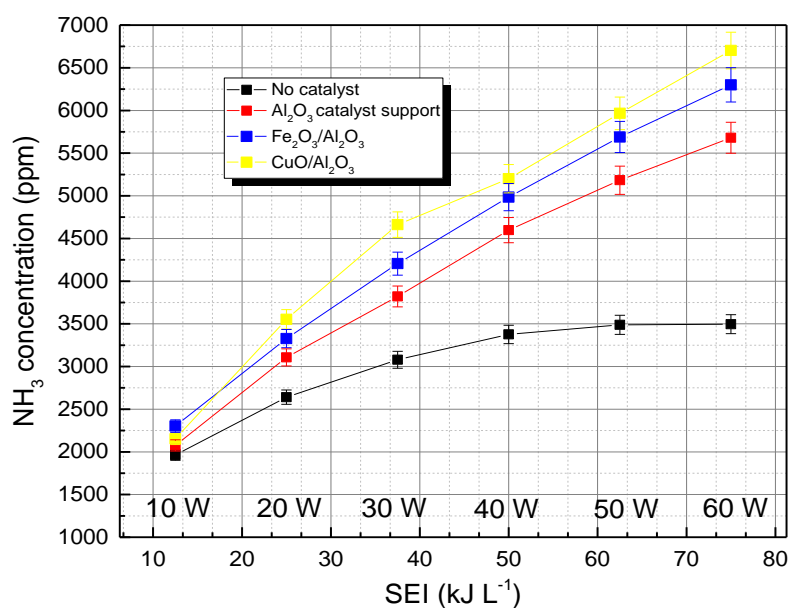


Figure 4.9 Ammonia concentration with different discharge powers: (a) No catalyst; (b) Packed with Al<sub>2</sub>O<sub>3</sub>; (c) Packed with Fe<sub>2</sub>O<sub>3</sub>/Al<sub>2</sub>O<sub>3</sub>; (d) Packed with CuO/Al<sub>2</sub>O<sub>3</sub> (N<sub>2</sub>/H<sub>2</sub> = 1:3, total flow rate 50 ml min<sup>-1</sup> and discharge power 10, 20, 30, 40, 50, 60 W).

Figure 4.10 compared the energy efficiency when different discharge power was applied. Surprisingly, the energy efficiency was found to have the optimum result at a relatively low discharge power input with a low specific energy input (SEI) of N<sub>2</sub>. Similar trends of variation of energy efficiency were observed from all of the four experiment objects and showed that as the power goes up the energy efficiency drops quickly. A possible explanation for this might be that the limited gas residence time leads to an inefficient process of ammonia synthesis.

Also, the extreme specific energy density might have enabled the dissociation of produced  $\text{NH}_3$  compounds, which further subtract energy efficiency.

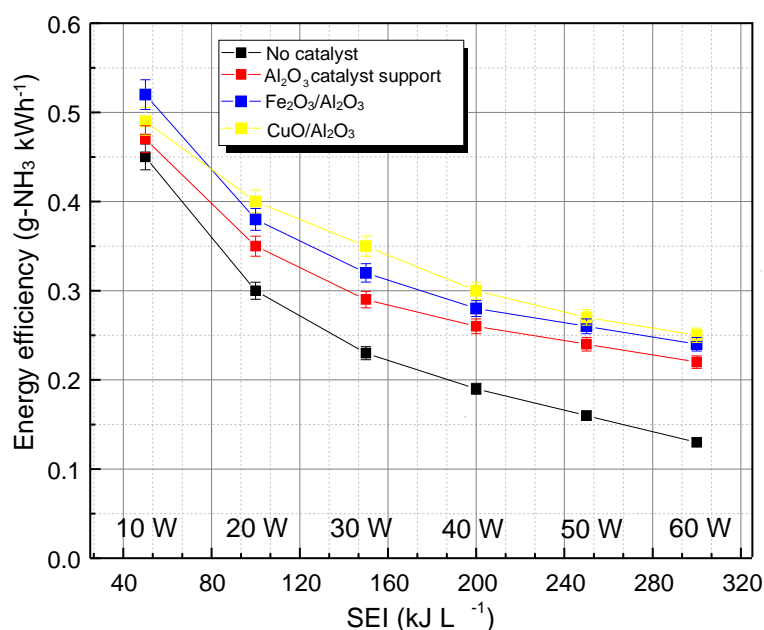


Figure 4.10 Energy efficiency with different discharge powers: (a) No catalyst; (b) Packed with  $\text{Al}_2\text{O}_3$ ; (c) Packed with  $\text{Fe}_2\text{O}_3/\text{Al}_2\text{O}_3$ ; (d) Packed with  $\text{CuO}/\text{Al}_2\text{O}_3$  ( $\text{N}_2/\text{H}_2 = 1:3$ , total flow rate  $50 \text{ ml min}^{-1}$  and discharge power 10, 20, 30, 40, 50, 60 W).

To recall, the definition of SEI (equation 2) describes the specific energy applied to the reactant gases. It can be changed by either adjusting the discharge power or changing the gas feed flow rate. For example, to increase the SEI from 12 to  $24 \text{ kJ L}^{-1}$ , it can either be realised by reducing the total feed flow rate from 100 to  $50 \text{ ml min}^{-1}$  (Figure 4.8); or increasing the discharge power from 10 to 20 W (Figure 4.9). For the first approach, the  $\text{NH}_3$  concentration increased from 1750 to 2688 ppm (an increase of 53.6%). Also, the second approach increased the  $\text{NH}_3$  concentration from 1963 to 2641 ppm (an increase of 35%). Meanwhile, the first approach decreased the energy efficiency of the plasma process from  $0.4\text{--}0.31 \text{ g-NH}_3 \text{ kWh}^{-1}$  and the second decreased the energy efficiency from  $0.45\text{--}0.3 \text{ g-NH}_3 \text{ kWh}^{-1}$ . This finding indicates that both total feed flow rate and the discharge power play an essential role in the

synthesis of  $\text{NH}_3$ . Moreover, the former one affects the  $\text{NH}_3$  concentration more, and the latter one affects energy efficiency more. This result agrees with the finding of other studies, in which Mei [78] investigated the effect of changing SEI on the  $\text{CO}_2$  decomposition in a rod electrode DBD reactor. In a word, the trade-off between total feed flow and discharge power needs to be considered to achieve a high  $\text{NH}_3$  concentration and high energy efficiency reaction.

#### 4.2.4 EFFECT OF TEMPERATURE

The plasma gas temperature in the plasma ammonia synthesis has been measured in the rod electrode DBD reactor according to the increasing SEI, as shown in Figure 4.11. It can be seen that the plasma gas temperature steady rises from 60 °C to 190 °C with the increase of the input power. However, the observed difference between plasma only, and that of packed with catalysts, was not significant.

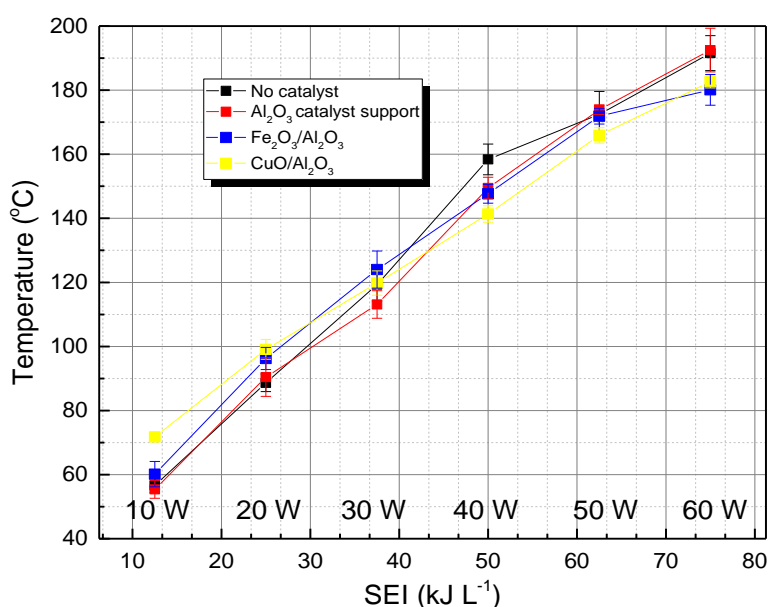


Figure 4.11 Plasma gas temperature of (a) No catalyst; (b) Packed with  $\text{Al}_2\text{O}_3$ ; (c) Packed with  $\text{Fe}_2\text{O}_3/\text{Al}_2\text{O}_3$ ; (d) Packed with  $\text{CuO}/\text{Al}_2\text{O}_3$  ( $\text{N}_2/\text{H}_2 = 1:3$ , total flow rate  $50 \text{ ml min}^{-1}$  and discharge power 10, 20, 30, 40, 50, 60 W).

#### 4.2.5 EFFECT OF METAL OXIDE-BASED CATALYSTS ON PLASMA DISCHARGES

Figure 4.12 shows the electric signals of packing with different metal oxide catalysts, including  $\gamma\text{-Al}_2\text{O}_3$ , plasma only,  $\text{Fe}_2\text{O}_3/\text{Al}_2\text{O}_3$  and  $\text{CuO}/\text{Al}_2\text{O}_3$ . It is observed that the number of micro-discharges and the amplitude of spikes are getting more intensive when packed with  $\gamma\text{-Al}_2\text{O}_3$  and also gives higher  $\text{NH}_3$  concentration. This is because of the high dielectric constant of  $\gamma\text{-Al}_2\text{O}_3$  that restrains the electrical conduction, in this case, plasma. Also, no significant differences in micro-discharge were found when packing with metal catalysts. This may occur due to the limited amount of catalysts loaded (10 wt%) that leads to a limit exposition to the plasma or otherwise suggests that the presence of metal catalysts does not seem to affect the discharge characteristics. This finding suggests that the catalyst supporter plays an important role in this DBD plasma discharge, while catalysts mainly contribute to the reaction process. The gap voltage is also presented when different catalysts were used for the plasma  $\text{NH}_3$  synthesis. There was no notable difference found on the gap voltage, that may because the catalysts or supporter were only partially packed, and therefore very limit affects the gap voltage.

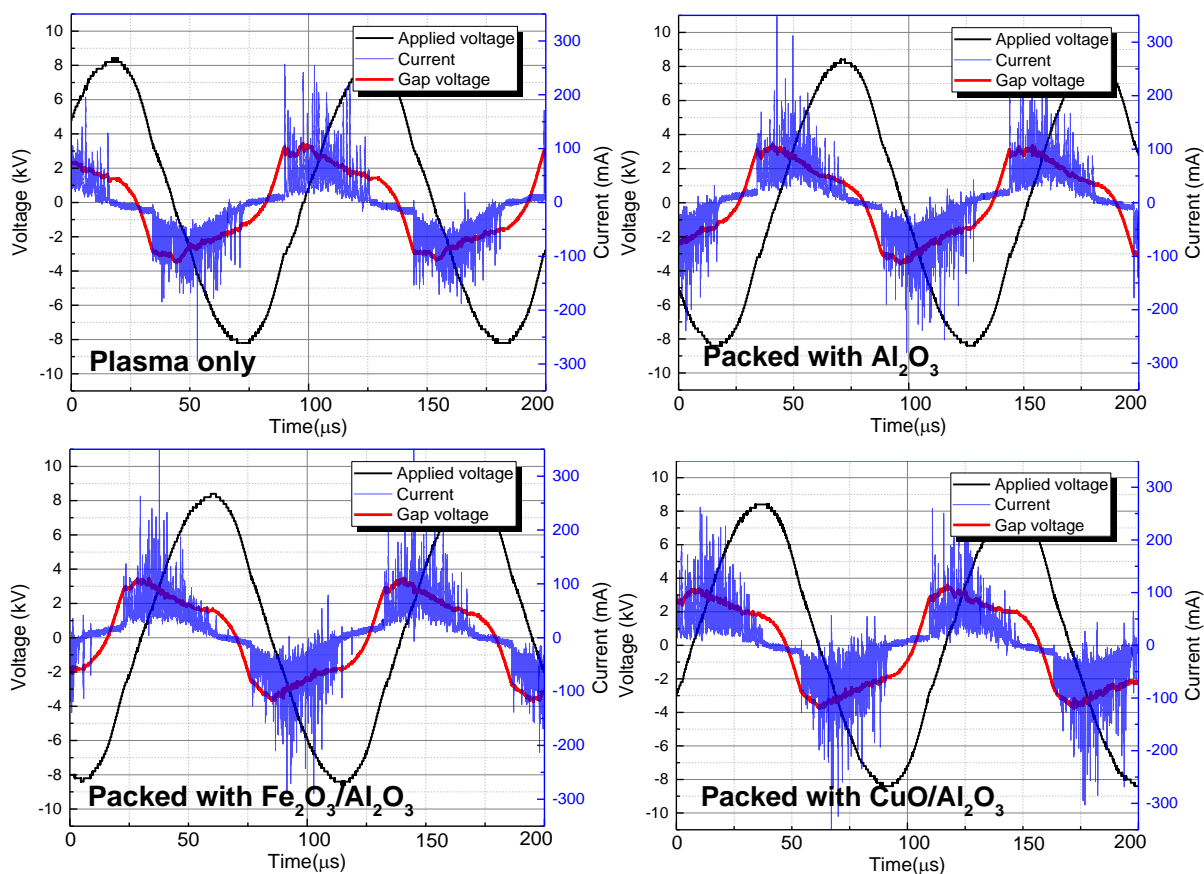


Figure 4.12 Typical discharge waveform of the plasma-synthesis of  $\text{NH}_3$  using metal oxide catalysts. ( $\text{N}_2/\text{H}_2 = 1:3$ , total flow rate  $50 \text{ ml min}^{-1}$  and discharge power  $60 \text{ W}$ ).

#### 4.2.6 THE ENHANCEMENT MECHANISM OF $\text{CuO}/\text{Al}_2\text{O}_3$

The present study was designed to determine the effect of using different metal-oxide based catalysts in plasma synthesis. As mentioned in the results,  $\text{CuO}/\text{Al}_2\text{O}_3$  gave out the best result. There are several possible explanations for this result. First, the presence of different active species and their transformation in the gas phase was detected using the optical emission spectra (OES). The OES spectrum of each sample can be found in Figure 4.13. From the spectrum, we can see the existence of  $\text{N}_2$  ( $\text{C}^3\Pi_u \rightarrow \text{B}^3\Pi_g$ ) second positive system (SPS) and the weak band of  $\text{N}_2$  ( $\text{B}^3\Pi_g \rightarrow \text{A}^3\Sigma_u$ ) first positive system (FPS), which indicates the presence of electronically excited nitrogen ( $\text{e} + \text{N}_2 \rightarrow \text{e} + \text{N}_2^*$ ). In addition, the existence of  $\text{N}_2^+$  ( $\text{B}^2\Sigma_u^+ \rightarrow \text{X}^2\Pi_g^+$ ) first negative system (FNS) suggests the nitrogen was partially ionised in the reaction

( $e + N_2 \rightarrow e + N_2^+ + e$ ). Moreover, N ( $3p^2p_0-3s^2p$ ) atomic lines at 656.3 indicates the dissociation of  $N_2$  ( $e + N_2 \rightarrow e + N + N$ ). In summary, these results show that all of the three major reactions of nitrogen in a plasma system have occurred. It is difficult to explain the OES result, but it might be related to the higher intensity of excited species and radicals such as N,  $N_2^+$  and  $N^*$  in the  $N_2$ - $H_2$  plasma when packed with  $CuO/Al_2O_3$ .

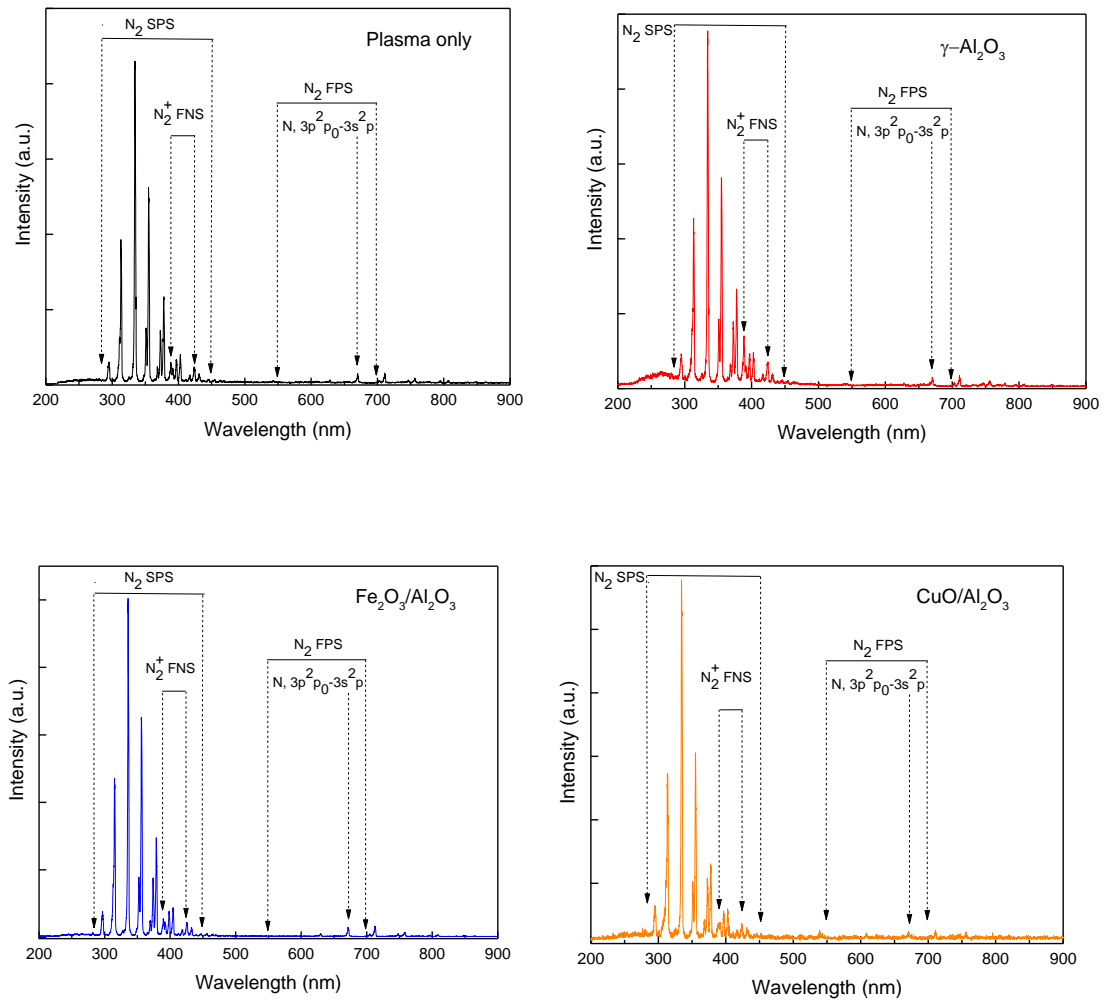


Figure 4.13 Emission spectrum for DBD: (a) plasma only (b) packed with  $Al_2O_3$  (c)  $Fe_2O_3/Al_2O_3$  and (d)  $CuO/Al_2O_3$  (SPS = second positive system; FPS = first positive system; FNS = first negative system)

A second possible explanation for this is that the strength of the M-N bond (metal nitrogen bond) on the catalyst surface may affect the dissociative adsorption of  $\text{NH}_3$ . Some authors have speculated that a higher M-N bond strength would encourage the dissociative adsorption on the catalyst surface while a weaker M-N bond may result in a smaller hydrogenation barrier and therefore promote the formation of  $\text{NH}_3$  [55], [64], [73]. More specifically, Y Wang, et al, measured the relative strength of the Fe-N, Ni-N and Cu-N bonds in plasma ammonia synthesis by  $\text{N}_2$ -TPD. They found a good correlation between the catalytic performance and the strength of the M-N bond which was inversely proportional to each other. This finding also agrees with other studies, in which Mehta, et al [64], combined experiments with DFT microkinetic modelling and determined that metals require lower hydrogenation barriers with a lower nitrogen binding strength.

This result may also be explained by the fact that the total acid sites have decreased when the metal-oxide is involved. The evaluation of the acid sites of each catalyst can be seen in the figure. The findings observed in this study mirror those of the previous studies that have examined the effect of acidity of the catalyst surface on the desorption of formed  $\text{NH}_3$ . As discussed by Wang, et al [55], the dissociation of  $\text{NH}_3$  happens mostly on the surface of catalysts. Therefore, a reduction in the total number of acid sites may contribute to the desorption of ammonia. Indeed, this also accords with earlier observations of XPS results where the amount of  $\text{NH}_3$  species on the surfaces of the catalyst is inversely proportional to the catalytic performance. Whereas, it boosts the formation of  $\text{NH}_2$  intermediates on the catalyst surface.

### 4.3 CONCLUSION

In this work, plasma only,  $\text{Al}_2\text{O}_3$ ,  $\text{Fe}_2\text{O}_3/\text{Al}_2\text{O}_3$  and  $\text{CuO}/\text{Al}_2\text{O}_3$  catalyst were tested on their performance in a rod electrode DBD reactor. First, it was found that in a rod electrode DBD reactor, hydrogen-abundant environment improves the  $\text{NH}_3$  concentration by suggesting the best  $\text{N}_2/\text{H}_2$  molar ratio to be 1:3. Also, the total flow rate and power input were investigated. It has shown the ability of both factors in changing the SEI. However, the total flow rate affects the  $\text{NH}_3$  concentration more, and the power input affects energy efficiency more. Second,  $\gamma\text{-Al}_2\text{O}_3$ ,  $\text{Fe}_2\text{O}_3/\text{Al}_2\text{O}_3$  and  $\text{CuO}/\text{Al}_2\text{O}_3$  were packed into the DBD reactor individually. When varying the power input from 10 W to 60 W, all objects gave out the same trend of  $\text{NH}_3$  concentration that was nearly proportional to the power input wherein  $\text{CuO}/\text{Al}_2\text{O}_3$  achieved the best result of about 6700 ppm ( $\text{N}_2/\text{H}_2 = 1:3$ , total flow rate:  $50 \text{ ml min}^{-1}$ , discharge power: 60 W), which is the best  $\text{NH}_3$  concentration in the research for this thesis. Third, discharge characteristics were evaluated when partially packed with different catalysts. It was observed that the addition of catalysts or catalyst support significantly increased the micro-discharge in the reactor, which therefore gives better results of  $\text{NH}_3$  concentration. Finally, the enhancement mechanism of  $\text{CuO}/\text{Al}_2\text{O}_3$  was discussed. It was found that a weaker M-N bond could lower the hydrogenation barrier of the nitrogen species, while the reduced total number of acid sites could increase the formation of  $\text{NH}_2$  intermediate as well as promote the desorption of ammonia from the catalyst surface.

## 5 CONCLUSIONS AND FUTURE WORK

### 5.1 OVERVIEW

The synthesis of ammonia is one of humanity's most massive volume manufactured chemical reactions. So far, about 88% of the human-made ammonia is broadly utilised in manufacturing nitrogen-based fertilisers. The industrialised Haber Bosch process requires severe operating conditions of temperature (400-600 °C) and pressures (200-400 atm). These conditions make the Haber Bosch process undesirable due to the substantial energy burden. Among other alternative methods of artificial ammonia synthesis, such as biological and electrochemical ammonia synthesis. Non-thermal plasma ammonia synthesis has the highest energy efficiency floor (303 g-NH<sub>3</sub> kWh<sup>-1</sup>) and therefore, is believed to have the potential of contributing to the ammonia market [15].

In this thesis, two kinds of dielectric barrier discharge reactors were evaluated on their performance of ammonia synthesis regarding the NH<sub>3</sub> concentration, energy efficiency and discharge characteristics. Chapter 3 has focused on using a wire electrode and the main findings were concluded as:

- The copper-wool electrode exhibited the highest concentration of produced NH<sub>3</sub> (2983 ppm) and the best energy efficiency (0.68 g-NH<sub>3</sub> kWh<sup>-1</sup>) at an N<sub>2</sub>/H<sub>2</sub> molar ratio of 1:1 and a flow rate of 100 ml min<sup>-1</sup>.
- By changing the total flow rate to 250 ml min<sup>-1</sup>, the energy efficiency for the NH<sub>3</sub> synthesis using a Cu electrode can be further increased to 1.04 g-NH<sub>3</sub> kWh<sup>-1</sup>.

Chapter 4 investigated the ammonia synthesis in a rod electrode DBD reactor. Effects of N<sub>2</sub>/H<sub>2</sub> flow ratio and total feed flow rate were discussed without packing. Then, catalysts of Iron and

copper oxide supported on alumina were partially packed into the reactor. The main findings of this part can be concluded as:

- Hydrogen-abundant environment improves the  $\text{NH}_3$  concentration by suggesting the best  $\text{N}_2/\text{H}_2$  molar ratio to be 1:3.
- The total flow rate and power input were investigated. It has shown the ability of both factors on changing the SEI. However, the total flow rate affects the  $\text{NH}_3$  concentration more, and the power input affects energy efficiency more.
- $\text{CuO}/\text{Al}_2\text{O}_3$  achieved the best result of about 6700 ppm ( $\text{N}_2/\text{H}_2 = 1:3$ , total flow rate: 50  $\text{ml min}^{-1}$ , discharge power: 60 W).
- The addition of catalysts or catalyst support significantly increased the micro-discharge in the reactor, which therefore gives better results of  $\text{NH}_3$  concentration.

## 5.2 LIMITATIONS

The non-thermal plasma ammonia synthesis would only be attractive for scaling up when the electricity is from renewable energy sources, and the  $\text{H}_2$  is coming from renewable sources such as from solar electrolysis/photolysis or biomass utilisation. Without the need for air compressor or heating device, plasma-driven  $\text{NH}_3$  synthesis can be carried out in smaller equipment and deployed in distant areas. For instance, the process of plasma synthesis can be installed on locations near wind farm where hydrogen is produced by electrolysis of water using waste/excessive electricity, or near a factory where hydrogen is produced from biomass. Another solution that could significantly enhance energy efficiency is to instantaneously separate the  $\text{NH}_3$  gas product. Solid or liquid sorbents should be involved and integrated with the plasma reactor to adsorb the produced  $\text{NH}_3$  and avoid its decomposition.

### 5.3 FUTURE WORK

According to the finding in chapter 4 that catalyst supporter plays a vital role on the discharge characteristics, and it suggests that different catalyst supporters such as  $\text{TiO}_2$  and active carbon can be tested on their ability to improve the plasma ammonia synthesis. Also, the effect of metal loading (weight percentage) of catalysts should be further investigated, for example, to test if a 20 wt%  $\text{CuO}/\text{Al}_2\text{O}_3$  would have a better result than that of using 10 wt%. At this stage, noble metal catalysts, for example, ruthenium-based, is strongly recommended since a higher  $\text{NH}_3$  was obtained from literature studies. Moreover, promoters for catalysts such as potassium and alkali that has been widely adopted in the study of conventional Haber Bosch process, are expected to be investigated.

Furthermore, the proper performance of packing glass beads suggests involving the dielectric materials. A new hypothesis is to smear the metal catalysts, for example,  $\text{Fe}_2\text{O}_3/\text{Al}_2\text{O}_3$  on the surface of dielectric materials. This method is expected to have a positive effect on promoting surface discharge and thus yield higher  $\text{NH}_3$  concentration.

## REFERENCES

- [1] D. E. Canfield, A. N. Glazer, and P. G. Falkowski, 'The evolution and future of earth's nitrogen cycle', *Science*, vol. 330, no. 6001, pp. 192–196, 2010.
- [2] Ceresana, 'Market Study: Ammonia', 2012.
- [3] R. R. Schrock, 'Reduction of dinitrogen', *Proc. Natl. Acad. Sci.*, vol. 103, no. 46, pp. 17087–17087, 2006.
- [4] U.S. Geological Survey, 'Mineral Commodity Summaries 2016', 2016.
- [5] E. Cowling *et al.*, 'Optimizing nitrogen management in food and energy production and environmental protection: summary statement from the Second International Nitrogen Conference.', *ScientificWorldJournal.*, vol. 1 Suppl 2, no. x, pp. 1–9, 2001.
- [6] J. W. Erisman, M. A. Sutton, J. Galloway, Z. Klimont, and W. Winiwarter, 'How a century of ammonia synthesis changed the world', *Nat. Geosci.*, vol. 1, no. 10, pp. 636–639, 2008.
- [7] J. M. Modak, 'Haber process for ammonia synthesis', *Resonance*, vol. 16, no. 12, pp. 1159–1167, 2011.
- [8] W. H. Avery, 'A role for ammonia in the hydrogen economy', *Int. J. Hydrogen Energy*, vol. 13, no. 12, pp. 761–773, 1988.
- [9] E. Morgan, J. Manwell, and J. McGowan, 'Wind-powered ammonia fuel production for remote islands: A case study', *Renew. Energy*, vol. 72, pp. 51–61, 2014.
- [10] R. Lan, J. T. S. Irvine, and S. Tao, 'Ammonia and related chemicals as potential indirect hydrogen storage materials', *International Journal of Hydrogen Energy*, vol. 37, no. 2, pp. 1482–1494, 2012.
- [11] J. S. J. Hargreaves, 'Nitrides as ammonia synthesis catalysts and as potential nitrogen transfer reagents', *Appl. Petrochemical Res.*, vol. 4, no. 1, pp. 3–10, 2014.
- [12] J. Dorning, 'The Haber Bosch Process'.
- [13] L. F. Razon, 'Life cycle analysis of an alternative to the haber-bosch process: Non-renewable energy usage and global warming potential of liquid ammonia from cyanobacteria.', *Environ. Prog. Sustain. Energy*, vol. 33, no. 2, pp. 618–624, 2014.
- [14] G. Council for Social and Economic Studies (U.S.) and R. George Mason University. Contemporary Economics and Business Association., 'The Journal of social, political, and economic studies.', *J. Soc. Polit. Econ. Stud.*, vol. 36, no. 4, p. 421, 1981.
- [15] N. Cherkasov, A. O. Ibhaden, and P. Fitzpatrick, 'A review of the existing and alternative methods for greener nitrogen fixation', *Chem. Eng. Process. Process Intensif.*, vol. 90, pp. 24–33, Apr. 2015.
- [16] F. Barbir, 'PEM electrolysis for production of hydrogen from renewable energy sources', *Sol. Energy*, vol. 78, no. 5, pp. 661–669, 2005.
- [17] P. Peng *et al.*, 'A review on the non-thermal plasma-assisted ammonia synthesis technologies', *J. Clean. Prod.*, vol. 177, 2018.
- [18] B. Hinnemann and J. K. Nørskov, 'Catalysis by Enzymes: The Biological Ammonia Synthesis', *Top. Catal.*, 2006.

- [19] X. Guo, Y. Zhu, and T. Ma, 'Lowering reaction temperature : Electrochemical ammonia synthesis by coupling various electrolytes and catalysts', *J. Energy Chem.*, vol. 26, no. 6, pp. 1107–1116, 2017.
- [20] V. Kyriakou, I. Garagounis, E. Vasileiou, A. Vourros, and M. Stoukides, 'Progress in the Electrochemical Synthesis of Ammonia', *Catalysis Today*. 2016.
- [21] T. Mizushima, K. Matsumoto, J. I. Sugoh, H. Ohkita, and N. Kakuta, 'Tubular membrane-like catalyst for reactor with dielectric-barrier- discharge plasma and its performance in ammonia synthesis', *Appl. Catal. A Gen.*, vol. 265, no. 1, pp. 53–59, 2004.
- [22] H. H. Kim, Y. Teramoto, A. Ogata, H. Takagi, and T. Nanba, 'Atmospheric-pressure nonthermal plasma synthesis of ammonia over ruthenium catalysts', *Plasma Process. Polym.*, vol. 14, no. 6, pp. 1–9, 2017.
- [23] K. Aihara, M. Akiyama, T. Deguchi, M. Tanaka, R. Hagiwara, and M. Iwamoto, 'Remarkable catalysis of a wool-like copper electrode for NH<sub>3</sub> synthesis from N<sub>2</sub> and H<sub>2</sub> in non-thermal atmospheric plasma', *Chem. Commun.*, vol. 52, no. 93, pp. 13560–13563, 2016.
- [24] M. Iwamoto, M. Akiyama, K. Aihara, and T. Deguchi, 'Ammonia Synthesis on Wool-Like Au, Pt, Pd, Ag, or Cu Electrode Catalysts in Nonthermal Atmospheric-Pressure Plasma of N<sub>2</sub> and H<sub>2</sub>'.
- [25] A. Gómez-Ramírez, J. Cotrino, R. M. Lambert, and A. R. González-Elipé, 'Efficient synthesis of ammonia from N<sub>2</sub> and H<sub>2</sub> alone in a ferroelectric packed-bed DBD reactor', *Plasma Sources Sci. Technol.*, vol. 24, no. 6, 2015.
- [26] A. Gómez-Ramírez, A. M. Montoro-Damas, J. Cotrino, R. M. Lambert, and A. R. González-Elipé, 'About the enhancement of chemical yield during the atmospheric plasma synthesis of ammonia in a ferroelectric packed bed reactor', *Plasma Process. Polym.*, 2017.
- [27] M. Bai, Z. Zhang, M. Bai, X. Bai, and H. Gao, 'Synthesis of Ammonia using CH<sub>4</sub>/N<sub>2</sub> plasmas based on micro-gap discharge under environmentally friendly condition', *Plasma Chem. Plasma Process.*, vol. 28, no. 4, pp. 405–414, 2008.
- [28] M. Bai, Z. Zhang, X. Bai, M. Bai, and W. Ning, 'Plasma Synthesis of Ammonia With a Microgap Dielectric Barrier Discharge at Ambient Pressure', *IEEE Trans. Plasma Sci.*, vol. 31, no. 6 II, pp. 1285–1291, 2003.
- [29] P. Peng, Y. Li, Y. Cheng, S. Deng, P. Chen, and R. Ruan, 'Atmospheric Pressure Ammonia Synthesis Using Non-thermal Plasma Assisted Catalysis', *Plasma Chem. Plasma Process.*, vol. 36, no. 5, pp. 1201–1210, 2016.
- [30] K. Sugiyama, K. Akazawa, M. Oshima, H. Miura, T. Matsuda, and O. Nomura, 'Ammonia synthesis by means of plasma over MgO catalyst', *Plasma Chem. Plasma Process.*, vol. 6, no. 2, pp. 179–193, 1986.
- [31] M. V. Khin Swe Yin, 'Plasma Chemical Synthesis. I. Effect of Electrode Material on the Synthesis of Ammonia Khin Swe Yin I and Mundiayath Venugopalan 1', *Chem. Plasma Process. Plasma*, vol. 3, no. 3, pp. 343–350, 1983.
- [32] H. Uyama and O. Matsumoto, 'Synthesis of ammonia in high-frequency discharges', *Plasma Chem. Plasma Process.*, vol. 9, no. 1, pp. 13–24, 1989.
- [33] H. Uyama and O. Matsumoto, 'Synthesis of Ammonia in High-Frequency Discharges . II . Synthesis of Ammonia in a Microwave Discharge Under Various Conditions Haruo Uyama ~ and Osamu Matsumoto ~', *Plasma Chem. Plasma Process.*, vol. 9, no. 3, p. 12, 1989.

- [34] J. Nakajima and H. Sekiguchi, 'Synthesis of ammonia using microwave discharge at atmospheric pressure', *Thin Solid Films*, vol. 516, no. 13, pp. 4446–4451, 2008.
- [35] J. H. Montoya, C. Tsai, A. Vojvodic, and J. K. Nørskov, 'The challenge of electrochemical ammonia synthesis: A new perspective on the role of nitrogen scaling relations', *ChemSusChem*, vol. 8, no. 13, 2015.
- [36] B. S. Patil, Q. Wang, V. Hessel, and J. Lang, 'Plasma N<sub>2</sub> -fixation : 1900 – 2014', *Catal. Today*, vol. 256, pp. 49–66, 2015.
- [37] P. Talebizadeh *et al.*, 'A coaxial DBD reactor'. 2015.
- [38] 'Plasma technology. What is Plasma? | Plasmatreat'. .
- [39] H Conrads and M Schmidt, 'Plasma generation and plasma sources', *Plasma Sources Sci. Technol.*, vol. 9, no. 4, p. 441, 2000.
- [40] 'Electric glow discharge - The Plasma Universe theory (Wikipedia-like Encyclopedia)'. .
- [41] R. Hippler, S. Pfau, M. Schmidt, and K. H. S. Eds, 'Low Temperature Plasma Physics'.
- [42] P. Lu, P. J. Cullen, and K. Ostrikov, *Atmospheric Pressure Nonthermal Plasma Sources*. 2016.
- [43] B. Eliasson, W. Egli, and U. Kogelschatz, 'Modelling of dielectric barrier discharge chemistry', *Pure Appl. Chem.*, vol. 66, no. 6, 1994.
- [44] U. Kogelschatz, 'Dielectric-barrier discharges: Their History, Discharge Physics, and Industrial Applications', *Plasma Chemistry and Plasma Processing*. 2003.
- [45] A. V. Pipa and R. Brandenburg, 'The equivalent circuit approach for the electrical diagnostics of dielectric barrier discharges: The classical theory and recent developments', *Atoms*, vol. 7, no. 1, 2019.
- [46] A. Fridman, *Plasma Chemistry*. Cambridge University Press, 2008.
- [47] M. Rycroft, F. Editor, and E. E. Publishers, 'Plasma gasification of waste: arcs and microwaves offer advantages', *EE Publishers*. 2016.
- [48] 'Moscow Radiotechnical Institute of Russian Academy of Sciences - Atmospheric-pressure microwave plasmotrons for synthesis of chemically pure nanopowders and plasma'. .
- [49] M. D. Bai, X. Y. Bai, Z. T. Zhang, B. Mingdong, B. Xiyao, and Z. Zhitao, 'Synthesis of ammonia in a strong electric field discharge at ambient pressure', *Plasma Chem. Plasma Process.*, 2000.
- [50] J. Hong, S. Prawer, and A. B. Murphy, 'Production of ammonia by heterogeneous catalysis in a packed-bed dielectric-barrier discharge: Influence of argon addition and voltage', *IEEE Trans. Plasma Sci.*, vol. 42, no. 10, pp. 2338–2339, 2014.
- [51] Y. Kubota, K. Koga, M. Ohno, and T. Hara, 'Synthesis of Ammonia through Direct Chemical Reactions between an Atmospheric Nitrogen Plasma Jet and a Liquid', *Plasma Fusion Res.*, vol. 5, pp. 042–042, 2010.
- [52] J. Hong *et al.*, 'Plasma Catalytic Synthesis of Ammonia Using Functionalized-Carbon Coatings in an Atmospheric-Pressure Non-equilibrium Discharge', *Plasma Chem. Plasma Process.*, vol. 36, no. 4, pp. 917–940, 2016.
- [53] P. Peng *et al.*, 'Ru-based multifunctional mesoporous catalyst for low-pressure and non-thermal plasma synthesis of ammonia', *Int. J. Hydrogen Energy*, vol. 42, no. 30, pp. 19056–19066, Jul. 2017.

- [54] P. Peng *et al.*, 'Atmospheric Plasma-Assisted Ammonia Synthesis Enhanced via Synergistic Catalytic Absorption', *ACS Sustain. Chem. Eng.*, vol. 7, no. 1, pp. 100–104, 2019.
- [55] and X. T. Yaolin Wang, Michael Craven, Xiaotong Yu, Jia Ding, Paul Bryant, Jun Huang, 'Plasma-enhanced catalytic synthesis of ammonia over a Ni/ Al<sub>2</sub>O<sub>3</sub> catalyst at near-room temperature: Insights into the importance of the catalyst surface on the reaction mechanism', *ACS Catal.*, 2019.
- [56] G. Akay and K. Zhang, 'Process Intensification in Ammonia Synthesis Using Novel Coassembled Supported Microporous Catalysts Promoted by Nonthermal Plasma', *Ind. Eng. Chem. Res.*, vol. 56, no. 2, pp. 457–468, 2017.
- [57] D. Xie, Y. Sun, T. Zhu, X. Fan, X. Hong, and W. Yang, 'Ammonia synthesis and by-product formation from H<sub>2</sub>O, H<sub>2</sub> and N<sub>2</sub> by dielectric barrier discharge combined with an Ru/Al<sub>2</sub>O<sub>3</sub> catalyst', *RSC Adv.*, vol. 6, no. 107, pp. 105338–105346, 2016.
- [58] K. ichi Aika, 'Role of alkali promoter in ammonia synthesis over ruthenium catalysts—Effect on reaction mechanism', *Catal. Today*, 2017.
- [59] Z. Ma, S. Zhao, X. Pei, X. Xiong, and B. Hu, 'New insights into the support morphology-dependent ammonia synthesis activity of Ru/CeO<sub>2</sub> catalysts', *Catal. Sci. Technol.*, 2017.
- [60] S. Tanaka, H. Uyama, and O. Matsumoto, 'Synergistic effects of catalysts and plasmas on the synthesis of ammonia and hydrazine', *Plasma Chem. Plasma Process.*, vol. 14, no. 4, pp. 491–504, 1994.
- [61] H. Kiyooka and O. Matsumoto, 'Reaction scheme of ammonia synthesis in the ECR plasmas', *Plasma Chem. Plasma Process.*, 1996.
- [62] H. Uyama, T. Nakamura, S. Tanaka, and O. Matsumoto, 'Catalytic effect of iron wires on the syntheses of ammonia and hydrazine in a radio-frequency discharge', *Plasma Chem. Plasma Process.*, vol. 13, no. 1, pp. 117–131, 1993.
- [63] M. Touvelle, J. L. M. Licea, M. Venugopalan, J. L. Mufioz Licea, and M. Venugopalan, 'Plasma Chemical Synthesis. II. Effect of Wall Surface on the Synthesis of Ammonia', *Plasma Chem. Plasma Process.*, vol. 7, no. 1, p. 101, 1987.
- [64] F. A. Herrera *et al.*, 'The impact of transition metal catalysts on macroscopic dielectric barrier discharge (DBD) characteristics in an ammonia synthesis plasma catalysis reactor', *J. Phys. D. Appl. Phys.*, 2019.
- [65] T. C. Manley, 'The Electric Characteristics of the Ozonator Discharge', *Trans. Electrochem. Soc.*, 1943.
- [66] X. Tu, H. J. Gallon, M. V Twigg, P. A. Gorry, and J. C. Whitehead, 'Dry reforming of methane over a Ni/Al<sub>2</sub>O<sub>3</sub> catalyst in a coaxial dielectric barrier discharge reactor', *J. Phys. D. Appl. Phys.*, vol. 44, no. 27, p. 274007, 2011.
- [67] D. Mei, X. Zhu, Y.-L. He, J. D. Yan, and X. Tu, 'Plasma-assisted conversion of CO<sub>2</sub> in a dielectric barrier discharge reactor: understanding the effect of packing materials', *Plasma Sources Sci. Technol.*, vol. 24, no. 1, p. 015011, 2014.
- [68] Y. Zeng, 'Conversion of CO<sub>2</sub> into valuable fuels and chemicals using non-thermal plasma', no. March, 2017.
- [69] Z. Falkenstein and J. J. Coogan, 'Microdischarge behaviour in the silent discharge of nitrogen - oxygen and water - air mixtures', *J. Phys. D. Appl. Phys.*, 1999.

- [70] R. Valdivia-Barrientos, J. Pacheco-Sotelo, M. Pacheco-Pacheco, J. S. Benítez-Read, and R. López-Callejas, 'Analysis and electrical modelling of a cylindrical DBD configuration at different operating frequencies', in *Plasma Sources Science and Technology*, 2006.
- [71] D. Mei, 'Plasma-catalytic conversion of greenhouse gas into value-added fuels and chemicals', no. June, p. 210, 2016.
- [72] 'OMNIC™ Spectra Software'.
- [73] L. Wang, Y. Yi, Y. Zhao, R. Zhang, J. Zhang, and H. Guo, 'NH<sub>3</sub>Decomposition for H<sub>2</sub>Generation: Effects of Cheap Metals and Supports on Plasma-Catalyst Synergy', *ACS Catal.*, 2015.
- [74] J. Hong, S. Pancheshnyi, E. Tam, J. J. Lowke, S. Prawer, and A. B. Murphy, 'Kinetic modelling of NH<sub>3</sub> production in N<sub>2</sub>-H<sub>2</sub> non-equilibrium atmospheric-pressure plasma catalysis', *J. Phys. D. Appl. Phys.*, 2017.
- [75] J. R. Shah, J. M. Harrison, and M. L. Carreon, 'Ammonia plasma-catalytic synthesis using low melting point alloys', *Catalysts*, vol. 8, no. 10, 2018.
- [76] C. Wang, X. Ma, Q. Ge, and H. Xu, 'A comparative study of PdZSM-5, Pdβ, and PdY in hybrid catalysts for syngas to hydrocarbon conversion', *Catal. Sci. Technol.*, 2015.
- [77] NIST, 'XPS database'. [Online]. Available: [https://srdata.nist.gov/xps/EngElmSrchQuery.aspx?EType=PE&CSOpt=Retri\\_ex\\_dat&Elm=N](https://srdata.nist.gov/xps/EngElmSrchQuery.aspx?EType=PE&CSOpt=Retri_ex_dat&Elm=N).
- [78] D. Mei and X. Tu, 'Conversion of CO<sub>2</sub> in a cylindrical dielectric barrier discharge reactor: Effects of plasma processing parameters and reactor design', *J. CO<sub>2</sub> Util.*, vol. 19, pp. 68–78, 2017.

## APPENDICES

Experiment results in the work of Chapter 3

Power: 20W Different materials (1:1 total flow rate of 100 ml)	SS Rod	NiCr 80	NiFe 70	SS	Ti	Ni	Cu
Peak Concentration (ppm)	1885	2561	2571	2649	2868	2940	2983
Energy Efficiency (g/kWh) Error: +-0.05	0.43	0.58	0.59	0.6	0.65	0.67	0.68
N2 conversion % +-0.02	0.19	0.26	0.26	0.27	0.29	0.29	0.3
Cu							
Effect of molar ratio N2:H2=	01:03	01:02	01:01	02:01	03:01		
	N2:H2=25 ml: 75 ml	N2:H2=35 ml: 65 ml	N2:H2=50 ml: 50 ml	N2:H2=65 ml: 35ml	N2:H2= 75 ml:25ml		
Peak Concentration	2466	2838	2983	2769	1943		
Energy Efficiency	0.56	0.65	0.68	0.63	0.44		
N2 conversion	0.49	0.41	0.3	0.21	0.13		
Cu 1:1							
Effect of Total Flow rate	50	100	150	200	250		
	N2:H2= 25 ml:25ml	N2:H2= 50 ml:50ml	N2:H2= 75 ml:75ml	N2:H2= 100 ml:100ml	N2:H2= 125 ml:125ml		
Peak Concentration	3833	2983	2526	1952	1822		
Energy Efficiency	0.44	0.68	0.86	0.89	1.04		
N2 conversion	0.38	0.3	0.25	0.2	0.18		

Experiment results in the work of Chapter 4

<b>N2:H2=1:3</b>	<b>Flow rate test</b>	<b>Power: 20W</b>	<b>Temperature</b>	<b>Calibrated FTIR peak area</b>			<b>Average FTIR area</b>	<b>NH<sub>3</sub> yield (ppm)</b>	<b>Energy efficiency (g-NH<sub>3</sub> kWh<sup>-1</sup>)</b>
N2		H2		10min	20min	30min			
12.5	50 ml	37.5	85.9-91.4	1.22787	1.29615	1.29443	1.29529	2687.72675	0.305968893
25	100 ml	75	84.6-93.8	0.859115	0.842172	0.827934	0.843073667	1749.37786	0.398295852
37.5	150 ml	112.5	83.8-95.6	0.584313	0.578378	0.567124	0.576605	1196.45538	0.408610876
50	200 ml	150	83.4-92.3	0.444933	0.435269	0.434793	0.438331667	909.538208	0.41416472
<b>Total flow rate 50 ml</b>	<b>Gas ratio test</b>	<b>Power: 20W</b>	<b>Temperature</b>	<b>Calibrated FTIR peak area</b>			<b>Average FTIR area</b>	<b>NH<sub>3</sub> yield (ppm)</b>	<b>Energy efficiency (g-NH<sub>3</sub> kWh<sup>-1</sup>)</b>
N2		H2		10min	20min	30min			
12.5	01:03	37.5	85.9-91.4	1.22787	1.29615	1.29443	1.29529	2687.72675	0.305968893
17	01:02	33	85.6-92.6	0.975159	0.991522	0.983216	0.983299	2040.34543	0.232271466
25	01:01	25	87.1-93.3	0.622913	0.633572	0.623213	0.626566	1300.12445	0.148005239
33	02:01	17	77.9-83.5	0.289159	0.292779	0.286765	0.289567667	600.852908	0.068400666
37.5	03:01	12.5	83.5-88.7	0.170547	0.168559	0.168354	0.169153333	350.993167	0.039956811
<b>N2:H2=1:3</b>	<b>Power test</b>	<b>Total flow rate 50 ml</b>	<b>Temperature</b>	<b>Calibrated FTIR peak area</b>			<b>Average FTIR area</b>	<b>NH<sub>3</sub> yield (ppm)</b>	<b>Energy efficiency (g-NH<sub>3</sub> kWh<sup>-1</sup>)</b>
N2		H2		10min	15min	20min			
12.5	10 W	37.5	54.4-58.8	0.89237815	0.96913508	0.976349788	0.945954	1962.855	0.45
12.5	20 W	37.5	85.9-91.4	1.22787	1.29615	1.29443	1.272817	2641.095	0.3
12.5	30 W	37.5	114.2-124.4	1.425528042	1.5106414	1.515421056	1.483864	3079.017	0.23
12.5	40 W	37.5	153.6-163.2	1.56871256	1.65335306	1.65893968	1.627002	3376.029	0.19
12.5	50 W	37.5	165.3-179.6	1.641171068	1.72161676		1.681394	3488.892	0.16
12.5	60 W	37.5	186.1-197.0	1.648431062	1.72131752		1.684874	3496.114	0.13

Experiment results in the work of Chapter 4

Power test Al <sub>2</sub> O <sub>3</sub> /Al <sub>2</sub> O <sub>3</sub>	N <sub>2</sub> :H <sub>2</sub> =1:3	Total flow rate: 50ml		Average FTIR area	NH <sub>3</sub> yield (ppm)	Energy efficiency (g- NH <sub>3</sub> kWh <sup>-1</sup> )
Power (W)	N <sub>2</sub>	H <sub>2</sub>	Temperature			
10	12.5	37.5	52.6-58.2	1.000111	2075.23	0.472485
20	12.5	37.5	84.4-96.5	1.49724	3106.773	0.353673
30	12.5	37.5	108.8-117.4	1.84143	3820.967	0.289984
40	12.5	37.5	146.1-152.8	2.2159	4597.993	0.261716
50	12.5	37.5	172.4-175.4	2.49759	5182.499	0.235989
60	12.5	37.5	185.7-199.3	2.73751	5680.333	0.215548
Power test Fe <sub>2</sub> O <sub>3</sub> /Al <sub>2</sub> O <sub>3</sub>	N <sub>2</sub> :H <sub>2</sub> =1:3	Total flow rate: 50ml				
Power (W)	N <sub>2</sub>	H <sub>2</sub>	Temperature			
10	12.5	37.5	56.2-64.1	1.10956	2302.337	0.524193
20	12.5	37.5	92.8-99.7	1.6037	3327.678	0.37882
30	12.5	37.5	118.2-129.8	2.02663	4205.257	0.319149
40	12.5	37.5	144.7-150.6	2.40227	4984.71	0.283728
50	12.5	37.5	169.4-174.3	2.7419	5689.443	0.259073
60	12.5	37.5	175.3-184.9	3.03615	6300.011	0.239063
Power test CuO/Al <sub>2</sub> O <sub>3</sub>	N <sub>2</sub> :H <sub>2</sub> =1:3	Total flow rate: 50ml				
Power (W)	N <sub>2</sub>	H <sub>2</sub>	Temperature			
10	12.5	37.5	71.1-72.4	1.03819	2154.244	0.490475
20	12.5	37.5	96-102.2	1.71205	3552.504	0.404414
30	12.5	37.5	116.0-123.6	2.24703	4662.587	0.353857
40	12.5	37.5	138.8-143.9	2.5062	5200.365	0.296003
50	12.5	37.5	163.5-168.3	2.87534	5966.331	0.271681
60	12.5	37.5	180.7-184.6	3.23002	6702.292	0.254328